國立交通大學

工學院半導體材料與製程設備學程

碩士論文

光阻烘烤製程的不均勻性對CD之影響

The Impact of Non-Uniformity in Photoresist Processing on Critical Dimension

研究生：卓慶華
指導教授：呂志鵬　教授

中華民國九十九年六月

光阻烘烤製程的不均勻性對 CD 之影響

The Impact of Non-Uniformity in Photoresist Processing on Critical Dimension

研 究 生：卓慶華　　Student：Ching Hua Cho

指導教授：呂志鵬　　Advisor：Jihperng(Jim)Leu

國 立 交 通 大 學

工學院半導體材料與製程設備學程

碩 士 論 文

A Thesis

Master Degree Program of Semiconductor Material and Processing Equipment

College of Engineering

National Chiao Tung University

in Partial Fulfillment of the Requirements

for the Degree of

Master of Science

In

Program of Semiconductor Material and Processing Equipment

June 2010

Hsinchu, Taiwan, Republic of China

中華民國 九十九 年 六 月

光阻烘烤製程的不均勻性對CD之影響

學生:卓慶華　　指導教授:呂志鵬 博士

國立交通大學工學院半導體材料與製程設備學程

摘要

隨著電腦科技的進步,記憶體晶片的容量需求越來越大,像動態隨機存取記憶體(dynamic random access memory, DRAM)以及快閃唯讀記憶體(flash read-only memory, flash-ROM)等晶片,積體電路(IC)製造者勢必想用最小的晶圓面積作出最大的記憶容量,因此必需不斷的減小元件特徵尺寸來持續的降低成本。而提高IC電路製程光微影(lithography)解析度的方法有很多,但是最有效的方法卻只有不停的縮短波長,而使用的波長越短光源能量就越弱,若直接加長曝光時間雖也能有足夠能量傳給光阻進行光反應,但是這樣作會嚴重損失產能及曝光穩定性。所以現階段較可行的方式是利用化學放大型光阻(chemically amplified photoresist, CAPR)製程,另將光阻獲得能量的方式,分成曝光及烘烤兩個部份。因為烘烤關係到CAPR H^+連續催化反應的能量,所以對關鍵尺寸(critical dimension, CD)的影響和曝光一樣的重要,此外,烘烤步驟中光阻的溫度均勻性因為矽晶圓與烘烤硬體之接觸問題,接觸熱傳導的均勻性無法能夠像光一樣的精準正確,因此曝光前烘烤(pre bake, PB)及曝光後烘烤(post exposure bake, PEB)的接觸問題,會直接影響CAPR內部光化學反應的均勻性，而會造成晶圓半邊的CD異常及一半的良率損失現象。

為了探討光阻烘烤製程的不均勻性對CD之影響,我們利用wafer與烤盤接觸瞬間,熱由高溫傳導至低溫,使的plate的溫度下降了ΔT,因為下降的程度與wafer和plate接觸面積大小有關,因此可利用此參數ΔT方便我們來判斷Wafer

烘烤製程之狀況。

一般而言PEB的主要功能是提供CAPR內部H^+連續催化反應的能量,影響CD應該是最直接且最重要的,但是實驗結果,發現不論是 248 nm或 193 nm 的PB影響都大於PEB,因此PB比PEB更為重要。並且發現 PB 與 PEB 對CD的影響方向相反,例如當DUV photoresist 在wafer與plate之間有一 0.5 mm 的間隙Tilt,而且相同的條件下, PB使線距增加 94~340Å,而PEB卻使線距減少 61~109Å。然而I-Line雖然對線寬有些微影響,但因為規格較寬鬆,因此可不考慮CD的變化。

我們也利用 ANSYS 軟體建立了一個簡化的三維有限元素模型。此模型預測的晶片表面溫度與實際 T-Map 儀器所量測的數據差異小於±2℃。預測的 wafer 與 plate 接觸瞬間 plate 內部溫度下降ΔT 與實際 plate 溫度下降ΔT 的數據差異小於±0.2℃。而且此模型針對各種不同的 tilt 試片所預測的 CD 與溫度測試實驗有著極佳的相關性。最後我們發現了足於代表光阻的 PB/PEB 烘烤製程狀況的 plate 溫度下降參數ΔT,並且驗證了ΔT 與 CD 的直接關聯性,可利用此模型來協助預測新產品或新製程條件能忍受的範圍。

The Impact of Non-Uniformity in Photoresist Processing on Critical Dimension

Student: Ching Hua Cho Advisor: Dr. Jihperng Leu

Program of Semiconductor Material and Processing Equipment
College of Engineering
National Chiao Tung University

Abstract

The advancement of the computer science and technology has resulted in an increasing demand for memory chips such as dynamic random access memory (DRAM) and flash read-only memory (Flash-ROM) chips, etc. Manufacturers aim to develop chips that have maximum possible memory capacity with minimum chip area while simultaneously reducing the cost. With reference to Moore's law, many methods can be used to improve IC circuit image resolution; however, the most effective method is to use the increasingly shorter wavelengths, which require weaker light source. By extending exposure time will allow sufficient energy to pass through photoresist, thus enabling the photoacid reaction to proceed; however, this will result in heavy losses, which can produce and expose stability. Hence a more feasible solution by the usage of chemically amplified photoresist (CAPR) process is created. The CAPR process has been said to obtain the energy of the photoresist and can be divided into exposed and baked components. Bake heat-conduction by wafer and hot plate contact control uniformity is unlike light, which is perfect and correct. In addition, contact issues on pre-bake (PB), post-exposure bake (PEB) and direct

influence uniformity of the photochemical reaction within CAPR can usually cause yield loss on half of the wafer. Method to guarantee the performance baked by CAPR is an extremely important subject in the semi-conductor manufacturing at the moment.

Generally speaking, the main function of PEB is to support the energy of CAPR H^+ continuous catalysis, which is the most direct and important influence on critical dimension (CD). The experimental result has found that regardless of the PB of 248 nm or 193 nm, PB influence is still greater than PEB, thus PB has proven to be more important than PEB. The finding of PB contrary to the direction of PEB impact on CD will also be conducted. For example, if DUV photoresist wafer is 0.5 mm on both PB and PEB plate gap, PB will increase line distance by 94~340Å while PEB will reduce line distance by 61~109Å. Although I-line has little influence on some CDs, the relatively loose specification will not consider the change in CD. We will utilize software to set up a simple and limited element model in three-dimension. The wafer surface temperature predicted by the model and actual T-Map instrument data difference examined by quantity is less than ±2℃. Wafer and instantaneous plate-plate contact temperature drop ΔT, actual plate temperature drop ΔT and ΔT data difference are predicted to reach below ±0.2℃. Impacts will be seen in CD temperature, 248 nm photoresist at PB 0.34 nm/℃, PEB –0.21 nm/℃ in addition to 193 nm photoresist at PB 1.23 nm/℃ and PEB –0.39 nm/℃. The model used to predict CD wafer and temperature to all gaps of contact experiment has proved to possess extreme reliability.

In conclusion, PB/PEB was found capable in representing ongoing photoresist bake plate, which uses drop temperature ΔT parameter in addition to the direct relationship with the one with verified ΔT and CD. This model can be used to assist in the prediction of the standing range for new products or new process conditions.

Acknowledgements

碩士學程終於要接近完成的階段了, 首先我僅由衷的致上最誠摯的敬意, 感謝我的指導教授呂志鵬博士, 平日老師嚴格謹慎的要求, 與不斷的悉心指導與教誨使本文能夠導向正確的方向並順利完成, 在這過程中不僅使我在學術研究上得到寶貴的專業知識, 並使平常工作邏輯思考方向上皆獲得相當的助益。

接著我要感謝學校, 專班, 研究實驗室, 老師及學長助教及同學們, 大家營造了一個如此優良的學習環境。雖然利用下班時間晚上及假日上課代價很辛苦, 但是這最後一切成果都非常的值得。

再來要感謝我的旺宏電子的工作夥伴們, 及上級長官的鼓勵與支持, 使的黃光斜片二代系統能順利開發完成, 並成功的使用於線上, 這使我的論文獲得許多實務資料, 以及微影工程部一年多來協助幫忙完成此系統, 並提供許多實驗數據。

最後我要感謝我的家人, 一直以來默默的在背後幫我處理生活上的瑣事, 讓我回到家都能把今日一身的疲憊通通清除, 迎接明日更艱苦的挑戰, 如此得以專心的去處理學校與工作上的事務。

Contents

List of Tables

List of Figures

Chapter 1 Introduction

As semiconductor manufacturing technology advances, integrated circuit industry had used laser light source of shorter wavelength (193 nm) together with chemically amplified photoresist (CAPR) in order to improve resolution for enabling device scaling in accordance to Moore's Law. However, the energy of laser light source originated from deep ultraviolet (DUV) ray is much lower in the range around 10-30 mJ/cm^2, which is ~1/10 times of I-line light sources of traditional ultraviolet ray with mercury light source energy about 300-500 mJ/cm^2 as listed in Table 1.1 [1]. In order to compensate such low energy, scientists had implemented an additional post exposure bake (PEB) immediately after the exposure of DUV resist in which PAG generates proton upon radiation. Protons H^+ created by PAG upon exposure can subsequently catalyze polymer's acid labile protecting group (ALPG) and de-protecting chemical reaction during PEB step (~120-140 ℃) with other new by created proton H^+ again. The proton H^+ will continue and catalyze other ALPG de-protecting reaction. Through such chain reaction, the number of times of de-protecting reaction will expand by several hundred folds [2].

As a result, poor temperature control during PEB step and H^+ dissolution rate may have adverse effect on the resist patterning as illustrated by the examples of critical dimension (Table 1.2) and line edge roughness (LER)[3-4]. When the gate width/length is concerned, the variation of CD will influence the threshold voltage, V_{th}, leakage current, and I_{off} characteristics [5-7]. More over the dissolution rate and H^+ have been reported to affect LER significantly as illustrated in Figure 1.1 [8]. According to the International Technology Roadmap for Semiconductor (ITRS), there is a great demand of solutions and control for CD and line edge roughness (LER)

(Table 1.3) [9].

So far, the industry has addressed this problem by implementing a CD measurement step and reworking the lithography step for CD unlisted in the specifications. When DUV technology is introduced, numbers of measuring instruments and sampling frequency have been increased to send out-of-specifications wafers bake to rework and patterning step incurring increased equipment cost, production queue time. Recently, resist profile measurement based on scatterometry [10] has been adopted to provide accurate feedback and readjust the process parameters under exposure and PEB.

In this thesis, we will focus on the investigation of the hardware temperature control in PEB steps and its correlation between ΔT parameter and CD. The objective is to use a simple ΔT parameter to reduce rework rate and yield loss without incurring too much cost.

In order to examine the correlation between ΔT and CD variation, a high resolution SEM is used to examine CD with resolution of 1 Å which is capable of observing any CD variation induced by heat and the changing behavior of photoresist material CD. To be specific, we use three types of photoresist, *namely*, I-line photoresist, DUV 248 nm photoresist, and DUV 193 nm photoresist using two kinds of bakes, PB and PEB. Spacers of six different thicknesses (2.5 mm, 2.0 mm, 1.5 mm, 1.0 mm, 0.5 mm, and 0 mm) are used to place and hinder the wafer from placing higher than the plate.

According to the measurement result influences of CD variation are found when PB is greater than PEB. Because the insufficient harden PR, photo-acid generator (PAG) in room temperature will be constant during the period of diffusion and micro flow, and in the subsequence PEB heat energy driven PAG move more violet. H^+ micro flow of the exposure area is actually non-directional due to the result of un-hardening which has led to the mass out warding of proton diffusion of CD

making. When it is insufficient to bake with PEB, the opposite direction of influence will cause diminish in the CD.

In addition, a three-dimensional finite-element model using commercial software, ANSYS^{TM} was employed to examine the wafer surface temperature of various hardware and contact gap conditions. Such as particle contamination, wafer tilt, and ring type backside contamination. This model can be employed to simulate narrow gap case, when the spacer thickness smaller than 400 μm. In the real apparatus is too difficult to put on the plate and take out of plate, in such thin spacer is likely to be crocked and make the experiment data unstable. In addition, model is used to predict 100 μm particle at backside center of wafer surface temperature drop from 120 ℃ to 110.6 ℃ and via CD shift 11.5 nm. Also, it is use to simulate the case of a ring pattern pollution on wafer backside, because there is no good method to do a ring pattern coating at wafer backside for experiment. Modeling resume predict for 100 μm pollution on wafer backside at backside center of wafer surface temperature drop from 120 ℃ to 106.4 ℃ and the via CD shift 16.7 nm.

This thesis is organized into five chapters, which are briefly described below:

Chapter 1 introduction

Chapter 2 describes the literature review of key photoresist technologies and the motivations of this study.

Chapter 3 illustrates the theorems of interferometry and finite element analysis, and describes the procedures of sample preparation.

Chapter 4 covers experimental, results and discussion.

Chapter 5 summarizes key findings and contributions of this thesis.

Table 1.1 Selected excimer laser for lithography [11-13].

Company	Product	Type	Wavelength (nm)	Bandwidth FWHM (pm)	Repetition rate (Hz)	Power (watts)	Pulse energy (mJ)	Energy dose stability/ # of pulses
Cymer	EX-5000	KrF	248	<100	1,000	15	15	≤±0.8%/50
	ELS-5000	KrF	248	<0.8	1,000	10	10	≤±0.8%/50
	ELS-5010	KrF	248	0.6	1,000	10	10	±0.6%/40
	ELS-6000	KrF	248	≤0.6	2,000	20	10	≤±0.5%/32
	ELS-6010	KrF	248	≤0.5	2,500	20	8	≤±0.35%
		ArF	193	0.5	2,000	10	5	±0.4%/40
		ArF	193	0.5	4,000	20	5	±0.2%/80
	ELX-6500F_2	F_2	157	0.3			5	
Komatsu	KLES-G10K	KrF	248	<0.5	1,000	10	10	±0.5%/40
Lambda Physic	K1010	KrF	248	<0.6	1,000	10	10	±0.5%/50
	K2010	KrF	248	<0.6	2,000	20	10	±0.5%/50
	K2020	KrF	248	25	2,000	30	15	±0.5%/50
	A2010	ArF	193	<0.6	2,000	10	5	±0.8%/50
	A2020	ArF	193	25	2,000	20	10	±0.5%/50
	F620	F_2	157	<1.5	600	6	10	±1%/50
	F630	F_2	157	<1.5	600	6	10	±1%/50
	F1020	F_2	157	<1.5	1,000	10	10	±0.5%/5
	F1030	F_2	157	not narrowed	1,000	10	10	±0.5%/50

Table 1.2 Effect of PEB bake temperature on CDs [14-15]

PR	Type of PR	Supplier	Sensitivity (nm/℃)
APEXE	248 nm DUV	Shipley	16.0
UV2HS	157 nm DUV	Shipley	7.5
Version 1B	193 nm DUV	IBM	3.8
UV6	248 nm DUV	Shipley	2.6
TM-461	248 nm DUV	JSR	2.6
DP-024	248 nm DUV	TOK	1.8
ARCH 2	248 nm DUV	Arch	0
R2J	248 nm DUV	JSR	0

Table 1.3 Critical dimension memory technology based on ITRS 2007

Year of production	2008	2009	2010	2011	2012	2013	2014	2015	2016
DRAM pitch (nm)	57	50	45	40	36	32	28	25	23
Flash pitch (nm)	45	40	36	32	28	25	23	20	18
DRAM/Flash CD control (3 sigma nm)	4.7	4.2	3.7	3.3	2.9	2.6	2.3	2.1	1.9
Gate CD control (3 sigma nm)	2.3	2.1	1.9	1.7	1.5	1.3	1.2	1	0.9
Absorber LER (3 sigma nm)	3.2	2.8	2.5	2.2	2	1.8	1.6	1.4	1.3

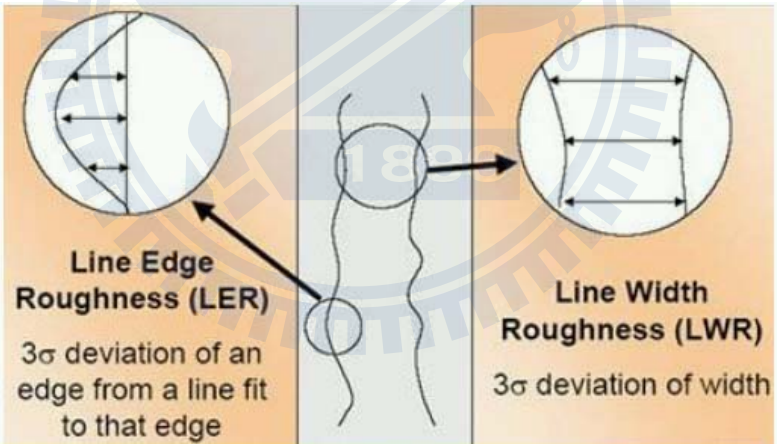

Figure 1.1 Schematic diagrams and, definitions of line edge roughness (LER) and line width roughness (LWR)

Chapter 2 Literature review

2.1 Characteristics of photoresist material:

Photoresist needs to endure wet/dry etching, in order to enable pattern etching. Several characteristics must be added to the photosensitivity, such as acid resistance in the process and resistance to with stand plasma etch and high dose ion implantation process. When photoresist is used for IC fabrication, the coatings must be able to form a thin uniform film and a lessee pin hold; with good adhesion onto the underlying substrate. In addition, while sensitive to the exposure wavelength of radiation utilized, the photoresist should be capable of printing the minimum feature size. Furthermore, significant difference in the development rate between the exposure and unexposed areas without pattern distortion must be demonstrated and removable for the process to follow with endurance to the bake process in absence of pattern distortion. In addition, photoresist material cannot be used if there is unacceptable health hazard [16].

2.1.1 Photoresist bake

The photoresist high polymer is dispersed in the solvent with molecule state packed inside the bottle. Storage in the refrigerator with temperature 6~8℃ will force the solvent to remain in a saturated condition. Equalization of the evaporation and condensation rate is to ensure a steady solvent concentration. Polymer molecule at this stage is mutually unable to get close and difficult to reciprocate, let alone buffered by the surrounding solvent molecule. The usage of solvent will enable the polymer and the sensitization of uniform distribution to liquid through hydrogen bond. The usage of the spin-on method will enable photoresist dispense to create a coating on the wafer with follow-up bake process; solvent will be removed smoothly by

evaporation. Thickness and uniformity are controlled by the spin speed. Photoresist wafer coating is currently used in lithography photoresist types such as G-Line (436 nm), I-Line (365 nm), and DUV (248/193 nm) [17].

Course of hardening during photoresist bake:

(1) A hot plate is being heated to take out of the solvent vapor constantly in order to help solvent steam molecule leave the chamber of the bake unit.

(2) The solvent molecular motion between the two-phase gaseous and liquid form is found on wafer surface with its motion energy offered by the heat energy. Near surface liquid member will leave the interface to enter into the gaseous phase. Capable of increasing polymer molecular weight, these two factors will enable polymer molecule to go near each other before falling into the same solvent cage. The chemical bond of these two single monomers is then combined to make solidified polymers.

(3) A large amount is combined into a macromolecule.

(4) Massive polymer will begin to solidify on the substrate, as shown in Figure 2.1.

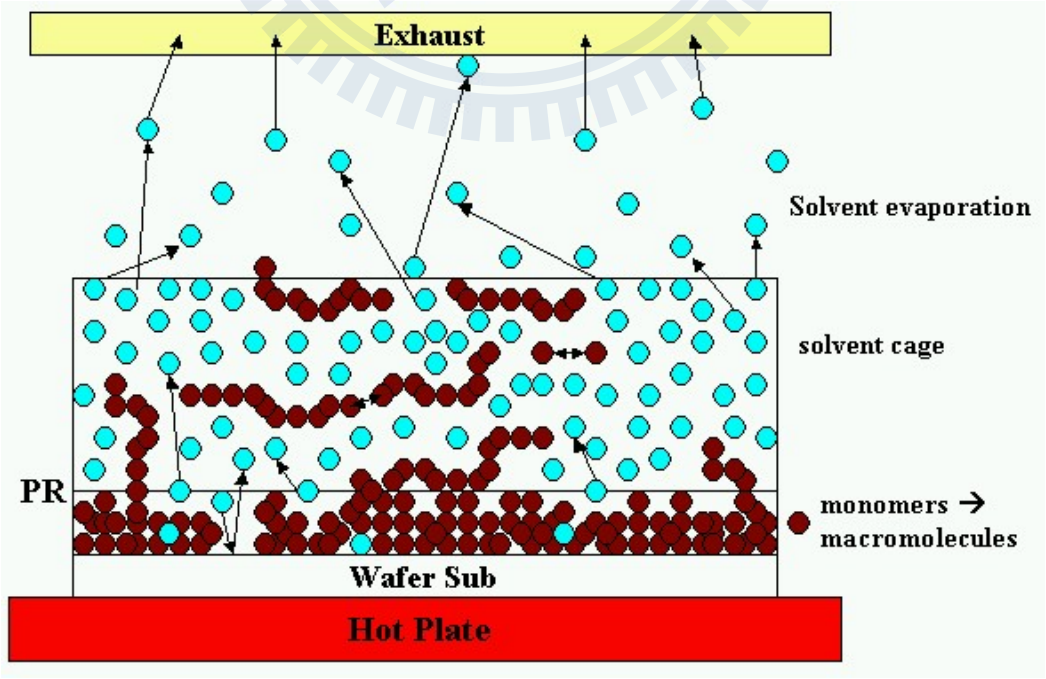

Figure 2.1 During photoresist the course of hardening

As shown in Figure 2.2, the structure of the photoresist is composed of oxygen, carbon, hydrogen atom in the polymer, and solvent. The strong covalent bond of H-O polarization is due to the size of the oxygen atom, which is bigger and capable in attracting electrons with strength. The making of the oxygen with higher electronic density had succeeded with little negative electricity. With small fraction of weaker attraction to the electron at the core, hydrogen is thus slightly positively charged, indicating the uneven attraction of the electron covalent bond between the two atoms. In carbon and hydrogen, electron in the covalent bond are generally under normal state with two extremely equalized core with most C-H and C-C not polarized (similar to H_2 and F_2). The main break-up point is between C-O and O-H, bond but not C-C bond [18]. Hydrocarbon position of the C-H molecule with the occurrence of changes in the function base and joined carbons have little or no influence. The juncture of structure δ^+, δ^- is at a point of broken bond position or at the site where new bond position is produced by the bond [19].

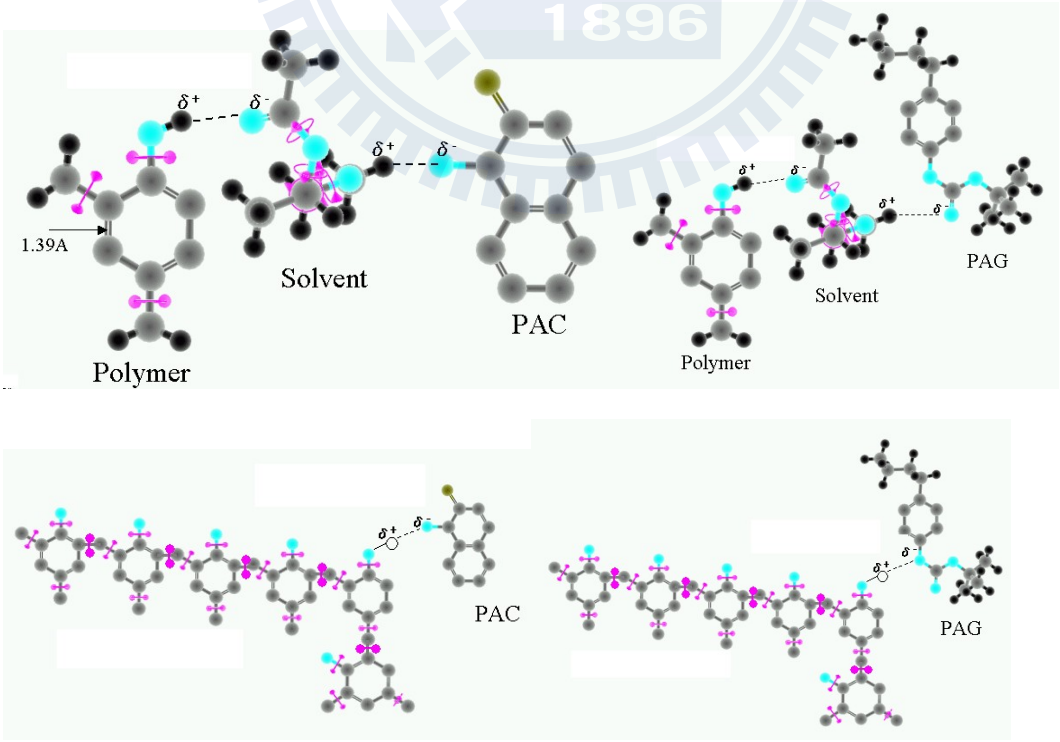

Figure 2.2 Hydrogen bond of liquid photoresist

2.2 Brief introduction on photoresist

An actual photoresist is generally composed of three major components: polymer (20%), photoactive compound (PAC DAQ/PAG 5%), and solvent (75%) [20]. Polymer is the backbone of the photoresist and major constituent of the patterned photoresist film. PAC is the constituent of the photoresist that will undergo a reaction when exposed to light and may be combined with the polymer. The solvent will keep the photoresist in liquid form until after coating with photoresist classified as either negative or positive photoresist.

Common organic function group in photoresist are mainly composed of 4 groups: hydroxyl (-OH), carbonyl (-C=O), carboxyl (-COOH) and amido base (R-C=O) with common light source UV/DUV/X-ray, electron beam, ion beam, etc. There are two kinds of traditional organic straight-type photoresist principle:

(1) Low polarity to high polarity: normally under low polarity, PAC will possess high polarity after exposure. Weak and acidic, the high polarity PAC may be dissolved in high polarity alkaline developer liquid; and

(2) Molecular weight will fall sharply when the main chain of the macromolecule breaks after exposure. In addition, such molecule can be dissolved in organic developer liquid.

2.3 I-Line photoresist

Mainly composed of hydrogen compound bond, the traditional I-line DNQ positive photoresist and photoactive compound (PAC) diazonaphthoquinonc (DAQ)~15% can, utilize nitrogen atom near the base to produce an unstable phenomenon in the detachment of N_2 after contact with light, which will then turn into ethylene ketone (solid) after rearrangement. With the vapor reaction in the air, acid base (liquid) will be produced and can be neutralized in alkaline NaOH developer. Failure in exposure

is caused by the interference of failure to dissolve the material as shown in Figure 2.3.

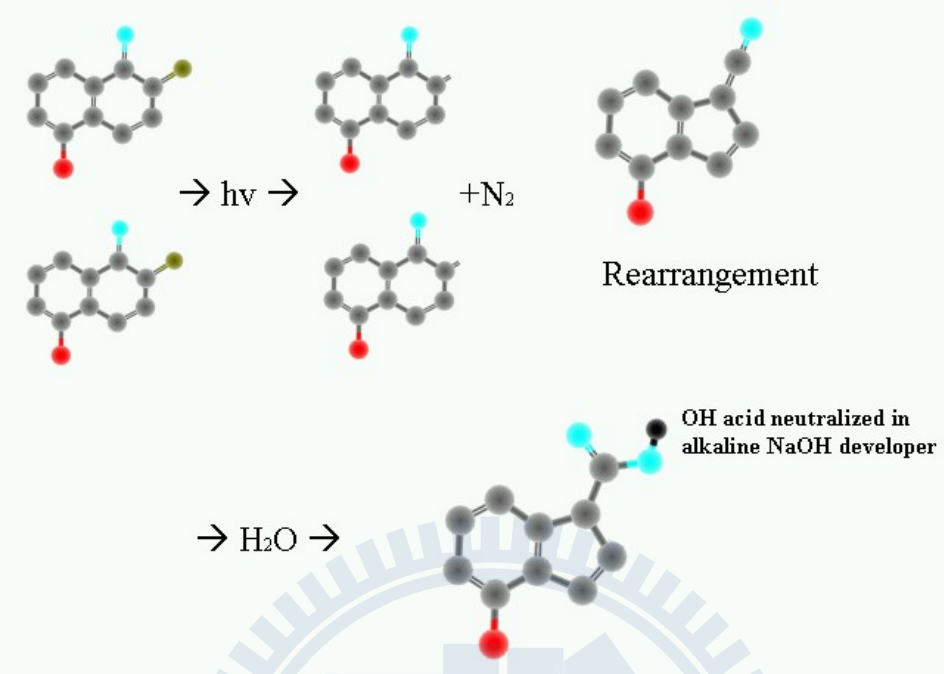

Figure 2.3 Exposure and developing of PAC and I-line DNQ photoresist [21]

2.3.1 DAQ/Novolak system

The DAQ (Di-Azonaphtho-Quinone) or Di-azo-Naphtho-Quinone (DNQ)/Novolak system is a positive photoresist system most frequently used by the I-line 365 nm at the present. DAQ is a photoactive compound whilst Novolak resin is composed of the combination of cresol and formaldehyde, which is also a substance of photoresist matrix. Oskar Suss, a chemist at the German Kalle Company in 1940, has used DQN to duplicate the project blueprint at first. It was not until 1970, DQN was produced by Bell Lab in USA for semiconductor fabrication. The combination of DAQ Diazo, $=N_2$ activity base photoactive group (PAG) and ballasting group (BG) will undergo a photolytic decomposition to an unstable keto-carbene and nitrogen when it is exposed to leading to light naphthoquinone diazide sulfonylchloride as shown in Figure 2.4 [22].

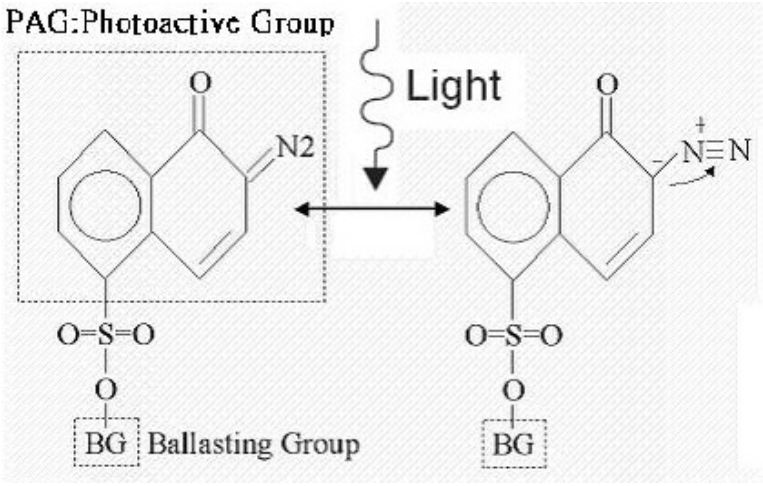

Figure 2.4 PG of DAQ leads to the naphthoquinone diazide sulfonylchloride reaction upon light exposure

Synthetic reaction of chemistry of DAQ:

$PAG\text{-}SO_2Cl+HO\text{-}BG \rightarrow PAG\text{-}SO_2\text{-}O\text{-}BG+HCl\uparrow$

$PAG\text{-}SO_2\text{-}O\text{-}BG = DAQ$

The DAQ after keto-carbene will immediately rearrange to a more stable ketene structure as shown in Figure 2.5. Highly hydroscopic, ketene structure can immediately react with water to form carboxylic acid. The indene carboxlic acid (ICA) is soluble in basic developers as shown in Figure 2.6. ICA can also dissolve in promoters such as TMAH developer liquid which is highly alkalinic in its polarity, whilst inhibitors can be dissolved by low polarity DAQ instead of unexposed acids.

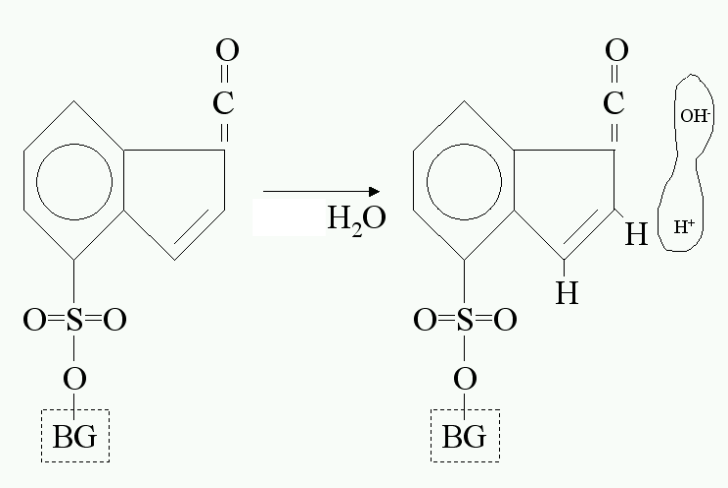

Figure 2.5 Hydroscopic ketene immediate reaction with water [23]

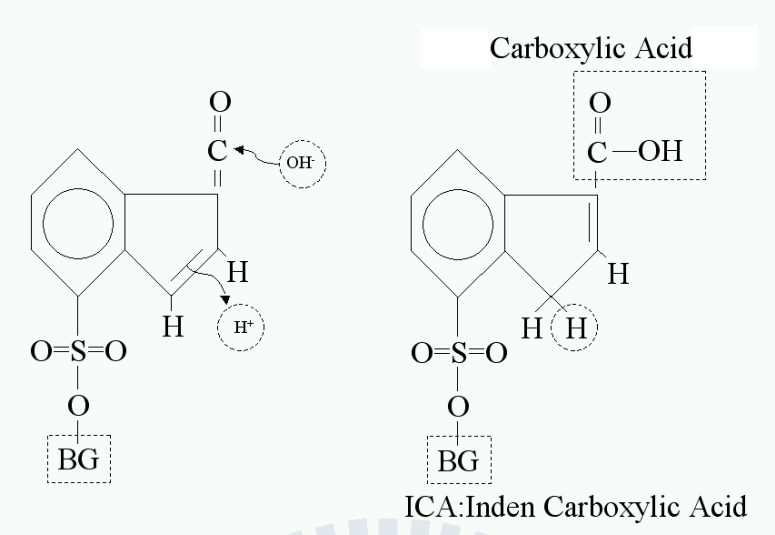

Figure 2.6 Acid compound ICA of high polarity [24]

The main function of DAQ BG is to adjust photoresist to a most suitable exposure wavelength with solubility resiststance to the etching. The single BG will join PAG with six kinds of selection as shown in Figure 2.7. However, if there are too many PGs, the promotion of the photoresist property will be inhibited due to PG dissolution. Novolak is normally 30:100 wt% in DAQ with relatively far PAG distance in DAQ. In addition, PAG dispersion and photoresist light sensitivity are relatively good with weak hydrophobic nature.

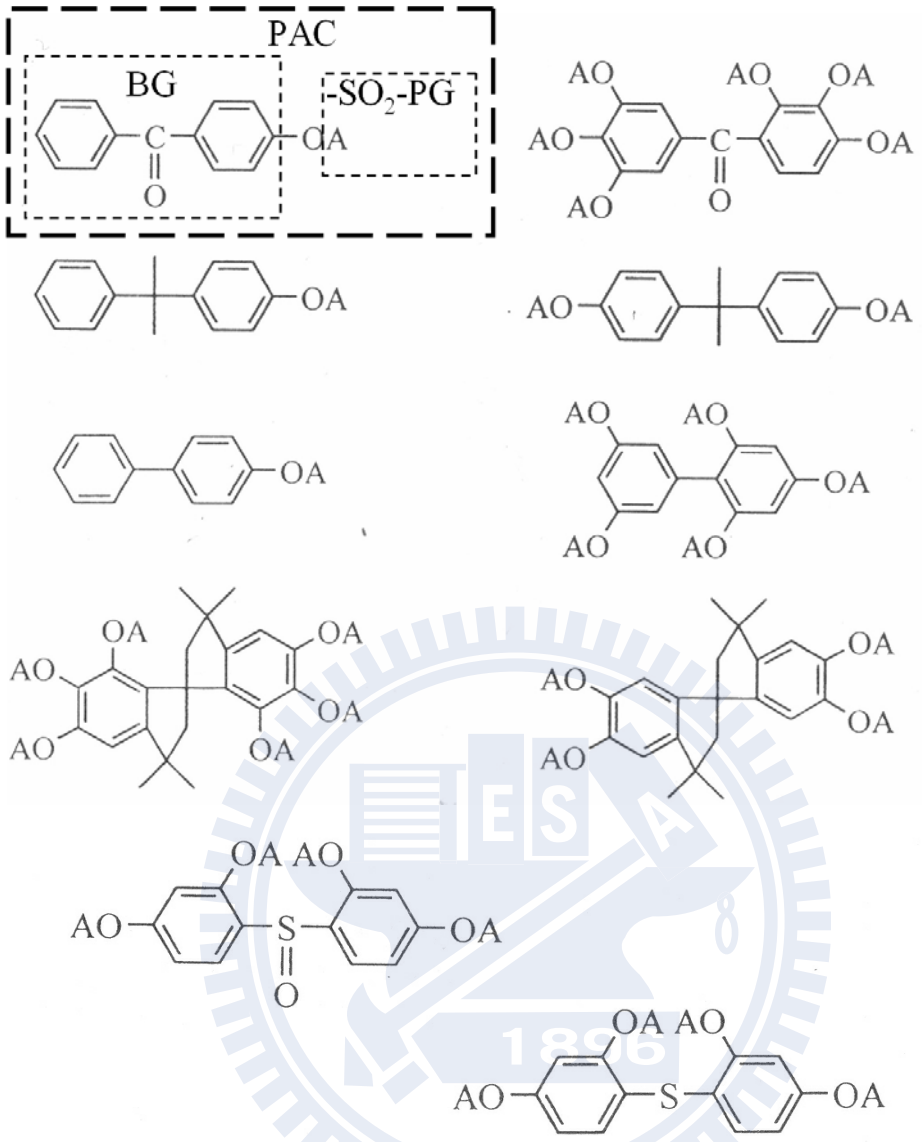

Figure 2.7 PAC compound and six kinds of BGs

DNQ will induce an overall drop in absorption due to post I-line exposure. With higher transparent rate, the light is allowed to pass through photoresist film by a function called “photobleaching”. On the other hand, Novolak shows no obvious overall change in its absorption under the exposure wavelength of the post-exposure I-line.

For 1 μm thickness of DNQ/Novolak after I-line exposure (100 mJ/cm^2), the absorption has dropped to 0.2~0.1 for NNQ as compared to 0.4~0.3 for Novolak as shown in Figure 2.8.

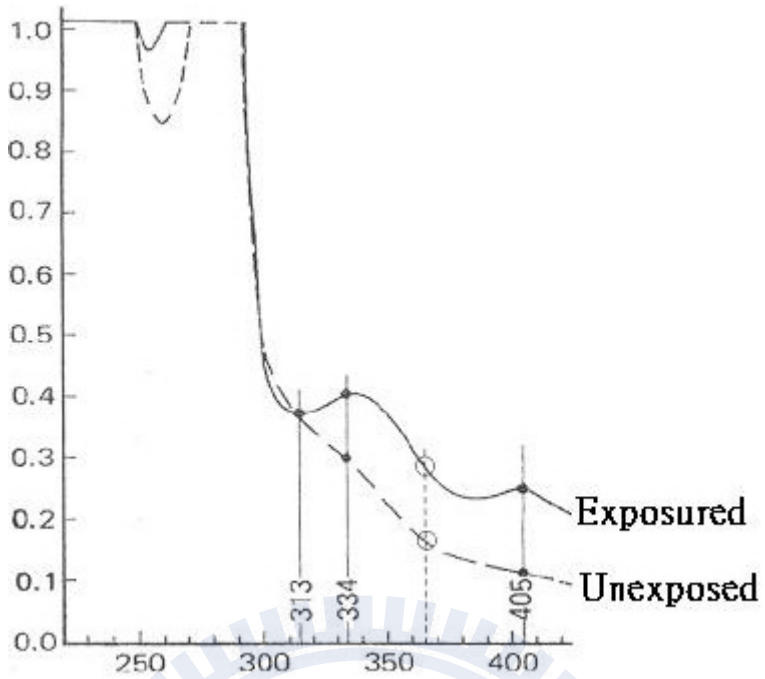

Figure 2.8 The absorption of DAQ/Novolak positive photoresist 1 μm thickness

A single nitrogen molecule or nitrogen atom and carbon have a nitrogen base (R-N) bond called single-nitrogen base (Azo). Two azo will form a heavy nitrogen base (Diazo) such as (R =N_2) and three azo will form a pile of nitrogen bases (Azide) such as (R-N_3). Two Azide will form one pair of nitrogen base (Bisazide) such as (N_3-R-N_3) with ammonia (NH_3) in its gaseous state and amine (R-NH_2) as organic matter. Ammonium (NH_4OH) is an alkaline inorganic matter with, properties in the likeness of sodium potassium which is also a source for metal ammonium pollution as shown in Figure 2.9.

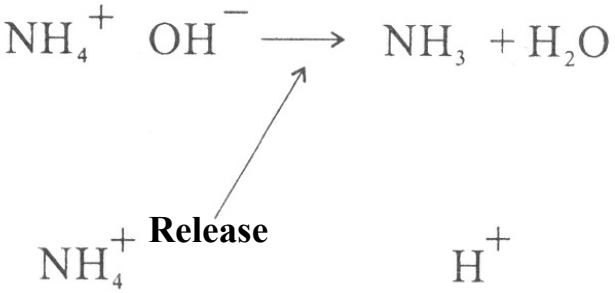

Figure 2.9 Metal pollution sources ammonium (NH_4OH)

2.3.2 Novolak

The matrix substance of the photoresist film is not macromolecule photoactive compound DAQ because it does not dissolve in the alkaline developer but dissolve inhibitors in liquid TMAH. Yet the matrix substance of the photoresist film is the macromolecule with a lot of OH bases and the weak and acidic Novolak. It can dissolve in alkaline developer liquid TMAH but will not dissolve in DAQ/Novolak equivalent or extremely low TMAH solutions. Regarded as a membrane matrix substance, Novolak's multi–functional purpose can also participate in nitrogen azo coupling, self crosslink and ester cross link photochemical reaction. Single while getting together for Novolak by cresol, the main chain of the electronic resonance structure of the phenol base must connect with the oxyhydrogen base (-OH base) in its ortho-position or counterpoint as shown in Figure 2.10. Thus, it is possible to combine the activity together with ease. The average molecular weight is relatively heavy with distribution around 3000-5000, which is good to resist etching.

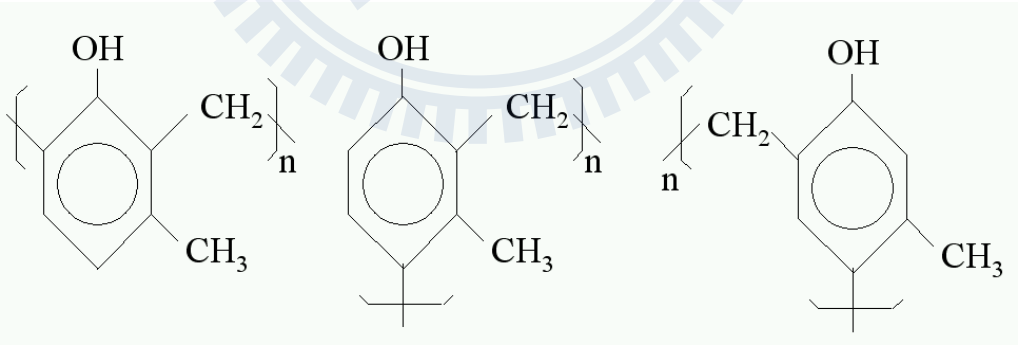

Figure 2.10 Three kinds possible cresol structures

Because o-cresol or p-cresol has already occupied an ortho-position or counterpoint, there is only one kind of possible structure to get together but with low possibility. Numbers for getting together for activity are: m-cresol 11.1, p-cresol 1.35, and m-cresol 1.0, as shown in Figure 2.11

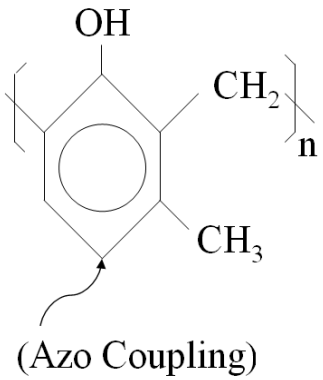

Figure 2.11 Best structure of Novolak

2.3.3 Dissolution rate in exposed and unexposed areas

Basic principle of low polar DAQ under exposure can produce acid compound ICA of high polarity. Under exceptional circumstances, the matching of DAQ and Novolak capable of increasing extra difference in dissolution as shown in Figure.2.12 with the following 4 reasons:

(1) Novolak counterpoint vacancy (Para_Vacancy) couple to nitrogen. Alkaline developer liquid can catalyze the dark area of photoactive base PG and Novolak of DAQ couple (Azo Coupling) nitrogen chemical reaction with increase in molecular weight. To develop TMAH within the little member of the liquid is more difficult than to spread in the Novolak, which can cause the increase in the dark area and inability to dissolve. Two azo coupling may happen if single mother base BG in DAQ contain more than two PG, with DAQ as the Novolak bridge formation pharmaceutical by doubling the molecular weight double to lower the solubility of the dark area as shown in Figure 2.13.

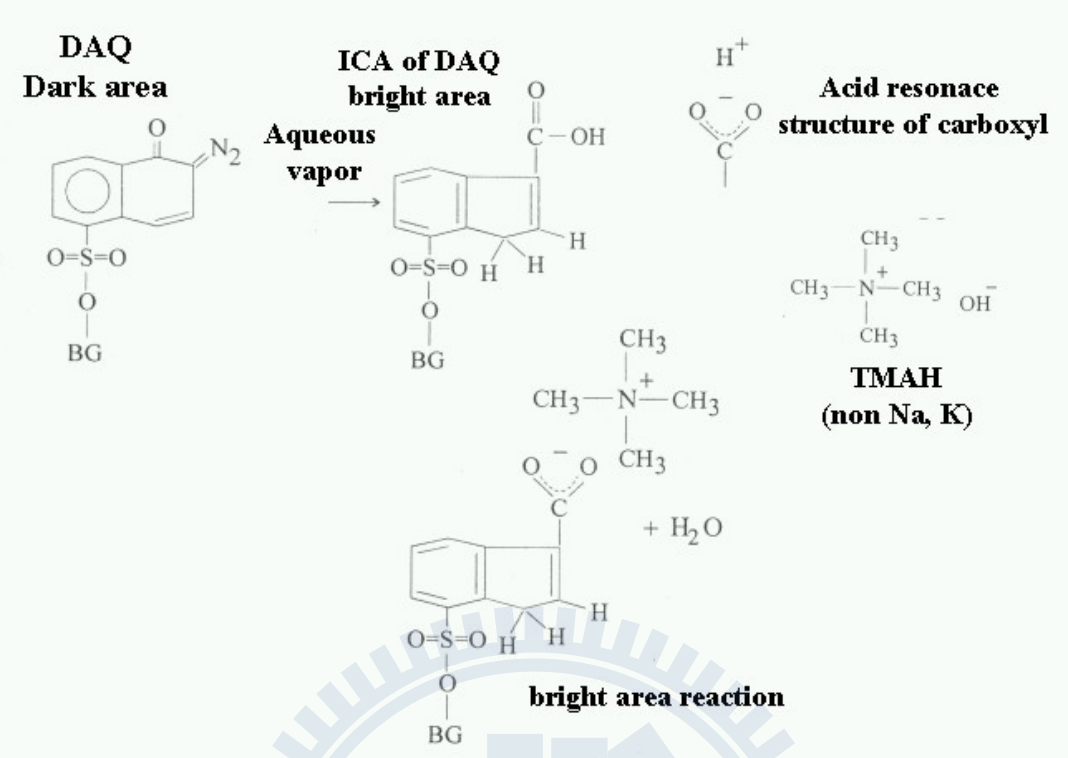

Figure 2.12 Bright area ICA of DAQ and TMAH reaction [25]

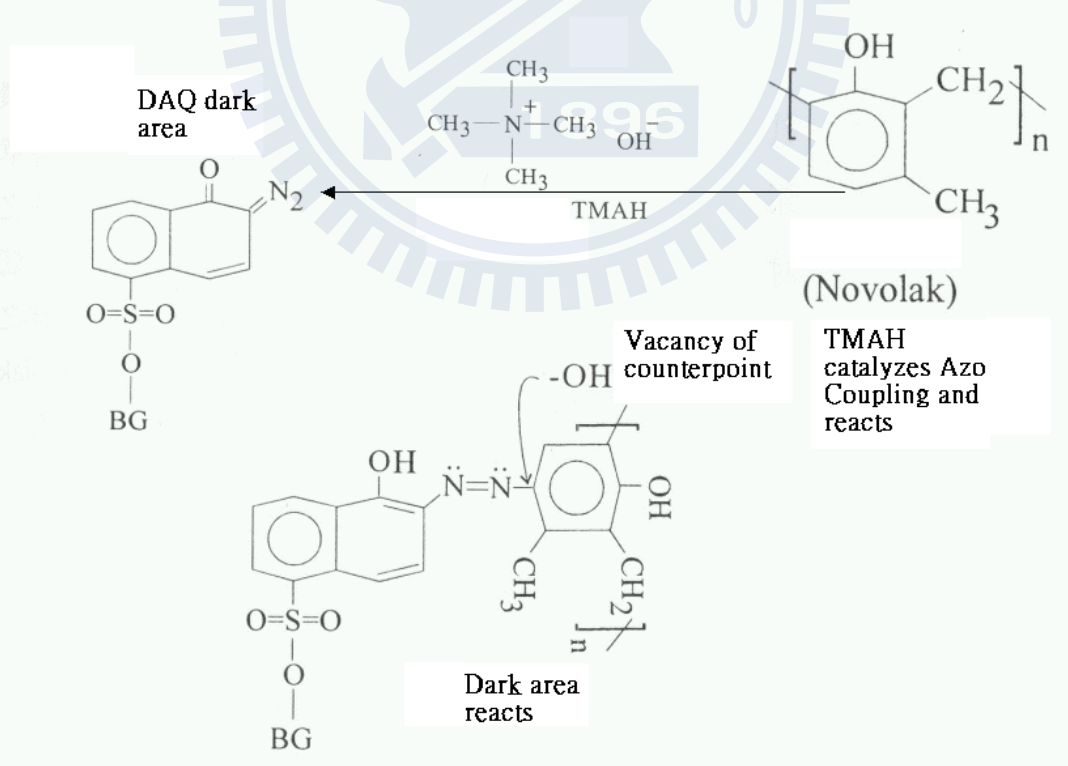

Figure 2.13 Dark area DAQ Azo Coupling [26]

Because the electronic resonance structure of the phenol base may produce negative charge in the -OH base in its ortho-position or counterpoint, PG thus possess heavy nitrogen (Diazo), which is positively charged in the DAQ resonance structure. It is easy to carry on with the electrophilic reaction (ER) in this negative charged seat seen in the examples of nitrogen coincidence function. The probability of vacancy in coincidence function is higher than the ortho-position because the space is less crowded with a relatively small stereoscopic obstacle as shown in Figure 2.14.

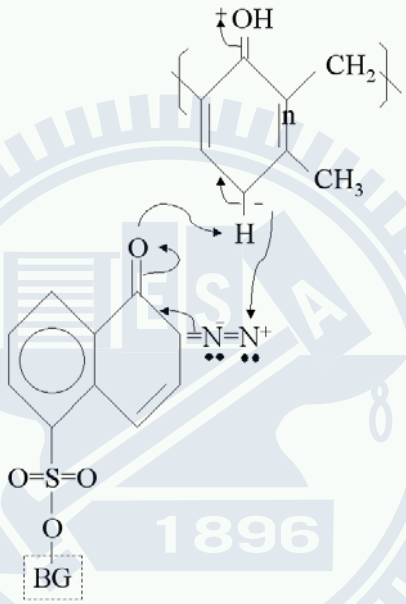

Figure 2.14 Electronphilic reaction (ER) of diazo [27]

(2) Stonewall:

The lower molecular weight of the unexposed areas of Novolak and new compound after coupling with DNQ; the surrounding non-coupling Novolak with higher molecular weight than Novolak like stonewall is easy to twine but will hinder coupling and reduce the solubility of the unexposed area. For a multifunctional DNQ, the azocoupling reaction could lead to crosslinking of Novolak chains, which increases the molecular weight and therefore decreases the dissolution rate.

(3) Host-Guest Complex:

Contributed eight OH base by a long bond of about 3-4 Novolaks, OH base has

enclosed itself into an inward ring. The intra-annular can hold just one DAQ molecule with Novolak as form host and DAQ complex as guest. This complex is composed of hydrogen bond. According to Van Der Waals Force, an intra-annular DAQ molecule will attract eight OH base, making the TMAH unable to enter the ring with its dense structure.

(4) Octopus-Pot:

Six Novolak has six long bonds, each offer three benzene ring, three OH base, 18 benzene ring and 18 OH base enclosed to form a pot with one DAQ attracted to the middle of the pot by hydrogen bond gravitation. One BG is on the top with several active base BGs at the bottom. PG include OH base of nitrogen oxygen and Novolak which will form a new hydrogen bond. This structure will reduce the solubility of the unexposed area [28].

2.4 Chemically amplified photoresist (CAPR)

Chemical amplifier positive photoresist has two kinds of prescriptions:

(1) Photoacid Generator, PAG:

PAG works through ultraviolet ray with electron beam focused on the ion and x-ray post exposure. It can initiate all chemical reaction and produce proton acid including proton H^+ (Bronsted acid) or “photo-acid”.

(2) Acid Labile Protecting Group, ALPG:

Proton in ALPG is a high polymer proton acid with H^+ as acidity cation, a necessary heat energy that the bake can offer in the activation of reaction protection removal after exposure. Catalyze polymer prop up chain ALPG protection removed reaction will produce $-COO^- H^+$ or acid base of $-O^- H^+$ with polymer polarity from low to high. When the polarity is changed significantly, it will become an acid and make the exposure area capable of dissolving in alkaline developer liquid.

2.4.1 PAG photoresist exposure and development

It can initiate a chemical reaction that generates an optic reacting photon such as cross link or chain rupture, etc. The 100 pieces of photon can initiate 30 pieces of chemical reaction to produce a 0.3 quantum yield for the making of 100 pieces of proton acid (H*) by PAG. As shown in Figure 2.15, the reaction of the protected polymer PBOCST with an acid (H^+), after PEB is heated, it will produce an unprotected polymer PHOST + CO_2 and an additional acid. Generation of H^+ during the de-protection reaction will allow a single photo event to catalyze the de-protection of multiple PBOCST molecules. This proton acid is a catalyst, a type of chemistry like the de-protecting reaction, which can produce another proton acid when the response finishes. This reaction can terminate due to oxygen, pollution, etc, when the proton acid is consumed. A photon can initiate the de-protection reaction by 800 times. Several hundred folds through chemistry can enlarge the number of de-protecting reaction. This type will hinder the pharmaceutical and is generally called chemically amplified photoresist (CAPR). Following the exposure, a PEB is required to aide in the diffusion of the photon to drive catalytic reaction. A problem will occur with CAPR when the photoresist is exposed to amines between exposure and PEB steps. Amines can neutralize the acids in the surface of the photoresist and lead to overhangs or T tops on the photoresist lines. Improvements in photoresist formulations and filtrations to remove amines to <1ppb are effective in eliminating T-toppings .

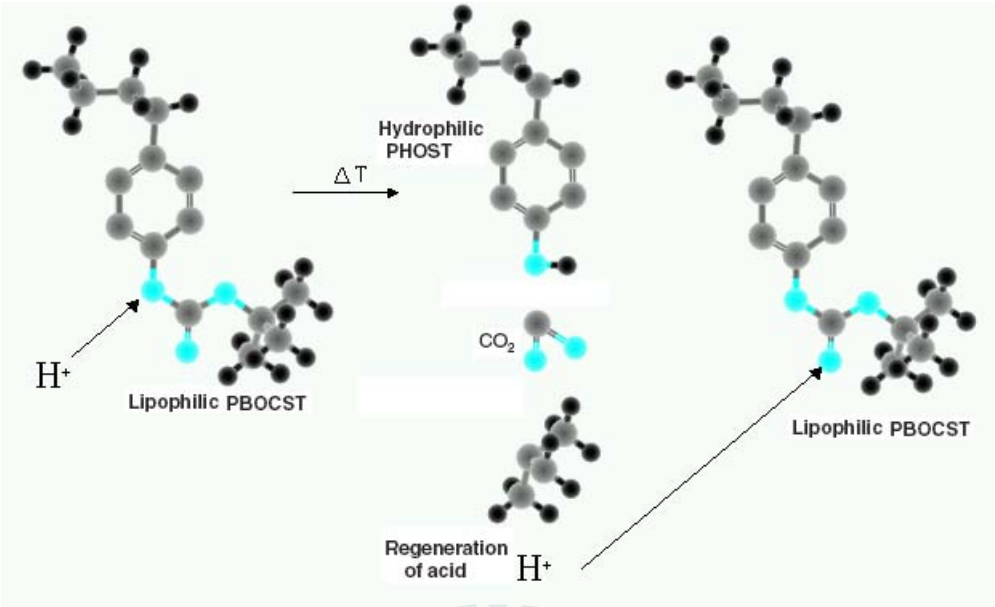

Figure 2.15 The tBOC photoresist deprotection mechanism

A proton with high polar phenol base or benzene oxygen base of acid course that produces constantly is weak and acidic. This can be dissolved in the alkaline developer liquid, volatile compound CO_2, $CCh_3Ch_3Ch_2$, and H^+ de-protected again.

Composition and functions of ALPG:

(1) Acid quencher: Usually alkaline ammonium salt or amine, its purpose is to buffer H^+ protons in the exposed/unexposed interface area without diffusion characteristics, reduce the rate of diffusion and the quantity of the proton. This controls the wide change of line after development. The shortcoming is that exposure dosage needs to be increased to produce enough proton H^+.

(2) Dissolution inhibitor: Unexposed and has not reacted to inhibit dissolvent. The purpose is to improve the exposed/unexposed ratio of development.

(3) Little member alkaline: Inhibits the pollution of the alkaline.

(4) Antioxidant: Prevents the oxidation of each composition.

(5) Stable pharmaceutical: Prevent all acids from producing PAG for decomposition.

(6) Active pharmaceutical of interface: Prevents the agglutination and precipitation of every composition.

(7) Free radical scavenger and little member exposure; volatile and will continue to react.

(8) Solvent: Dissolves every composition in the prescription and is also used for spin coating.

(9) Thickening agent: Thickening the coating of the photoresist film for use.

2.4.2 There are two common classes of photoacid generator (PAG):

(1) Ion type PAG such as iodonium and sulfoniums compound is referred to as onium salt. The proton acid H^+ source will be produced after exposure took PAG. There are two methods that can create H^+. The first is that the solvent or macromolecule needs to be able to support the protons. And the second is the H^+ from PAG, donors does not need to support the protons.

(2) Non-ion type PAG:

(a) Non-polarity covalent bond: Electric charge is distributed when equilibrium between two atoms of exposed bond breaks and need to support the protons. This type of PAG is more sensitive to mere light than the ion types, such as MeSB, NTPI.

(b) Polarity covalent bond: Exposure that causes breaking in bonds or rearrangement of two atoms that distributes electric charges uneven to polarity. It does not need to support the protons.

Labile polymer acid labile protection and de-protecting reaction will take place in polymers found in acid ALPG in its contact with unstable acid in the decomposition of its de-protection, and DUV wavelength, which has no effect. Controlled by the acid consistency of protons and the main intensity temperature time of PEB, reaction in the activation of de-protection will initiate as shown in Figure 2.16.

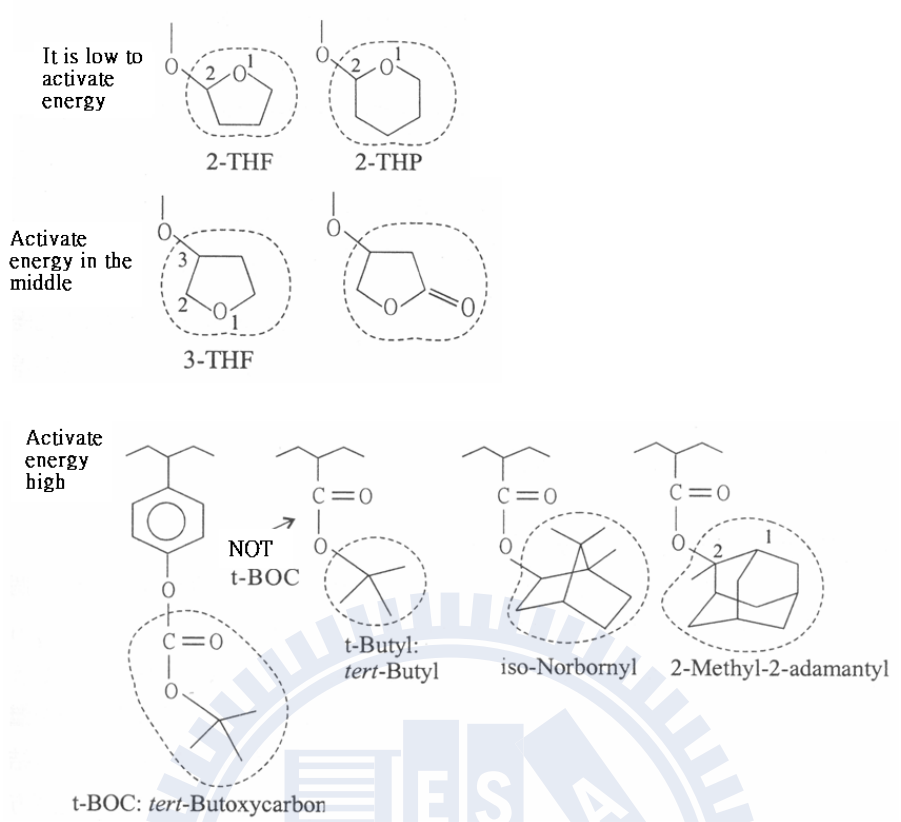

Figure 2.16 Activation energy of ALPG

The de-protecting reaction usually produces two kinds of acid bases:

(1) -COO-ALPG → $-COO^-H^+$. Carboxylic acid in which the polarity is high.

(2) -O-ALPG → $-O^-H^+$. Phenolic acid in which the polarity is relatively low.

The molecular weight of the polymer is distributed in a narrow range where more identical polymer photoresist is made up, and the contrast ratio gamma (γ) is relatively high therefore bonding of the polymer resolution is good. Purification of separation is very tedious and difficult. It will produce -OH after de-protecting the t-BOC and oxygen bond atoms. It also produces -COOH after the de-protection of t-Butyl. These two ALPGs are structurally similar, but results are extremely different. The protons have not been lost, therefore it can continue to catalyze de-protecting ALPG repeatedly until encountering oxygen or other pollutants, etc. In which the proton acid will enable termination. The traditional photoresist dosage =energy*time about 100 mJ/cm^2, CAPR dosage 5-30 mJ/cm^2.

2.4.3 The Development of CA positive PR

After CA positive photoresist de-protection finishes, it usually produces a high polarity and an acid of -COO^-H^+ or - O^-H^+. It is the same for the developer which also uses TMAH of ~0.26N as DAQ/Novolak.

2.5 KrF 248 nm CAPR

(1). A single polymer, also known as homo-polymer, is not a copolymer. Regarding tert-butoxycarbonyl (t-BOC) as ALPG, its function is for the protection base to serve as phenol base –OH. After exposure, PAG will produce a proton acid H^+, and after appropriate PEB bake, the proton acid H^+ in being catalyzed in ALPG de-protecting reaction and the phenol based -OH which produces high polarity will both also release simultaneously. This new H^+, which is adjacent to another ALPG reaction, releases another new H^+ and so the cycle goes on until the activity is stopped, but the main chain is not broken. After a large number of phenol base -OH is produced, the polymer polarity will change from low to high, present acidity, so it can be dissolved in the alkaline developer. This photoresist advantage contains phenyl which is strong in resisting etching. Its shortcoming is that no existing single polymer structure has a better -COOH carboxyl's acid base which is unable to offset various types of alkaline pollutant to neutralize proton acid destruction commonly seen in T– top. After the phenol base is produced by the de-protection, the de-protection polarity will not change much due to low acid and polarity, which in result will influence its development. Methods of improvement are needed in order to filter the air of the environment area with increased cost.

(2) Two single copolymer, tert-butyl (t-Butyl) and 2-Tetra-hydro-pyranyl (2-THP) which are ALPG exposed, baked, de-protected produce a low to high polarity -COOH will strengthen the acid, making the photoresist system capable in its dissolution in

the alkaline developer liquid. The main function of the prop up saturation heterocycle base originally found within the chain is to strengthen and resist etching. Alkaline pollutant, which neutralizes the external environment originally contained in the -COOH base, will not participate in the chemical reaction of photoresist which is environmentally stable (ESCAPR) [29].

(3) Ter-polymer: The formation of the metharylic acid (MAA) will act as a macromolecule backbone of the acryl acid. First an etch-resisting single saturation heterocycle will be included. The second will contain -COOH acid base to neutralize the alkaline pollutant. The third will include a single prop up chain containing tert-Butyl or 2-THP. NTNI regarded, as PAG exposed under low to high polarity will be the same as two monomers. The first two single will not to participate in the photochemistry or de-protecting reaction. The advantage of three single copolymers is that each monomer each has a characteristic function with good photoresist properties. The shortcoming is the difficulty in monomer separation, purification with complications in reaching the designated 1:1:1 proportion normally expressed under x: y: z.

2.6 ArF 193 nm CAPR

ArF positive photoresist has an extremely strong absorption in the 248 nm light wavelength due to its benzene ring. Acrylate based platforms with attached alicyclic structures in which acrylic provides a high resolution but relatively poor etch resistance. The semiconductor incorporation of the cycloaliphatic will side group in the polymer backbone to reduce etch rate. Cyclic olefins will provide an intrinsically good etch resistance, generally used to replace benzene ring in which the two will not bond in saturation in the heterocycle. The main difference between 248 nm photoresist and 193 nm photoresist is that PAG is usually <5wt% with pre-reaction

solvent C_6H_6 → C_6H_5+H to hold the ring to react with C_6H_6 → CH_3+C_5H_3 or C_2H_3+C_4H_3 and ionize and react with C_6H_6 → C_4H_4+C_2H_2+e or C_2H_4+C_4H_2+e etc. Normally a lithography wavelength intensity of absorbance <2.5 will be required by each micrometer thickness. If the degree is too high, the top layer photoresist dosage will also be too high; if the matrix floor photoresist is insufficient, the dosage will not be uniformed. Most photons will undergo no photochemical reaction through photoresist if the absorption is too low to produce little consistency of proton acid.

$$A=\varepsilon bc \tag{2.1}$$

Where A: Non-dimensional absorption degree,

ε: Absorption coefficient, absorbance or absorption coefficient, (dimensional mole^{-1}, L. CM^{-1}),

b: Direct light length (cm),

c: Consistency mole (L^{-1}).

ArF photoresist will regard norbornane as a macromolecule skeleton which is a two single copolymer called polynorbornene. The advantage of this skeleton is its automation and etch-resistance properties to fulfill all-around demands. After the low to high polarity de-protecting reaction, norbornene will no longer have pair bonds and will be known as a macromolecule called polynorbornene [30].

2.7 F_2 157 nm CAPR

The 248 nm photoresist often uses -C_6H_5OH phenolic group due to its possession of benzene ring. An acidity phenol, the benzene ring or “phenyl”, is very stable in its resistance to etching due to its double bond and 6π electronic resonance. Due to its strong absorption to benzene ring, the 193 nm photoresist will not use saturation heterocycle base with just one pair bond such as norbornane. The acid base which often use -COOH carboxylic acid and C=O carbonyl with double bond will not be

strong enough to absorb the 193 nm wavelength. Generally speaking, the 157 nm photoresist will include one pair of function bases of bond π electron with strong absorption of π-π^* in 157 nm wavelength such as benzene ring bond pair using C=O carbonyl as -COOH carboxyl acid which is unable to be used alone. The 157 nm absorbance is dominated by C (2π) electrons with bonding configuration expected to greatly influence absorption. Acrylic, phenolic, and cyclo olefin based photoresists can all achieve acceptable optical transmission at 157 nm if the photoresist thickness is <90 nm. However, industry experience has suggested that the defect density levels will be unacceptably high at such a thin photoresist thickness.

Design the direction in two directions:

(1) Use and exclude function base of π electron and reduce the degrees of absorption.

(2) Use the function base of π electron. May try relatively high bonding energy C-F bond 441kj/mole, instead of the lower bond energy C-H key 415kj/mole in the macromolecule structure in order to make O-O * absorption move to a shorter wave to produce hypsochrome (blue shift) and 157 nm wavelength absorption (A) reduction. Fluorine isopropanol (IPA) –OH will be regarded as a de-protection base with 6 C-F bonds in the replacement of 6 C-H bonds [31]. Aside from the reduction of absorption degree, the strong attraction from the highly negatively charged F will disperse electrically charged and stable oxygen anion acid, which can also strengthen alcohol base. <2.5 will be required by the 157 nm photoresist for each of its micrometer absorption degree A with >7.0 are normally used in the 248 nm / 193 nm photoresist, which uses t-BOC ALPG. The production of -COOH acid base will take place after the de-protection of two base pairs of π electron. All though the π electron has a strong absorption in 157 nm, it will continue to research and develop due to the lack in π electron. Use manpower / material resources / time course if problems should

occur in practice.

2.8 Motivation of this thesis

In order to keep with Moore's law, many methods can be used to improve IC circuit image resolution. However, the most effective method is to use the increasingly shorter wavelengths which requires a weaker light source such as DUV laser light with energy around 10-30 mJ/cm^2. In order to compensate such low energy of light source, additional post exposure bake (PEB) must be implemented immediately after DUV CAPR exposure. In other words, the acquisition of CAPR energy can be divided into exposed and baked components to promote an equal PEB impact on CD situation and exposure. Bake heat-conduction will be controlled by contact but the uniformity will not be in the likeness of the light, which is perfect and correct. Thus the contact questions of PB and PEB with its uniform and direct influence by the photochemical reaction within CAPR will usually cause yield loss (CD shift) on half of the wafer. Chemically amplified under DUV exposure resistance area, the photo-acid generator will produce protons H^+ that can subsequently catalyze the de-protecting chemical reaction of polymer ALPG during the PEB step with other new protons H^+ created again. Therefore, protons H^+ may continue and catalyze other ALPG de-protection reaction. Through such chain reaction, the number of times of de-protection reaction will enlarge by several hundred folds. The chain catalytic reaction will influence variation of CD if the place of gate width/length is taken, which in return will influence the threshold voltage (V_{th}) and leakage current (I_{off}), characteristic.

A more important question is the inefficiency in current PEB control. It has already caused FAB serious yield losses in which one must look for assistance from others to solve the problem. Because the heat-conducting principal can easily learn wafer and

plate contact with instantaneous plate temperature drop ΔT, the ΔT may be expressed as a direct state of the bake process.

In order to verify this inference, 3 types of photoresists are used to examine the correlation between ΔT and CD variation, namely, I-line PR, DUV 248 nm PR, and DUV 193 nm photoresist with two kinds of bakes such as PB and PEB being studied. The situation of using six kinds of different spacer thickness (2.5 mm/2.0 mm/1.0 mm/0.6 mm/ 0.1 mm /0 mm) will be used to put and hinder wafer from placing above the plate.

We will utilize software to set up a simple limited element model in three-dimension. Wafer surface temperature predicted by the model and actual T-Map instrument data difference examined by the quantity is less than ±2℃. The prediction of the wafer and instantaneous plat-plate contact with plate temperature drop ΔT, actual plate temperature drop ΔT and data difference of ΔT are all below ±0.2℃. This model will test the CD wafer and temperature predicted to all gaps in contact with extremely good experimental relevance.

We have now found the temperature of the drop parameter ΔT, which can represent PB/PEB of the photoresist bake state. The next step is to find 248 nm photoresist at PB 0.94 nm/℃ and PEB –0.61 nm/℃ and find 193 nm photoresist at PB 0.68 nm/℃ and PEB –0.57 nm/℃. We can make use of this model to assist the prediction on the range of the new products or new process condition standing which in addition can also conform to certain quality requirement of the wafer photoresist bake.

Chapter 3 Experimental Methods

3.1 Finite element analysis

There are two kinds of general numerical methods, finite difference method and finite element analysis. Finite difference method can be easily understood and applied to some simple mechanical problem. But in complicated geometric questions, finite difference method has become hard to put into use due to its extremely complicated geometric pattern. Thus we must conduct our analysis using finite element analysis [32].

3.1.1 Wafer and plate under exposure to conduct heat energy

There is 3 ways to transfer heat, namely: conduction, convection, and radiation. The fastest and the most direct way are by conduction.

The transmitting rate of energy by heat conduction through a medium can be described by eq. (3.1).

$$P = \frac{Q}{\Delta t} = KA\left[\frac{dT}{dx}\right] \tag{3.1}$$

Where P : Transmitting rate of energy,

Q : Heat (J),

Δt : Time (Second),

K : Heat-conduction coefficient,

A : Contact Area.

$$\left[\frac{dT}{dx}\right] = \frac{T_{hi} - T_{low}}{\Delta L} \tag{3.2}$$

Where T-hi : High side temperature (℃),

T-low : Low side temperature (℃),

ΔL : Conduct heat from a distance.

When a temperature gradient exists within the medium, the heat-conducting phenomenon will take place due to the activity of the molecule with medium high energy level as shown in Figure 3.1.

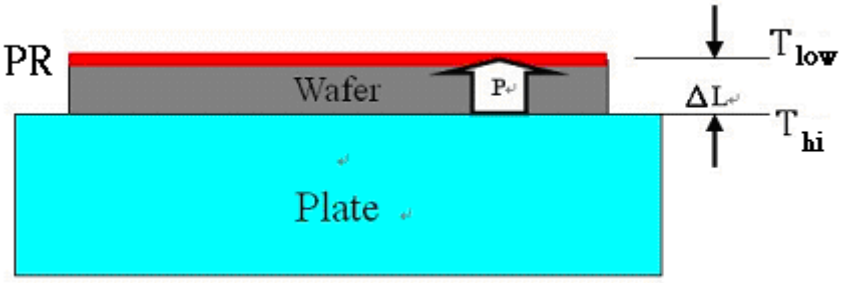

Figure 3.1 Heat energy transmission

3.1.2 Use ANSYS™ to analyze nodal heat conduction on the wafer

Because there are a lot of geometric patterns of different forms at the border of round wafer, the use of triangular element is found to be relatively suitable for the similaring of the curve of border, as shown in Figure 3.2. [33].

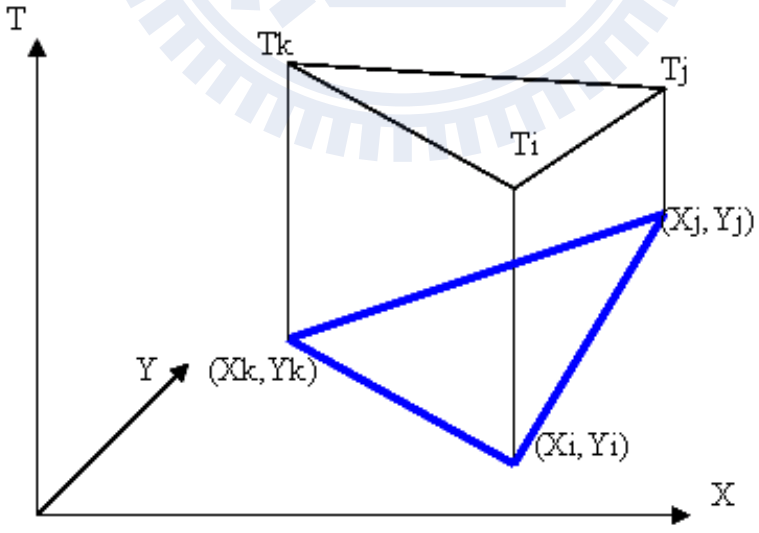

Figure 3.2 Component of triangular element

The temperature in the triangular area is defined by eq. (3.10) first.

$$T^{(e)} = a_1 + a_2 X + a_3 Y \tag{3.10}$$

Conditions to satisfy nodal temperature (3.11), (3.12), (3.13):

$$T=Ti \text{ at } X=Xi \text{ and } Y=Yi \tag{3.11}$$

$$T=Tj \text{ at } X=Xj \text{ and } Y=Yj \tag{3.12}$$

$$T=Tk \text{ at } X=Xk \text{ and } Y=Yk \tag{3.13}$$

Take (3.11), (3.12), (3.13) into (3.10).

$$Ti = a_1 + a_2 Xi + a_3 Yi \tag{3.14}$$

$$Tj = a_1 + a_2 Xj + a_3 Yj \tag{3.15}$$

$$Tk = a_1 + a_2 Xk + a_3 Yk \tag{3.16}$$

From (3.14), (3.15), (3.16) ask and solve: a_1, a_2, a_3.

$a_1 = (1/2A)[(X_j Y_k – X_k Y_j)\ T_i + (X_k Y_i - X_i Y_k)\ T_j + (X_i Y_j - X_j Y_i)\ T_k]$

$a_2 = (1/2A)[(Y_j – Y_k)\ T_i + (Y_k – Y_i)\ T_j + (Y_i – Y_j)\ T_k]$

$a_3 = (1/2A)[(X_k – X_j)\ T_i + (X_i – X_k)\ T_j + (X_j – X_i)\ T_k]$

A is the area of the triangular element: $2A = X_i (Y_j - Y_k) + X_j (Y_k - Y_i) + X_k (Y_i - Y_j)$

$$T^{(e)} = \begin{bmatrix} S_i & S_j & S_k \end{bmatrix} \begin{bmatrix} T_i \\ T_j \\ T_k \end{bmatrix} \tag{3.17}$$

Define the function S_i, S_j and S_k of the form:

$\alpha_i = X_j Y_k - X_k Y_j$, $\beta_i = Y_j - Y_k$, $\delta_i = X_k - X_j$

$\alpha_j = X_k Y_i - X_i Y_k$, $\beta_j = Y_k - Y_i$, $\delta_j = X_i - X_k$

$\alpha_k = X_i Y_j - X_j Y_i$, $\beta_k = Y_i - Y_j$, $\delta_k = X_j - X_i$

If $T_i >> T_j$ and $T_i >> T_k$

$$Si = \frac{a_1 + a_2 X + a_3 Y}{Ti} = \frac{a_1}{Ti} + \frac{a_2 X}{Ti} + \frac{a_3 Y}{Ti}$$

$$= \frac{1}{2A}\left(\alpha_i + \frac{\alpha_j T_j}{Ti} + \frac{\alpha_k T_k}{Ti}\right) + \frac{X}{2A}\left(\beta_i + \frac{\beta_j T_j}{Ti} + \frac{\beta_k T_k}{Ti}\right) + \frac{Y}{2A}\left(\delta_i + \frac{\delta_j T_j}{Ti} + \frac{\delta_k T_k}{Ti}\right) \quad (3.18)$$

$$S_i=(1/2A)(\alpha_i+\beta_i X+\delta_i Y) \quad (3.19)$$

If $T_j >> T_i$, $T_j >> T_k$

$$Sj = \frac{a_1 + a_2 X + a_3 Y}{Tj} = \frac{a_1}{Tj} + \frac{a_2 X}{Tj} + \frac{a_3 Y}{Tj}$$

$$= \frac{1}{2A}\left(\frac{\alpha_i T_i}{Tj} + \alpha_j + \frac{\alpha_k T_k}{Tj}\right) + \frac{X}{2A}\left(\frac{\beta_i T_i}{Tj} + \beta_j + \frac{\beta_k T_k}{Tj}\right) + \frac{Y}{2A}\left(\frac{\delta_i T_i}{Tj} + \delta_j + \frac{\delta_k T_k}{Tj}\right) \quad (3.20)$$

$$S_j=(1/2A)(\alpha_j+\beta_j X+\delta_j Y) \quad (3.21)$$

If $T_k >> T_i$, $T_k >> T_j$

$$Sk = \frac{a_1 + a_2 X + a_3 Y}{Tk} = \frac{a_1}{Tk} + \frac{a_2 X}{Tk} + \frac{a_3 Y}{Tk}$$

$$= \frac{1}{2A}\left(\frac{\alpha_i T_i}{Tk} + \frac{\alpha_j T_j}{Tk} + \alpha_k\right) + \frac{X}{2A}\left(\frac{\beta_i T_i}{Tk} + \frac{\beta_j T_j}{Tk} + \beta_k\right) + \frac{Y}{2A}\left(\frac{\delta_i T_i}{Tk} + \frac{\delta_j T_j}{Tk} + \delta_k\right) \quad (3.22)$$

$$S_k=(1/2A)(\alpha_k+\beta_k X+\delta_k Y) \quad (3.23)$$

$$S_i=(1/2A)(\alpha_i+\beta_i X+\delta_i Y) \quad (3.24)$$

$$S_j=(1/2A)(\alpha_j+\beta_j X+\delta_j Y) \quad (3.25)$$

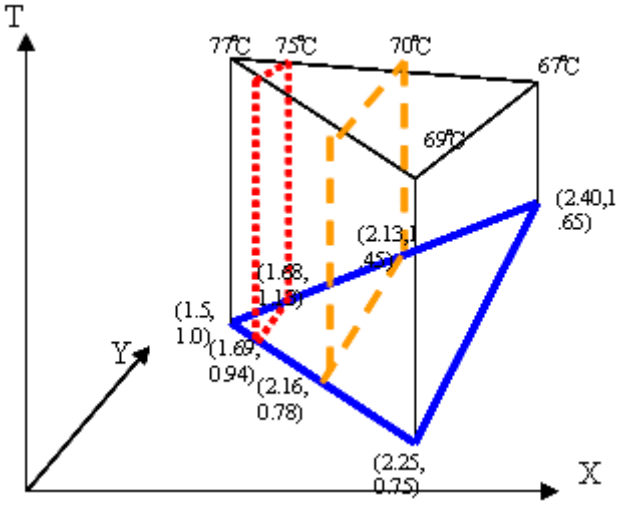

Figure 3.3 Triangular element calculated temperature of specific positions

Table 3.1 shows the define element type wafer and plate parameters for material properties In ANSYS, and create wafer and plate geometry 3D graphic by ANSYS volumes editor, and generate the triangular mesh by mesh tool smart size function, such as Figure 3.4.

Table 3.1 Characteristic parameter of Si wafer and Al alloy hot plate

Parameter	Unit	Al alloy	Wafer (Si)
Heat spreading rate	W/m.k	75	120
Specific heat C	J/kg.k	470	913
Density	Kg/m^3	6.8	2.52

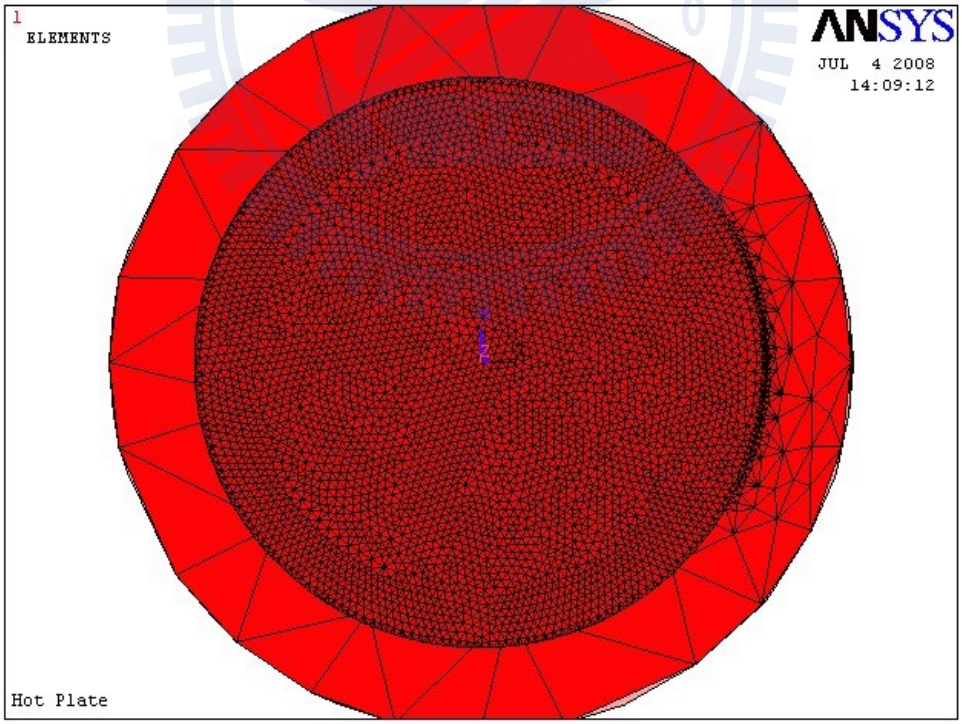

Figure 3.4 Wafer and plate geometry 3D graphic and triangular component

Apply displacement constraints and applied heat energy, review the results using the general postprocessor, exert the hot convection, define attitude analysis and initiate temporary conditions and finally find the result shown in Figure 3.5.

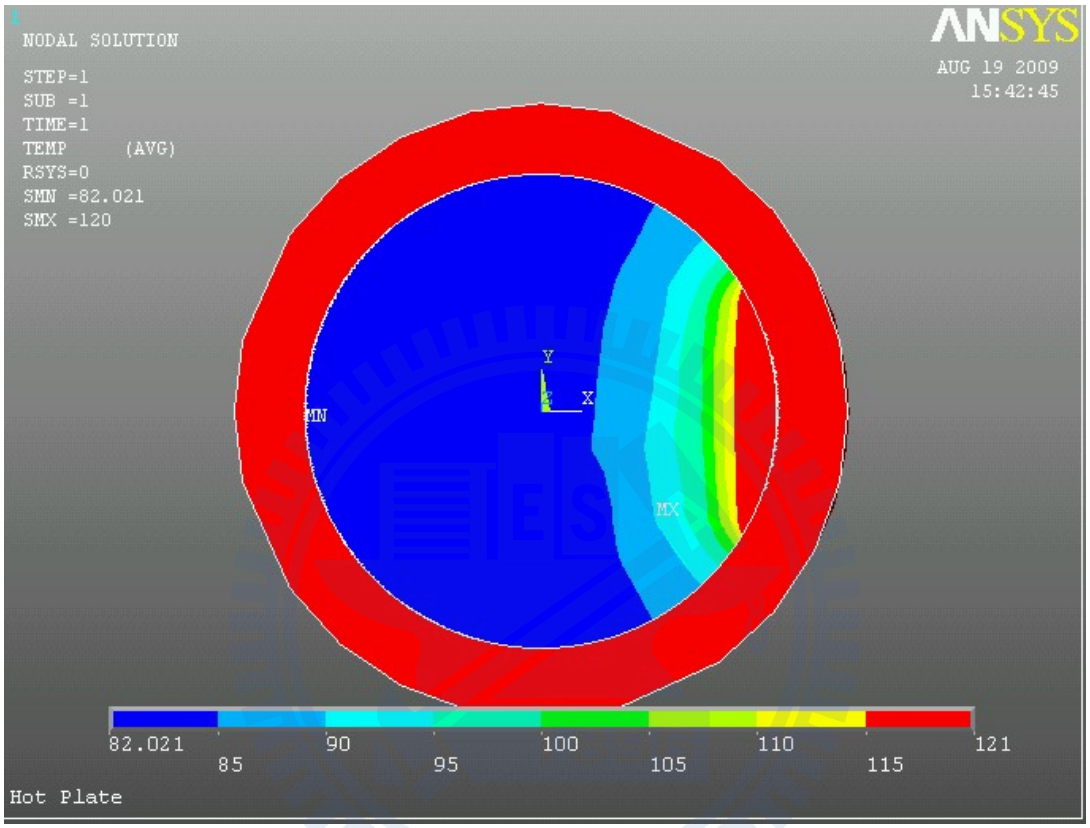

Figure 3.5 Calculation color temperature picture of wafer

3.2 Experiment steps

3.2.1 Standard lithography photoresist process flow

As shown in Figure 3.6, the typical flow of photolithography process in semiconductor industry. There are 7 main steps. In order to improve the wafer production output in each step, many units will be processed at the same time as shown in Figure 3.7 From here we can find 4 steps (1), (3), (5), (7) among the bake process.

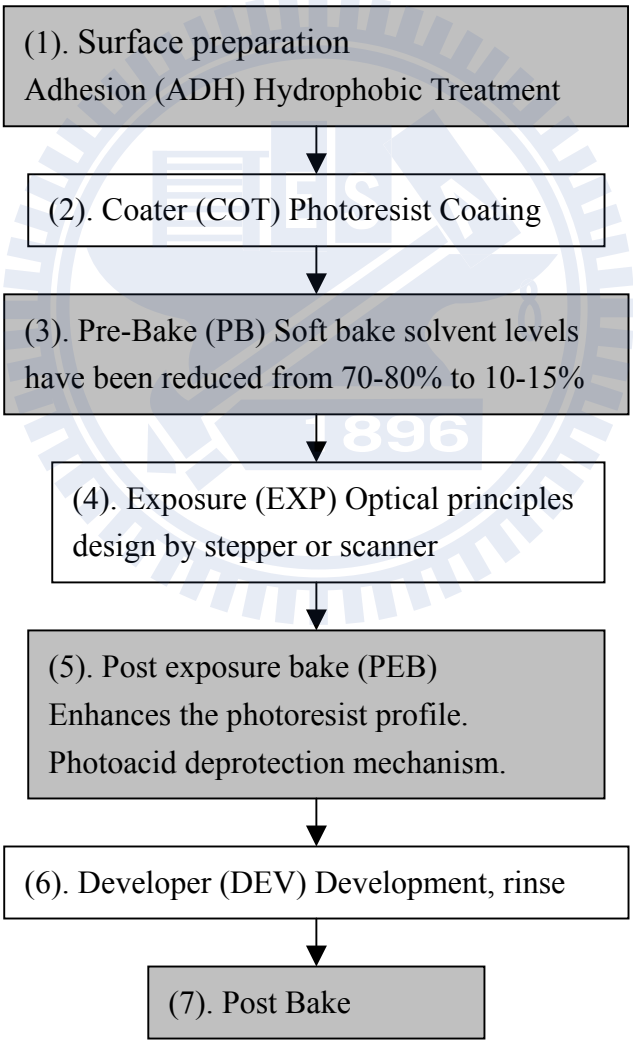

Figure 3.6 Standard lithography photoresist process flows

As shown in Figure 3.7, the Tokyo Electron Limited (TEL) track 5 blocks namely 1-X, 2-X, 3-X, 4-X, and 5-X. The block 1 includes wafer loader and unloader 1-1, 1-2, 1-3, 1-4, and 1-0 main arm. The 1-0 main arm will load wafer from 1-1 to 2-6, and unload wafer from 2-5 receive to 1-1. The block 2 include coater 2-1, 2-2, 2-3, and 2-4, the 2-7, 2-8, 2-9 are adhesion unit, 2-10, 2-11, 2-12 are cooling plate unit, 2-27, 2-28, 2-29 are pre exposure bake unit, 2-5, 2-6, 2-17, 2-18 are transfer buffer unit, and 2-0 main arm can load and unload wafer for all block 2 unit. The block 3 include developer 3-1, 3-2, 3-3, and 3-4, the 3-6, 3-7 and 3-8 are post exposure bake unit, and 3-12, 3-13, 3-18 are cooling plate unit, 3-10 and 3-11 are post develop bake unit 3-15, 3-16 are transfer buffer unit, and 2-0 main arm can load and unload wafer for all block 3 unit. The block 4 include 4-1, 4-2, 4-3 transfer buffer unit, and 4-0 main arms can load and unload wafer for all block 4 unit. The block 5 is stepper include 5-1 wafer aligner, 5-2 wafer leveling, 5-3 wafer exposure, 5-4 re-aligner, 5-5 output port. The X-0 main arm will automatically transfer wafer if target and source unit requested.

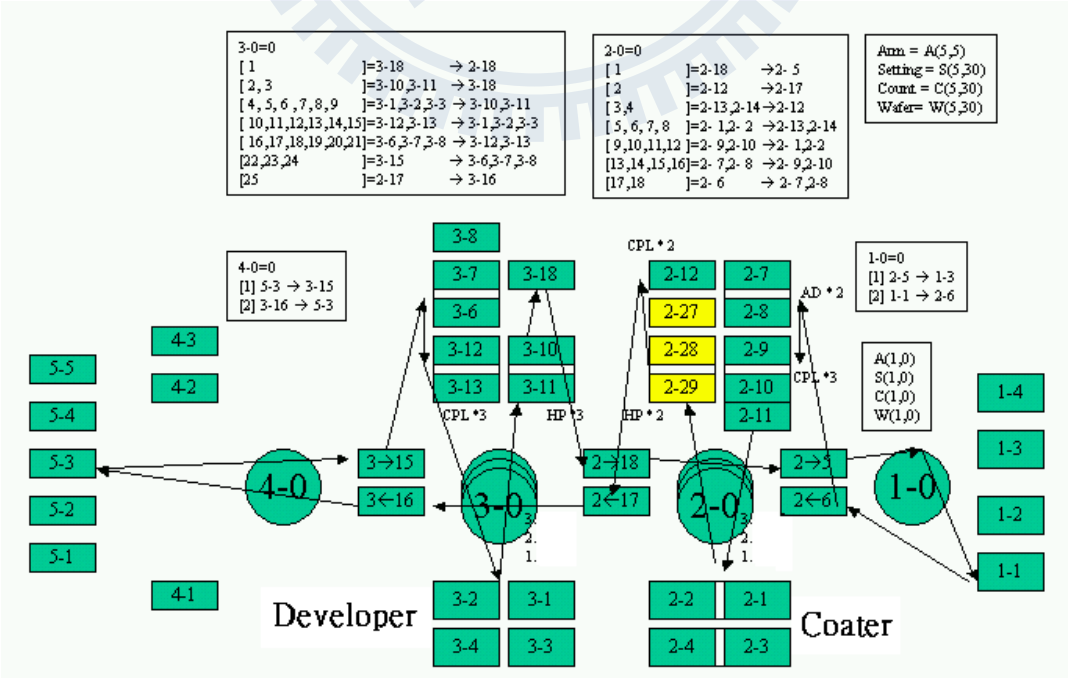

Figure 3.7 All units of Tokyo Electron Limited (TEL) track

3.2.2 Hot plate for primer

As shown in Figure 3.8, the hot plate for primer units will utilize heat energy to drive away the moisture content on the wafer surface (dehydration baking). In order to minimize moisture effects on the photoresist adhesion, a variety of surface pretreatment techniques are used. The most common is the application of Hexamethyldisilazane (HMDS), which will cover on wafer surface with a layer of hydrophobic material as shown in Figure 3.9. It is easy to join wafer and photoresist. As shown in Figure 3.10, the hydrophilic interface of the photoresist is difficult to stick to the wafer, which can cause photoresist to peel off during subsequent processing. This problem will also begrime the machine along with many other of the follow-up wafer. SiO_2 and metals are considered high-energy surfaces with surface free energy >103 dynes/cm. The photoresist is a form of solution with low surface energy (<36 dynes/cm) typical of a photoresist. Therefore, spontaneously wet SiO_2 and metal surfaces may be expected in addition to results in good adhesion [34].

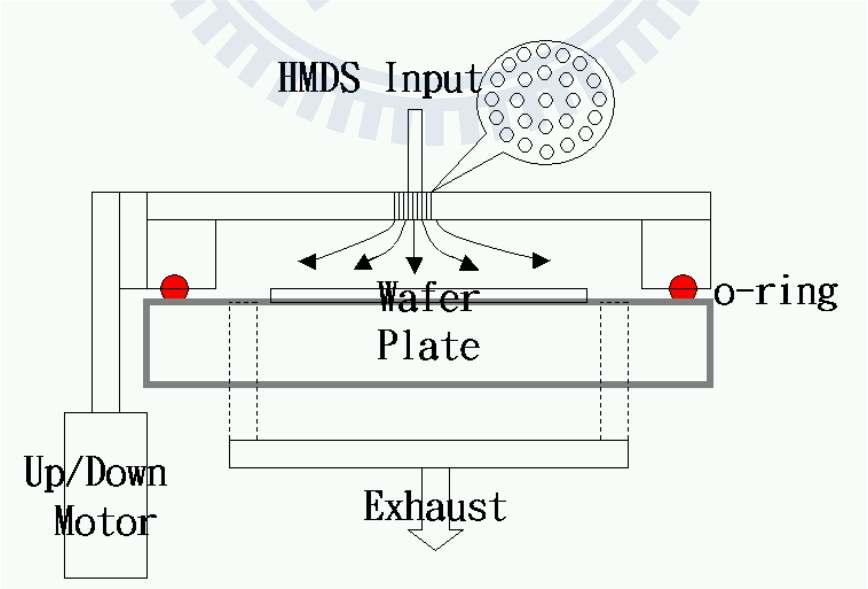

Figure 3.8 Hot plate for primer

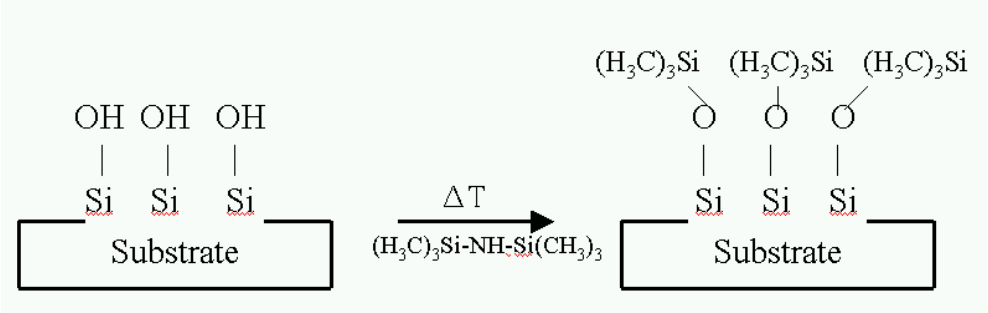

Figure 3.9 HMDS primer wafer surface hydrated to low moisture surface

There are three factors which can interfere with photoresist adhesion:

1. The solvent can push the resin away from the wafer surface. During soft bake, the solvent may evaporate with resins constrained by the photoresist film with the filling of the resulting gaps.

2. The resin will then form tight coils to minimize its energy and lower its interaction with the substrate. Resin-resin interaction can be stronger than the resin-substrate interface interaction particularly in poorly matched base solvent to resin.

3. Consider photoresist in interaction with SiO_2. Surface contamination, especially water moisture, has a very high affinity for SiO_2. From here one can see that moisture has a much stronger interaction. Moisture interaction with SiO_2 is a particular problem because the existing SiO_2 is already hydrated by the humidity.

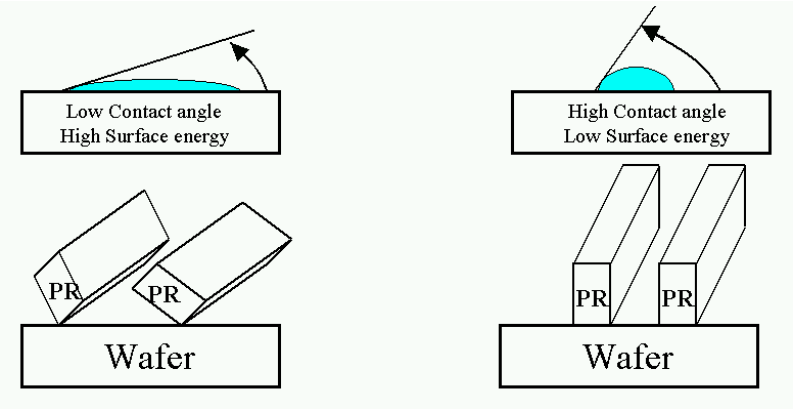

Resist pattern easy to peel **Resist pattern hard to peel**

Figure 3.10 Photoresist peel

3.2.3 Coater units of the photoresist spins

As shown in Figure 3.11, the arm of the photoresist spin coater units is a moving resistance nozzle heading in the direction of the wafer center. The photoresist spin coating process will begin by dispensing a controlled volume of photoresist which is then dispensed onto the center of the wafer. The wafer is spun at high speed to produce a uniform and partially dried photoresist film. The volume of the photoresist dispensed on the wafer size is typically 1 to 5ml (200 mm wafer). During coating, a solvent may be dispensed onto the outer-edge of the wafer to dissolve the edge-bead. This is a common method for line widths greater than approximately 0.5 mm. From the perspective of the edge-bead removal technique, the backside of the wafer is typically washed with an AZ_Ebr_7030 solvent to remove any photoresist that may accumulate on the backside during coating. Spin motor rotational speed is in inverse proportion to photoresist film thickness with static or rotation at a few hundred RPMs. General photoresist will control the temperature at 23℃. When the photoresist temperature is high, it will cause the thickness of wafer center to become relatively thin. In contrary, a low photoresist temperature will result in partial thickness of the wafer center. Coater exhaust must be carefully tuned and controlled to achieve uniform and repeatable photoresist films. The use of spin coating in IC fabrication is virtually universal, although there are several methods in which photoresist can be coated onto a wafer as shown in Figure 3.12.

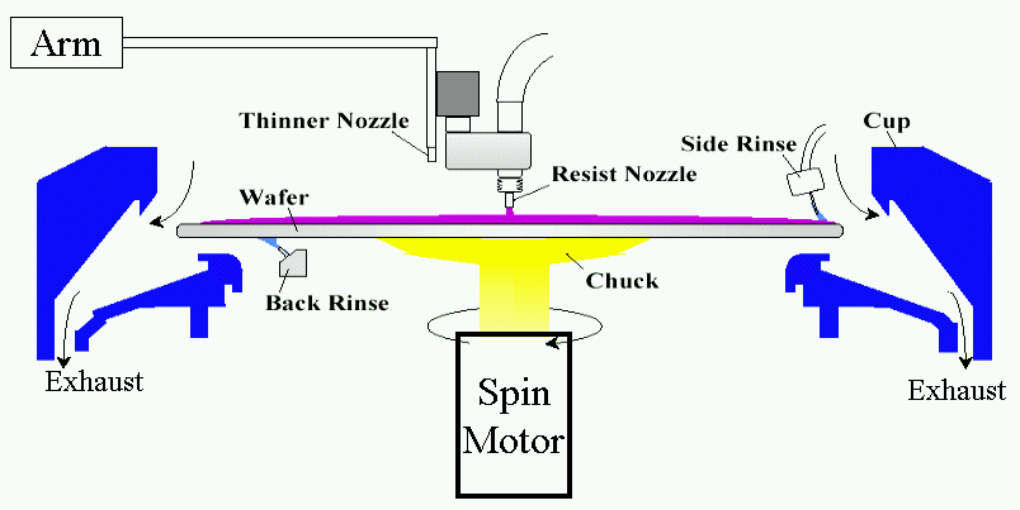

Figure 3.11 Coater unit

Parameter	Profile	Parameter	Profile
1. Rotation Speed	Thickness; Low; High	4. Cup Temp.	Thickness; High; Good; Low; Greatest effect on periphery
2. Resist Temp.	Thickness; High; Good; Low; Greatest effect on central region	5. Cup Humidity	Thickness; Low; Good; High; No change in profile but Thickness
3. Cooling Temp.	Thickness; High; Good; Low; Greatest effect on periphery	6. Exhaust Pressure	Thickness; High; Good; Low; Greatest effect on wafer edges

Figure 3.12 The photoresist coater parameters

3.2.4 Hot plate for pre-bake, PB (Soft Bake)

As shown in Figure 3.13, the pre-bake units following the coating of photoresist solvent levels have been reduced from 70-80% to 10-15% by heat energy in order to reduce residual solvent level in the PR. The reduction of photoresist free volume will reduce subsequent diffusion lengths for DUV resistance improvement resolution. The outer anneal residue will stress in the as-coated photoresist and improve adhesion in order to improve the difference in the development rate between the exposed and unexposed portions of the PR. Exhaust will take solvents produced by the evaporation away immediately to prevent depositing. Because hard bake is performed after pattern formation, the photoresist sensitizer will not limit bake temperature. The only limit on the hard bake temperature is by photoresist breakdown and or pattern distortion. Thus hard bake temperatures is much higher than soft bake temperature sometimes even higher than PEB temperature which can drive off residual solvents more efficiently. I-line photoresist Ar89 PB will bake for 90 seconds at 90℃; DUV248 nm SEPR203 photoresist PB will bake for 90 seconds at 100℃ and DUV193 nm G48 photoresist PB will bake for 90 seconds at 100℃ [35].

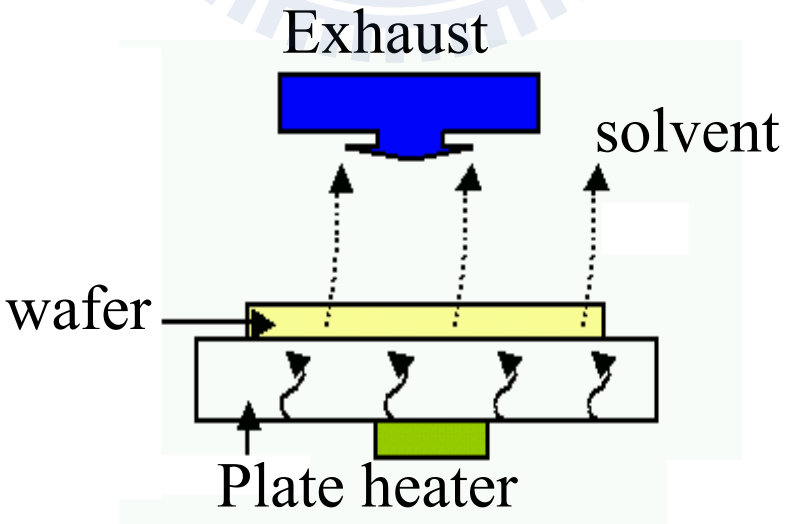

Figure 3.13 Hot plate unit

3.2.5 Exposure

As shown in Figure 3.14, the stepper exposure unit. The problems associated with making large diameter high NA lens has placed a practical threshold on the field size of the step and repeat systems. For a matching lens size, a step and scan system can achieve a larger field size than a step and repeat system. The basic principle of the step and scan is that a lens system can be taken to a location on the wafer with a slit imaged through the lens followed by scans of the reticle image onto the wafer. Defined by the reticle, the exposed and the unexposed area will then determine the keeping of the circuit pattern in accordance with photoresist characteristic. As shown in Figure 3.15, ten kinds of important process parameters under exposure with one to determine the quality of the exposure process. I-Line photoresist Ar89 exposure will use stepper UV 365 nm 350 mJ while DUV photoresist SEPR203 exposure use scanner laser 248 nm 15 mJ and DUV photoresist G48 exposure use scanner laser 193 nm 20 mJ [36].

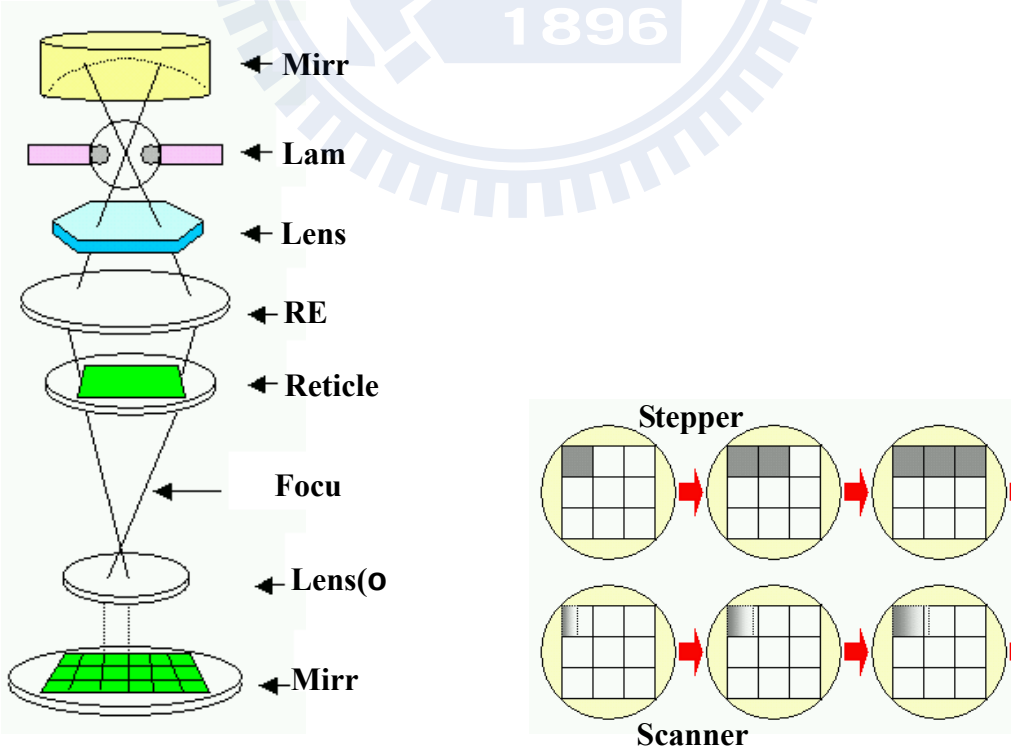

Figure 3.14 Exposure unit

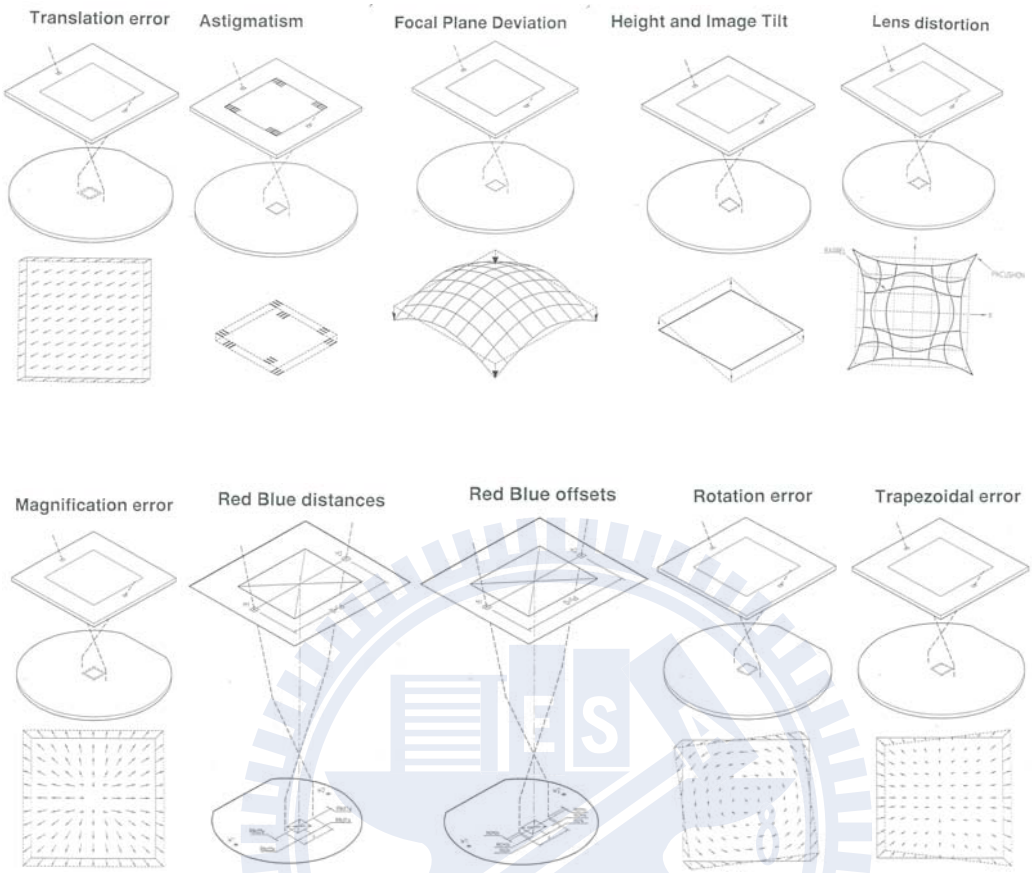

Figure 3.15 Exposure parameters [37]

3.2.6 Hot plate for post-exposure bake (PEB)

PEB is a bake step performed prior to development and after exposure. Heat energy is utilized in I-line photoresist to produce an averaging effect across the exposed /unexposed boundary. Aside from the inability to increase and stick to photoresist, PEB performed under 10 to 20℃ above the soft bake temperature can reduce standing wave effect with DQN photoresist. During PEB the PAC in the photoresist will diffuse from a high concentration region to low concentration region by reducing the differences in the development rate. With the advent of CAPR, PEB has taken on a new important role. CAPR will require a bake, typically between 90 - 140℃ for 1-2 minutes. PEB is required to allow the photo-generated acid to diffuse and accelerate the de-protection mechanism. DUV photoresist under immediate

exposure is designed with a photo-acid generator (PAG) for chemical amplification in the DUV-exposure resistance area. Photo-acid generator will then produce protons H^+, which can subsequently catalyze the de-protecting chemical reaction of the polymer acid labile protecting group (ALPG) during PEB step with other new protons H^+ created again. Therefore, protons H^+ can continue and catalyze other ALPG de-protecting reaction. Through such chain reaction, the number of times of de-protection reaction will enlarge by several hundred folds. Control of PEB temperature and time is critical to control the diffusion length of the photo-acid. If the photo-acid diffuse too far, broadening of the exposed areas may result. PEB has also been found to improve critical dimension control, exposure latitude and photoresist profile. Some researchers have reported additional benefits of PEB >30℃ and above soft bake temperature such as in contrast enhancement. PEB will be at 110℃ for 90 seconds in Ar89 photoresist with PEB at 110℃ for 90 seconds in SEPR203 photoresist and PEB at 110℃ for 90 seconds in G48 photoresist.

Effects of PEB temperature on CD shown in table 1.2 has listed several CAPR and CD change per ℃ for PEB. Note that while some photoresist are quite insensitive to temperature changes, resist such as APEX E are extremely sensitive. PEB at 100℃ for 2mins will result in diffusion length of ~5 nm. The chemical reaction in PTBOCST during PEB are quite complex with numerous side reactions which may occur depending on the exposure and PEB conditions. The side reaction can effect contrast and sensitivity depending on the processing conditions in addition to illustrate the importance of careful process control for CAPR.

3.2.7 Developer:

Due to the concerns in metal contamination, metal free developer currently in use is tetramethyl ammonium hydroxide (TMAH). The method of removing acidic material formed in the photoresist exposure area with preserved photoresist parts needed is currently the most frequently used. The spray of the developer will enable spin puddle at the same time. Rinsing of the DQN developers is done with DI water. Normally 2.38% of the TMAH developer will be sprayed on the photoresist first to force reaction under inactive state. Then it will be washed by rotation and spinned dry as shown in Figure 3.16 [38].

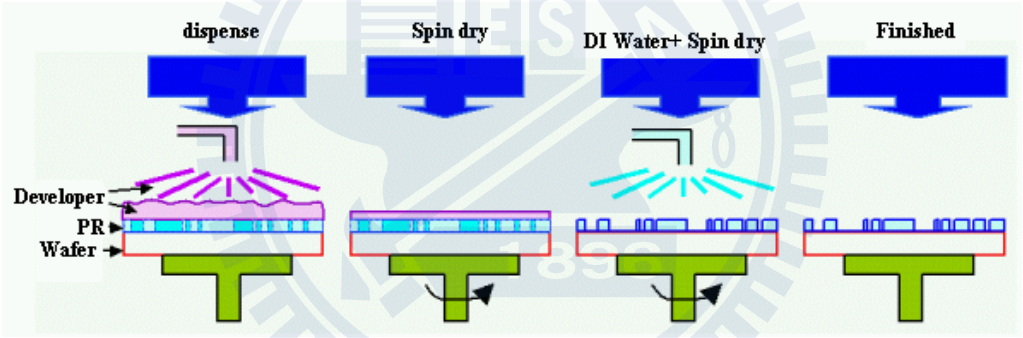

Figure 3.16 Developer steps

3.2.8 Hot plate for post development bake

Will utilize heat energy to remove residual solvents; improve adhesion; increase etch resistance and reduce pinholes and thin spots. PDB will be at 100℃ for 60 seconds in Ar89 photoresist with PDB at 100℃ for 60 seconds in SEPR203 photoresist and PDB at 100℃ for 60 seconds in G48 photoresist [39].

3.3 Experimental

3.3.1 Preparation of the tilt wafer

Wafer for normal condition should be placed in the center of the plate with equal distance between six guiding devices as shown in Figure 3.17. During the position shift of the arm, the position skew of the wafer is too big to act as a guiding device. In this range, the backfills will not run smoothly. Utilize the wafer (cold side) to stick to the plate (hot side) closely. For small and instant difference in temperature and the determination of wafer tilt is shown in Figure 3.18.

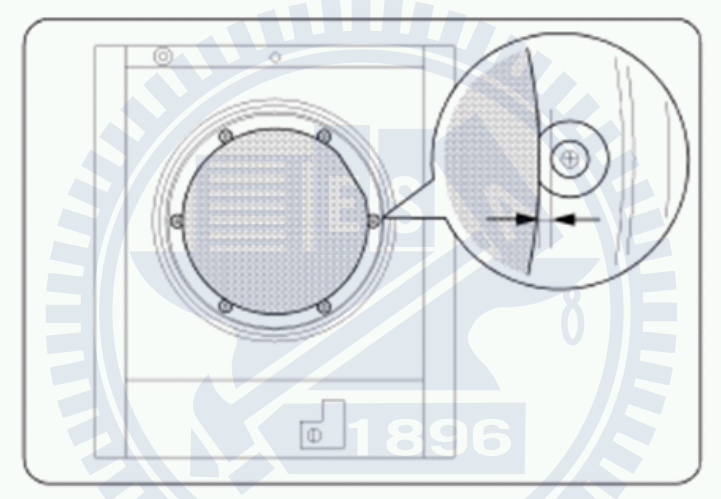

Figure 3.17 Top view of wafer and guide pins of hot plate

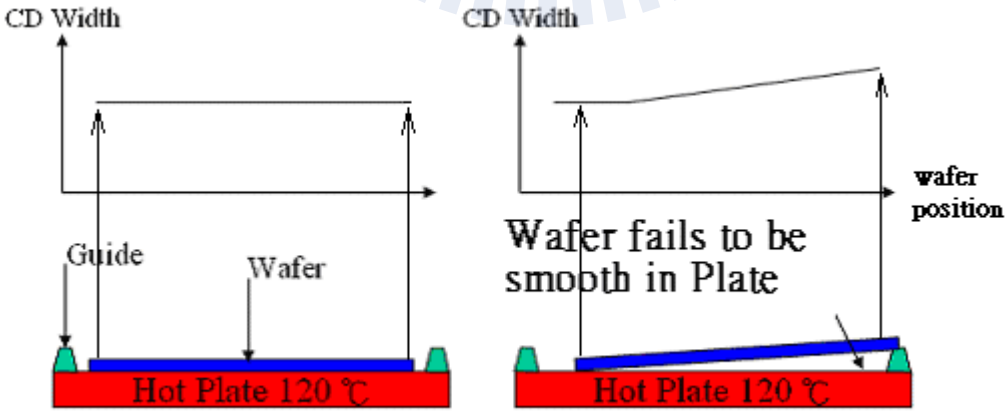

Figure 3.18 (a) normal position, (b) abnormal position for wafers during PB or PEB bake

Wafer must be in the guiding device block state, which does not allow the reoccurrence of the normal position of wafer skew. First set up and plan the recipe in accordance with standard wafer flow, then store the recipe. Place the cassette and combine the executive program. Before wafer moves to plate, press the arm pause button first. Put the first spacer on plate as shown in Figure 3.19-3.20. Release the arm pause button and continue to move the wafer. Wafer will be automatically placed in the plate and the process will begin. Wait for process to finish. The wafer will take out the next piece and continue to move in the plate. At this stage, press the arm pause button again. Put the second spacer on the plate and release the arm pause button to continue with the wafer movement. Wafer will be automatically placed in the plate to start the process. Carry out the steps described above repeatedly until all wafer tilt wanted by the experiment is complete (Wafer tilt spacer 2.5 mm, 2.0 mm, 1.0 mm, 0.6 mm, 0.1 mm, 0.05 mm, 0 mm). Afterwards, move these wafers to the thickness measuring instrument before moving to SEM.

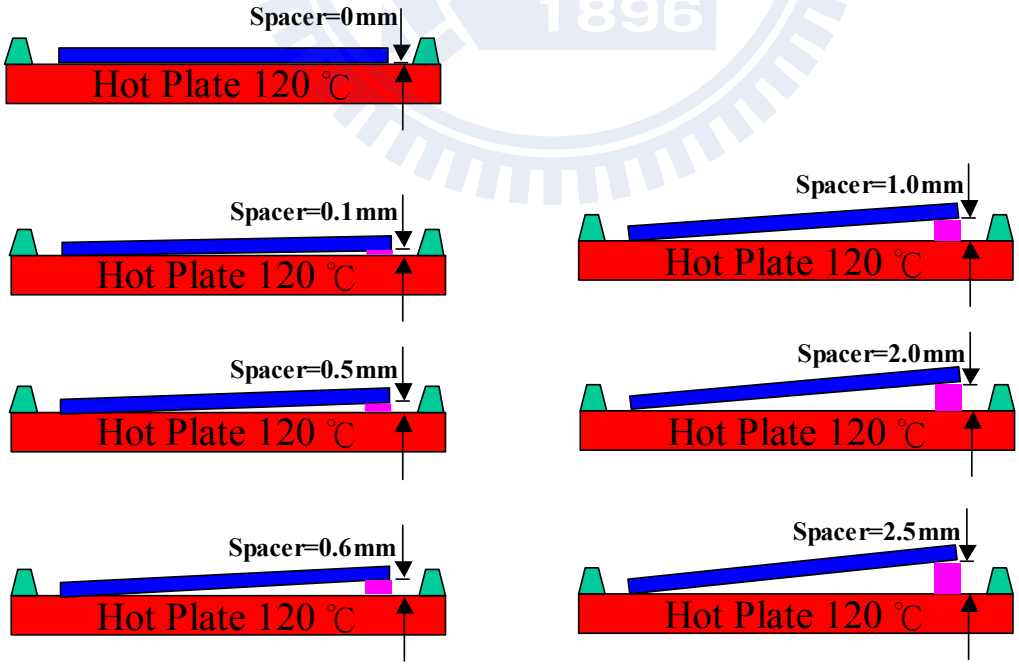

Figure 3.19 Various tilt conditions created by inseting spacers with different thickness

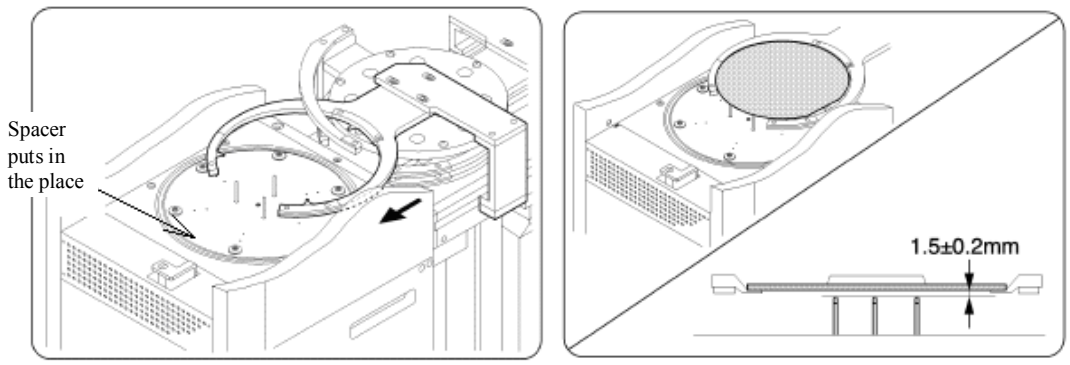

Figure 3.20 The schematic design of spacers relative to wafer transfer system and plate

3.4 Instruments for principle analysis

3.4.1 Thickness measuring instrument (THM)

This experiment will use UPTI to probe THERM-Wave 3290/2600 DUVI. This instrument mainly utilizes ellipsometry to carry out thickness measurement. The principle is when the light shine, the photoresist will reach wafer surface. The light is divided into two components with one part directly reflect to detector and the other as a line of light to enter in the photoresist. Reflection on the wafer sub layer surface will cause the light route of this component to leave and enter into the photoresist component. The thickness upon entering photoresist will influence the length of the route. The interference of these two lines of light will result in construction, interference and destructive interference. In accordance with the stripes of interference, calculate two lines of mere optical distance difference. Depending on the difference of optical distance and light incidence angle, the refract coefficient will calculate photoresist thickness, which can be done without contact and destruction to measure and examine film thickness as shown in Figure 3.21 [40].

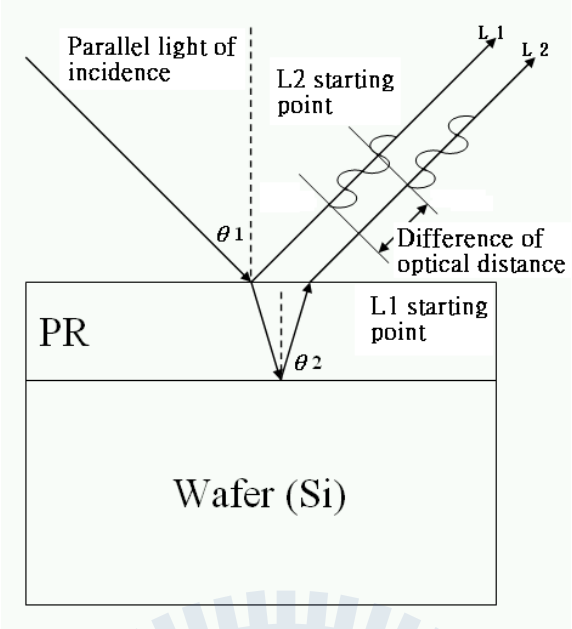

Figure 3.21 Principle of ellipsometry

Ellipsometers can provide both film thickness and index of refraction information. The name ellipsometer is derived from its use of elliptically-polarized light to measure film properties. In an ellipsometer, a laser beam is elliptically polarized and reflected from the specimen to be measured. The reflected beam will pass through an analyzer drum and onto a detector. The analyzer drum will then rotate to produce a minimum value under the light intensity reaching the photo-detector. By reading the polarizer and analyzer settings, the film thickness and index of refraction may be read. If a single reflectance angle is used, multiple film thicknesses can produce a null and the user must start with some idea of the expected film thickness in order to select a single value. If multiple angles are used, a single value may be obtained. Multi-domain tools in combination with multiple angles and wavelengths will allow multiple film stacks to be characterized as shown in Figure 3.22.

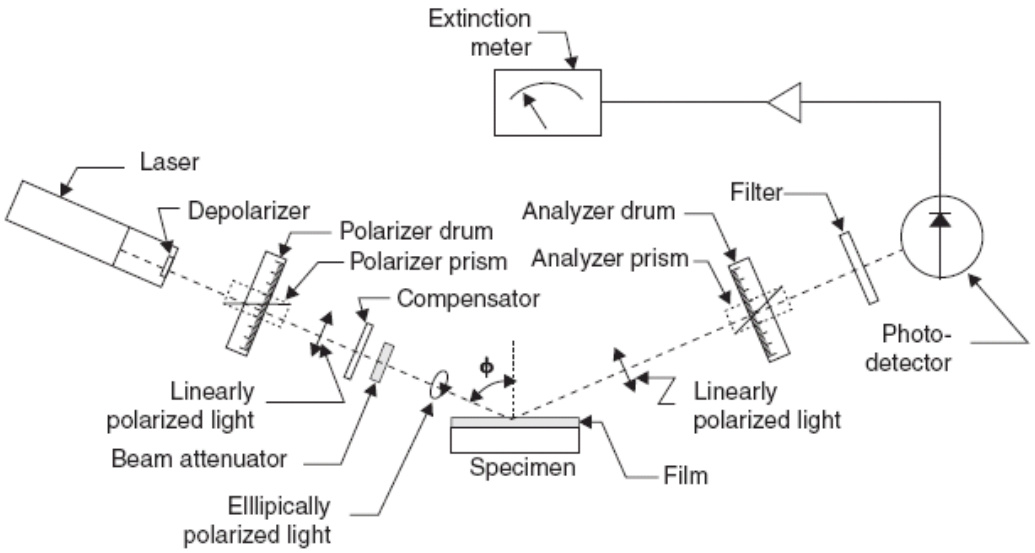

Figure 3.22 Set up schematic of an ellipsometer

3.4.2 Scanning electron microscope (SEM)

In order to isolate the interference of the gas molecule in the air, SEM must be carried out before measuring. The SEM chamber must be of a vacuum environment and the systems designed for in-line systems must be equipped with load-locks system and automatic pattern recognition under software control to shorten the time for vacuum and cassette to cassette wafer handling. The vacuum system is divided into three sections. First, is to rough pump about 10^{-3} torr from the dry pump. Second is to pump about 10^{-6} torr, from the turbo pump. And third, is to absorb about 10^{-9} torr from the ion pump. The energy of the electron beam will influence image quality directly. Energy that is lower than 2kev will reduce the damage to measuring the material, but energy that is too low will also influence the accuracy of the line width in which CD and SEM extends inspection into the deep sub micron regime. In a SEM, a column similar to the one illustrated in Figure 3.23 generates a focused electron beam. The electron beam penetrates through the matter to measure materials and the secondary electron after colliding. SEM can receive the second electron data by detecting the examining device and when the electron beam scans over the sample being inspected. One or more detectors may be used to detect electrons reflected or emitted by the

sample being scanned. After amplifying the signal, the signal will become controlled light and shades in a luminance CRT displayer. Using electron beam and CRT image synchronous to scan the position allows for drawing of the images with the contrast signal from the second electron which is recognizable by the computer imaging calculation CD. Field emission SEMs offer high resolution at low energies and are well suited to photoresist inspection where there are higher energy-charged electrons and/or may damage the photoresist film as shown in Figure 3.24 [41].

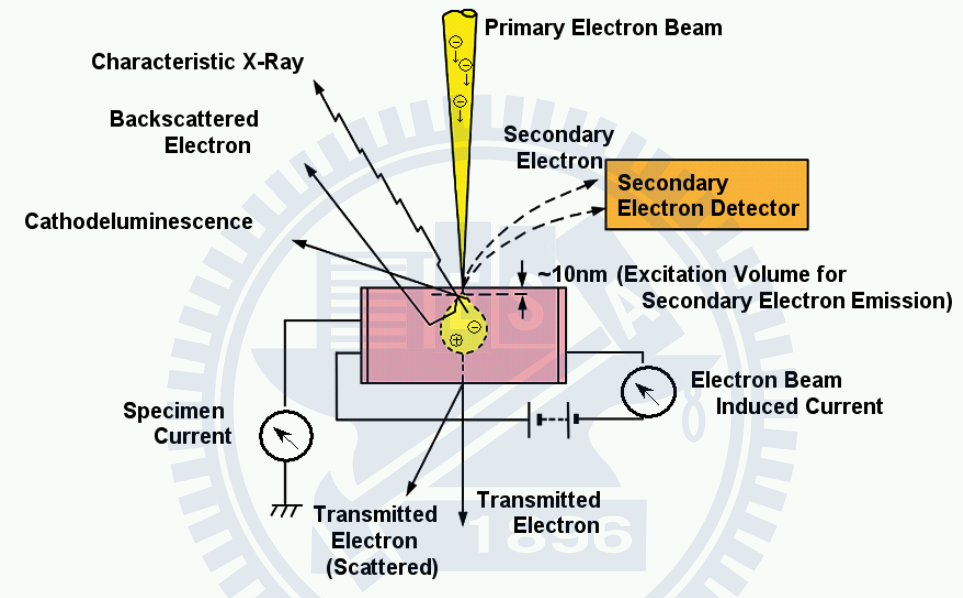

Figure 3.23 Scanning electron microscope

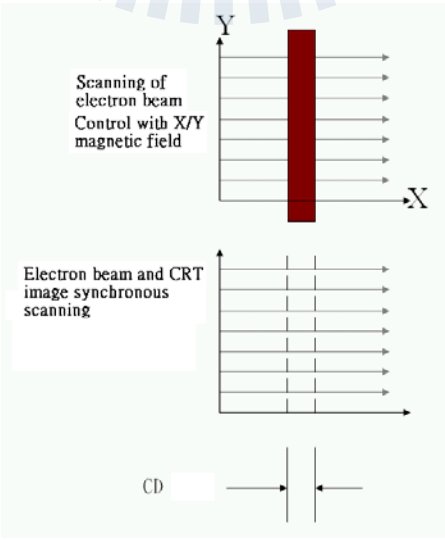

Figure 3.24 SEM X-Y scan formation of image

3.4.3 Temperature measuring instrument (T-MAP)

This instrument has 17 temperature sensors sticking on wafer surface, which are positioned uniform distribution. This tool measuring the 17 seats at the same time is in terms of voltage value to provide the temperature reading. This voltage signal is then changed into a digit signal with an A/D converter. Combine 17 temperature values by the controller and utilize COM RS232-Port to send out the result. After the computer receives the data, it will combine and use the T-MAP software for analysis, shown in Figure 3.25[42]

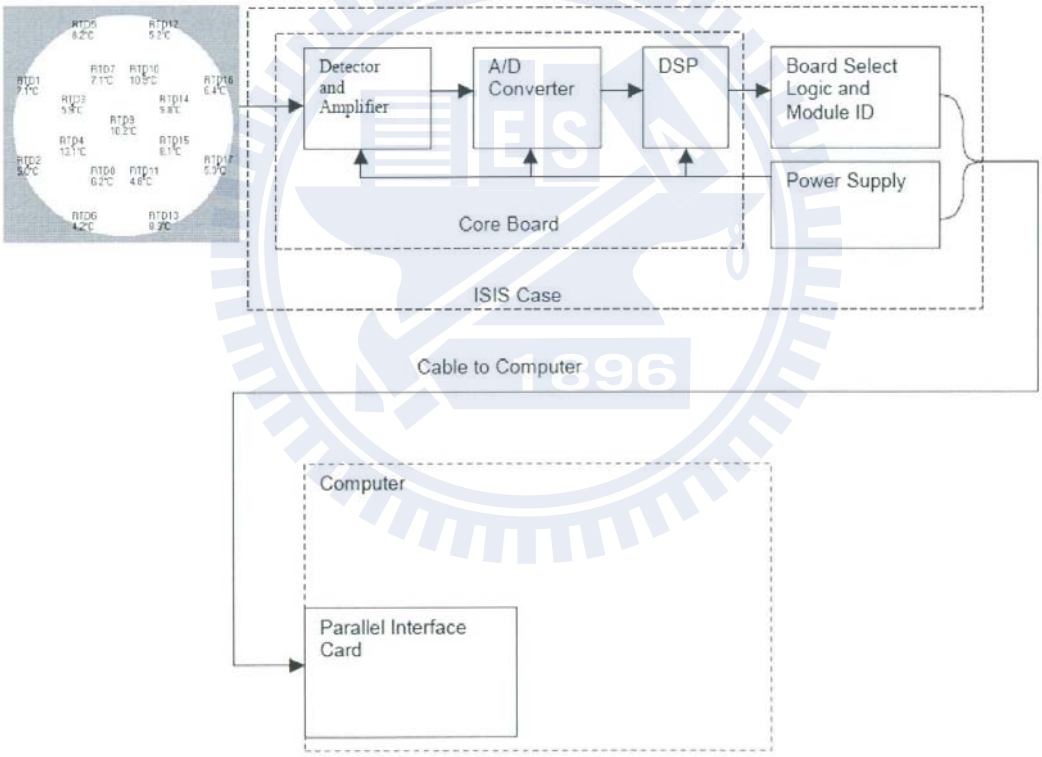

Figure 3.25 T-Map wafer surface temperature profile analysis

3.4.4 Obtaining plate ΔT:

Make an artificial intelligence microcomputer chip AT89S51 [43] to, plant into the machine which will bind perfectly with the machine as shown in Figure 3.26. Strengthen the performance and function of the machine as follow.

(1) Increase the sampled frequency of ΔT data and take a sample instead of once every 8 seconds, once every second.

(2) Confirm processing ΔT and correct the initial time signal.

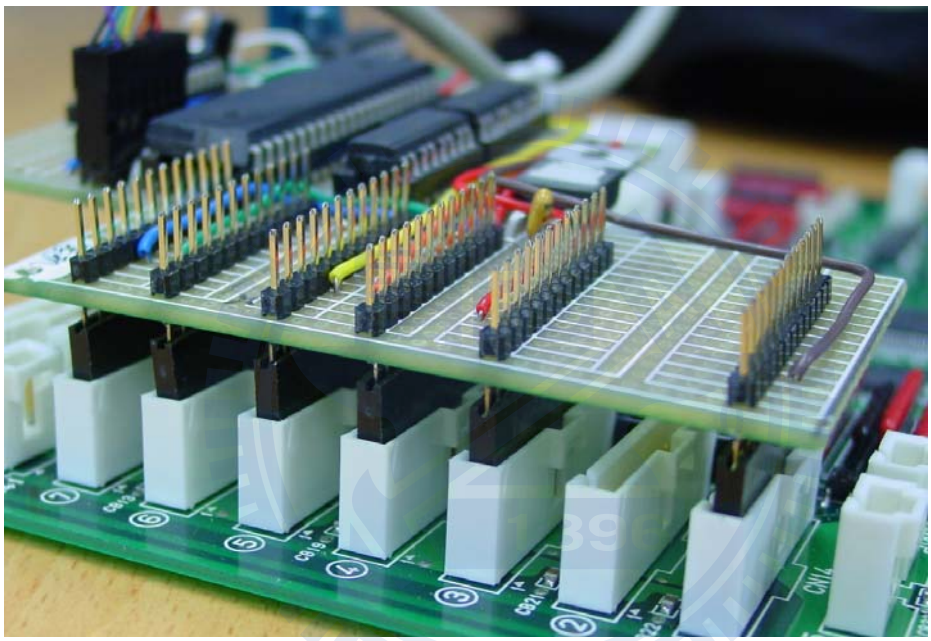

Figure 3.26 Setup microcomputer chip

3.4.5 Methods to increase ΔT and taking a sample

(1) The code to begin communication between the intercepting machine and the hot plate is to find out the initial code in the communication protocol which is "@". The code to end command is "*". Length of every sentence must be learned as shown in Figure 3.27.

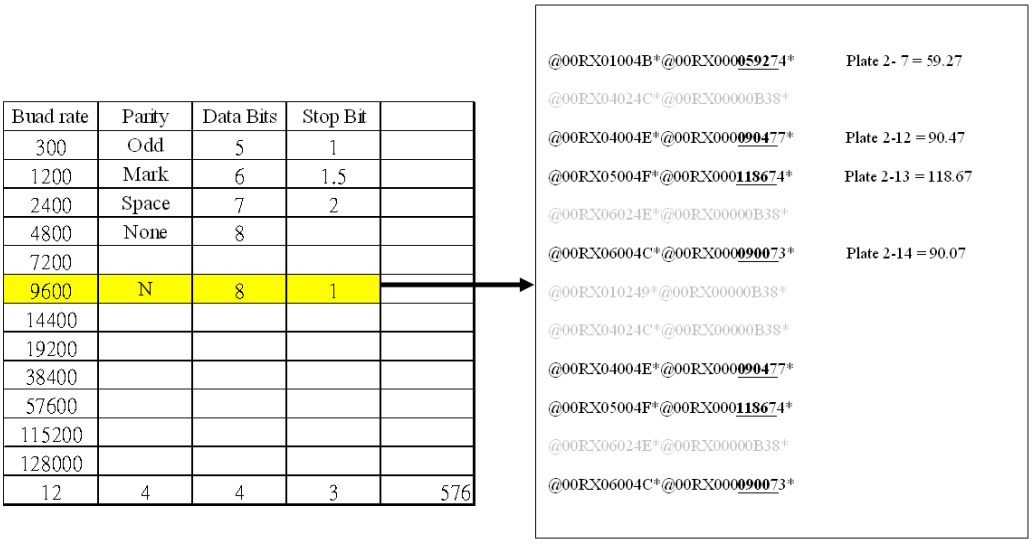

Buad rate	Parity	Data Bits	Stop Bit	
300	Odd	5	1	
1200	Mark	6	1.5	
2400	Space	7	2	
4800	None	8		
7200				
9600	N	8	1	
14400				
19200				
38400				
57600				
115200				
128000				
12	4	4	3	576

Figure 3.27 Communication code between the machine and hot plate

(2) Communication exists in every sentence between the machine and the hot plate. Find out the code that expresses temperature, and in order to confirm accuracy, must heighten or lower hot plate temperature designated. In the communication code of check-up, again, express temperature code, whether if one degree of change in rising or dropping in the temperature is within expectation.

(3) Try to procure hot plate temperature by observing the hot plate and replying the materials in which there is a temperature code.

(4) The communication code between the machine and hot plate could be found in repeated circulation cycle and during the stand-by cycle. Interrupt the cycle to send and ask for the temperature.

(5) If a haphazard code appears, when the machine is in standby state, the hot plate will receive a temperature to reply and thus influence the repeating circulation cycle. During appropriate times the masks will join which prohibits the machine from hearing the replies from the hot plate as shown in Figure 3.29.

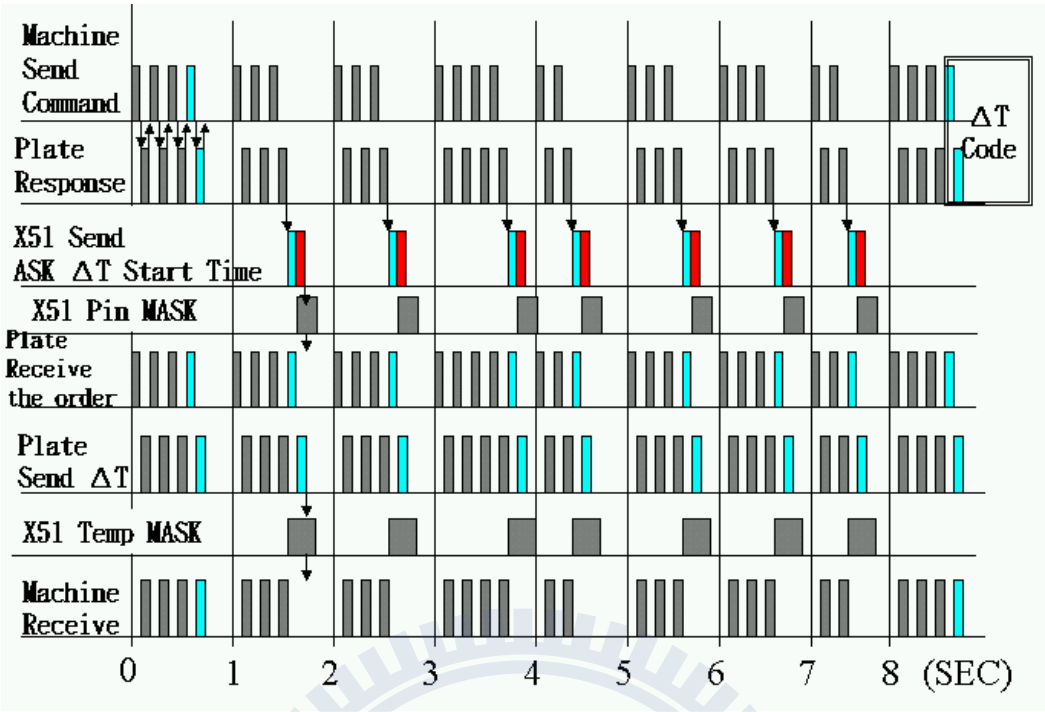

Figure 3.28 Increase ΔT sampled rate and haphazard code mask

(6) Hot plate temperature data collector as shown in Figure 3.28.

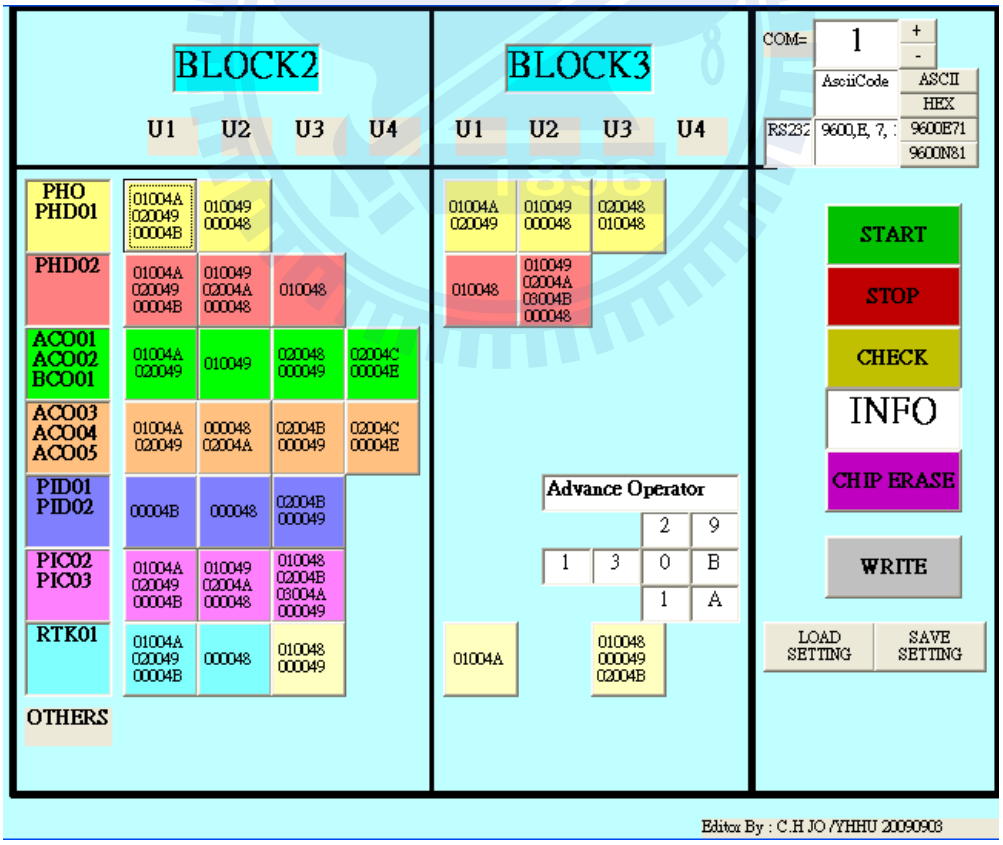

Figure 3.29 Hot plate temperature data collect software

3.4.6 Confirm process ΔT in real initial time

Use real pin to mark up/down signal; confirm the process, and correct initial time in order to compare the difference in temperature are shown in Figure 3.30.

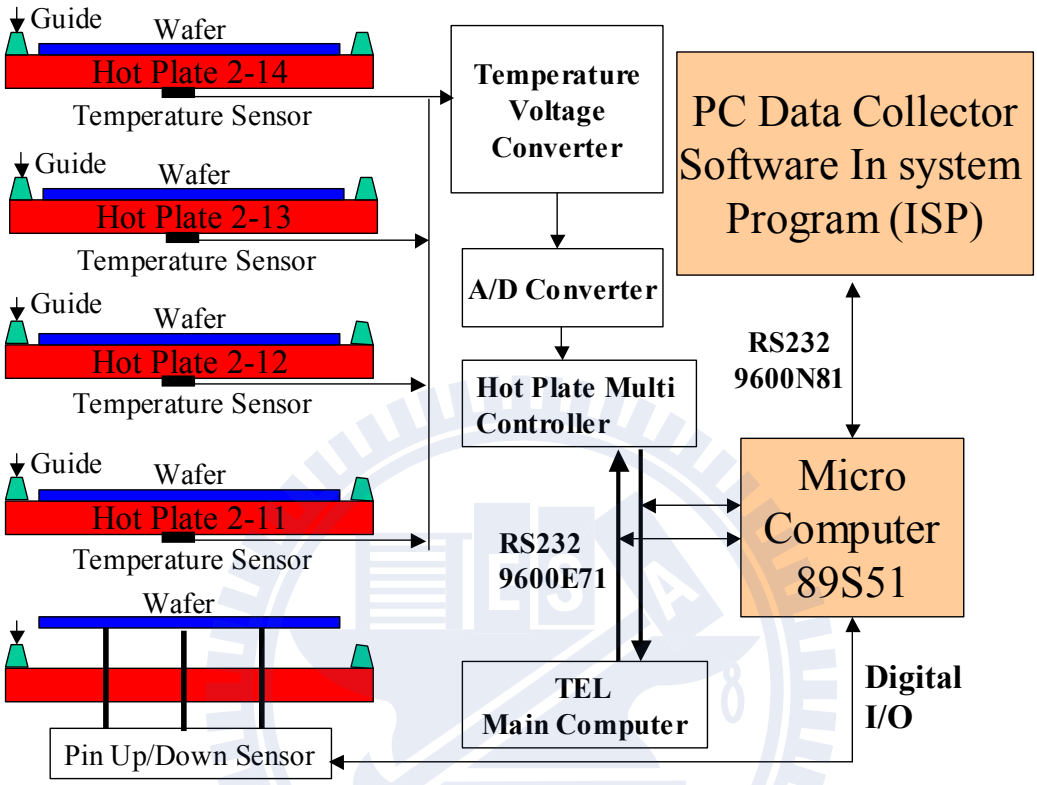

Figure 3.30 Hot plate temperature data collector

3.4.7 Bake the judging principle of unusual ΔT

Poor contact problem between wafer and plate will cause the temperature ΔT to drop drastically. It will be critical to judge whether the state of contact is good or bad. For example, when the instant the wafer touches the plate and pins down signal happens, there should be an immediate temperature drop about 0.9~1.2℃. Which is a normal temperature drop as shown in Figure 3.31 When the temperature drop is < 0.6℃, the contact is abnormal, as shown in Figure 3.32.

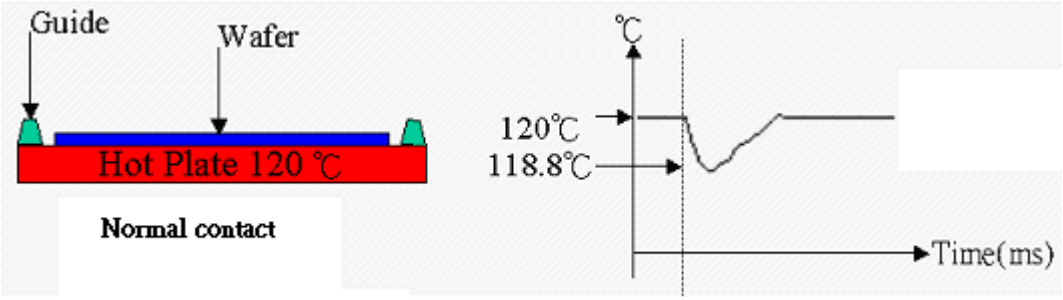

Figure 3.31 Temperature drop profile for normal contact between wafer and hot plate

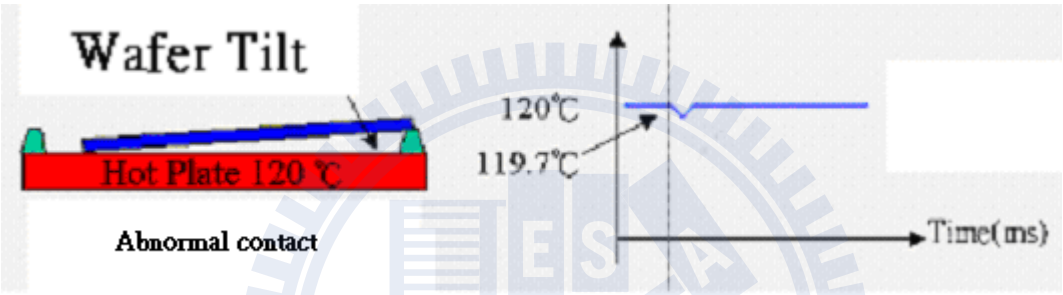

Figure 3.32 Temperature drop profile for abnormal contact between wafer and hot plate

3.5 Materials and utensils:

3.5.1 Silicon Wafer

(1) 8 inch Reclaim Wafer W803103, thickness of 705~745 μm was obtained from, Kinik Company Semiconductor Materials Co., Ltd.

3.5.2 Photoresist

(1) I-Line Photo Resist PFI-38A was obtained from SUMITOMO CHEMICAL COMPANY Co., Ltd.

(2) I-Line Photo Resist Ar89.

(3) DUV Photo Resist G48.

(4) DUV44-6 Anti-Reflective Coating (ARC) from Nissan Chemical industries, LTD.

(5) SEPR-203 8mPa's (cP) from Shin-Etsu Chemical Co., Ltd.

3.5.3 Solvents:

(1) AZ edge-bead removal (EBR) 7030 (90% PGMEA/10% Acetone) from AZ Electronic Materials Taiwan Co., Ltd.

(2) Hexamethyldisilazane (HMDS), Molecular Formula $(CH_3)3S_iNHS_i(CH_3)_3$, molecular weight: 161.39, Boiling Point: 126℃, Flash Point: 25℃, from Clariant Lsm (Florida) Inc.

3.5.4 Developer:

Tetramethyl ammonium hydroxide (TMAH), MD-3 Concentration 2.38wt%, Carbonate as CO_2< 0.03wt%, without surfactant.

3.5.5 Reticles

(1) TCE Photronlcs Semiconductor Mask Corp.

(2) DuPont PhotoMasks, Inc.

(3) Aligh Rite Linited.

3.5.6 Steppers

(1) ASML Stepper, Scanner 200, 500, 800, 1100.

(2) TEL Track M8, ACT8.

3.5.7 Lasers

(1) ELS 5610 248 nm Max Pulse Energy 50 mJ CYMER.

(2) ELS 6600 248 nm Max Pulse Energy 50 mJ CYMER.

(3) G42A4 ArF 193 nm Max Aver Power 200 Watts GIGAPHOTON.

Chapter 4 Results and Discussion

4.1 Temperature analysis

4.1.1 Plate temperature analysis

The plate drop temperature ΔT provides valuable insight into information regarding a bake condition, which can be related to the CD of the whole wafer. Temperature drop can thus be used to identify abnormal bakes of a wafer, as well as reduce the rework rate and yield loss without incurring too much cost.

4.1.1.1 Actual temperature of plate

When the wafer comes in contact with the plate, the wafer temperature is 23℃ and the plate temperature is 85℃. According to the heat conduction principle, heat is transferred from a high to a low temperature, resulting in a temperature drop (ΔT) in the plate. Contact area between the wafer and the plate influences the result of ΔT. Additionally, the state of the wafer baking process can be assessed by using this parameter. Figure 4.1 indicates that the ΔT under normal circumstances is 1.2℃. When the wafer and plate interface have a 0.1 mm gap, ΔT changes from 1.2℃ to 1.0℃. A larger gap leads to a smaller ΔT. When ΔT is about 0.25℃, the plate gap can be as large as 2.5 mm.

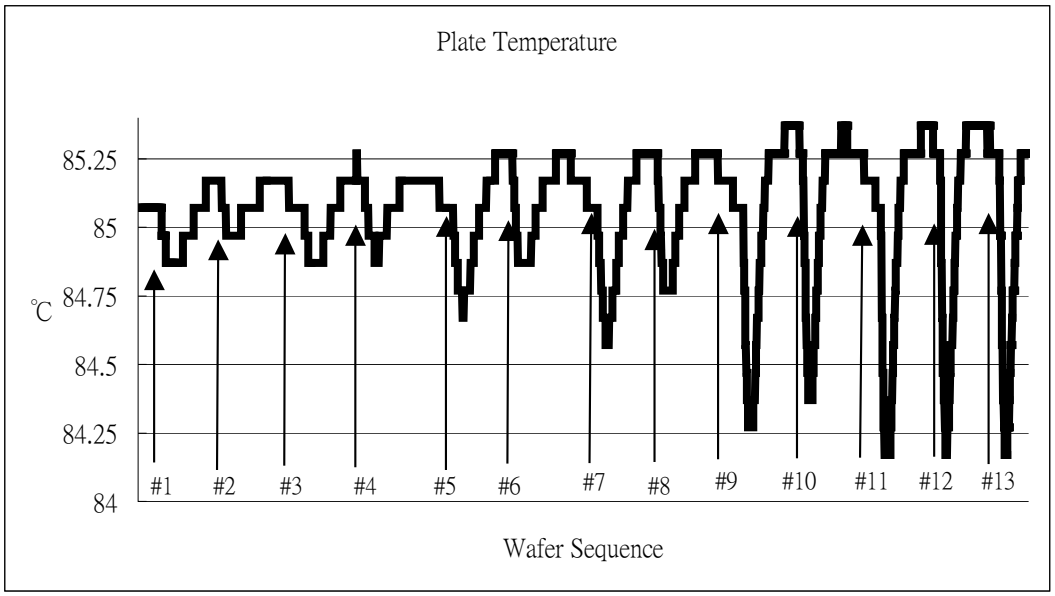

Figure 4.1 Plate temperature for wafer sequence (#1 to #13) at various gaps (0-2.5 mm) and plate set-point of 85℃

Table 4. 1 Summary of Plate temperature drop ΔT for gaps from 0 to 2.5 mm

Wafer No.	#1	#2	#3	#4	#5	#6	#7	#8	#9	#10	#11	#12	#13
Maximun	85.07	85.17	85.07	85.17	85.07	85.27	85.07	85.27	85.27	85.37	85.37	85.37	85.37
Minimum	84.87	84.97	84.87	84.87	84.67	84.87	84.57	84.77	84.27	84.37	84.17	84.17	84.17
ΔT (℃)	0.2	0.2	0.2	0.3	0.4	0.4	0.5	0.5	1	1	1.2	1.2	1.2
Gap (mm)	2.5		2.0		1		0.6		0.1		0		

Figure 4.2 shows the plate temperature drop, ΔT as a function of gap from 0 to 0.5 mm. In practice, performing experiments for a gap below 0.5 mm may be extremely difficult because a thin spacer is either warped or crocked to serve as a medium for a stable and reliability gap.

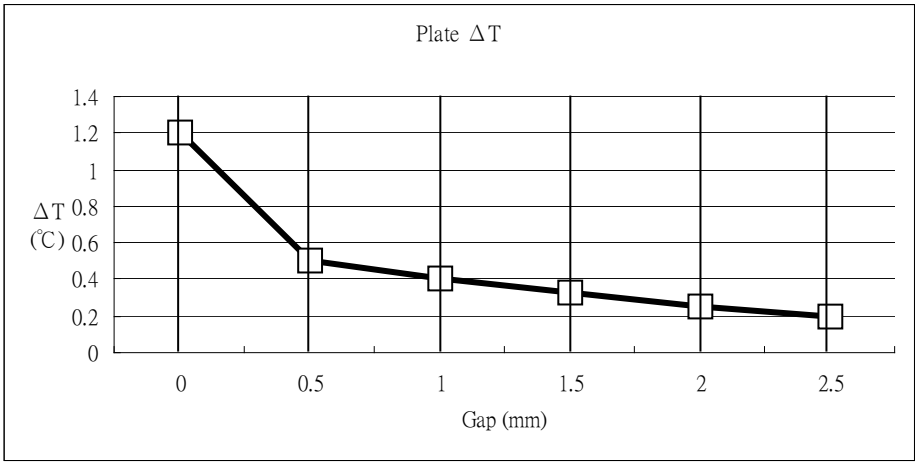

Figure 4.2 Plate temperature drop ΔT for gaps from 0 to 2.5 mm

The photoresist baking temperature generally ranges from 80℃ to 120℃, necessitating another experiment at 120℃. When the hot plate raises the temperature to 120℃, the wafer temperature is still 23℃. According to Figure 4.3, ΔT under normal conditions rises to 1.3℃ instantly, in comparison with an increase of 0.1℃ for the 80℃ ΔT when the slope is gentle. When the wafer and plate interface have a 0.1 mm particle, ΔT is changed from 1.3℃ to 1.1℃. When the slope is steep and the wafer and plate interface has a 2.5 mm particle, ΔT is 0.15℃, *i.e.* similar to the result of 80℃, as shown in Table 4.2.

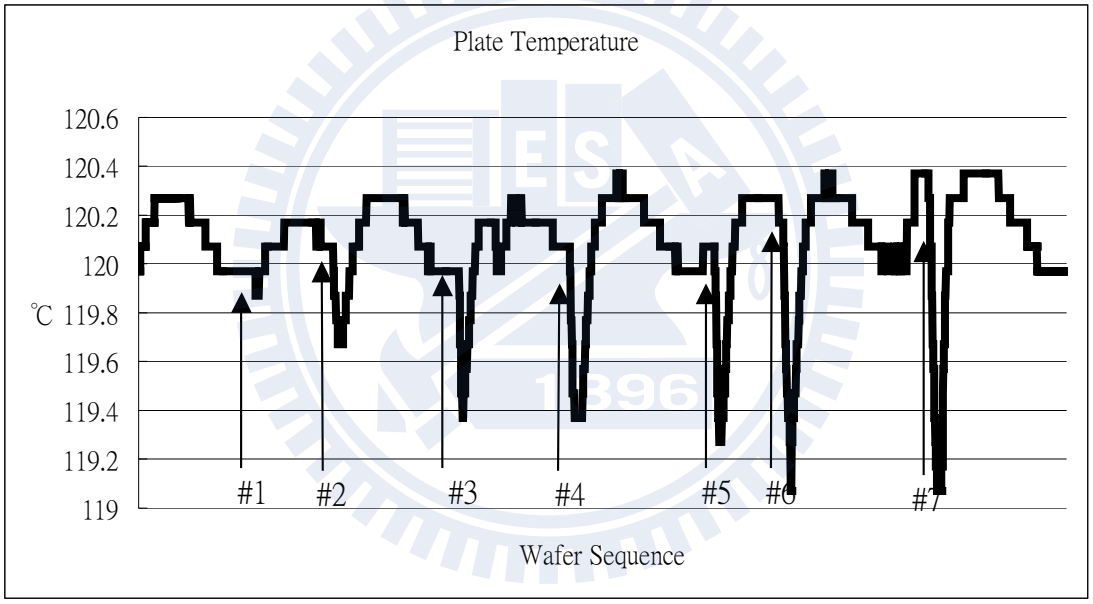

Figure 4.3 Plate temperature 120℃, wafer sequence #1 to #7

Table 4.2 Plate temperature drop ΔT for gaps from 0 to 2.5 mm

Wafer No.	#1	#2	#3	#4	#5	#6	#7
Maximun (℃)	119.97	120.07	119.97	120.07	120.07	120.27	120.37
Minimum (℃)	119.87	119.67	119.37	119.37	119.27	119.07	119.07
ΔT (℃)	0.1	0.4	0.6	0.7	0.8	1.2	1.3
Gap (mm)	2.5	2	1	0.6	0.5	0.1	0

Figure 4.1 and 4.2 compare the various tilts of 85℃ and 120℃ by deducting 85 ℃ ΔT from 120 ℃ ΔT, which results in the average increment of about 0.1℃ at different tilts. A higher plate temperature implies a more decisive change in ΔT, and can explicitly describe a bake process state, as shown in Figure 4.4.

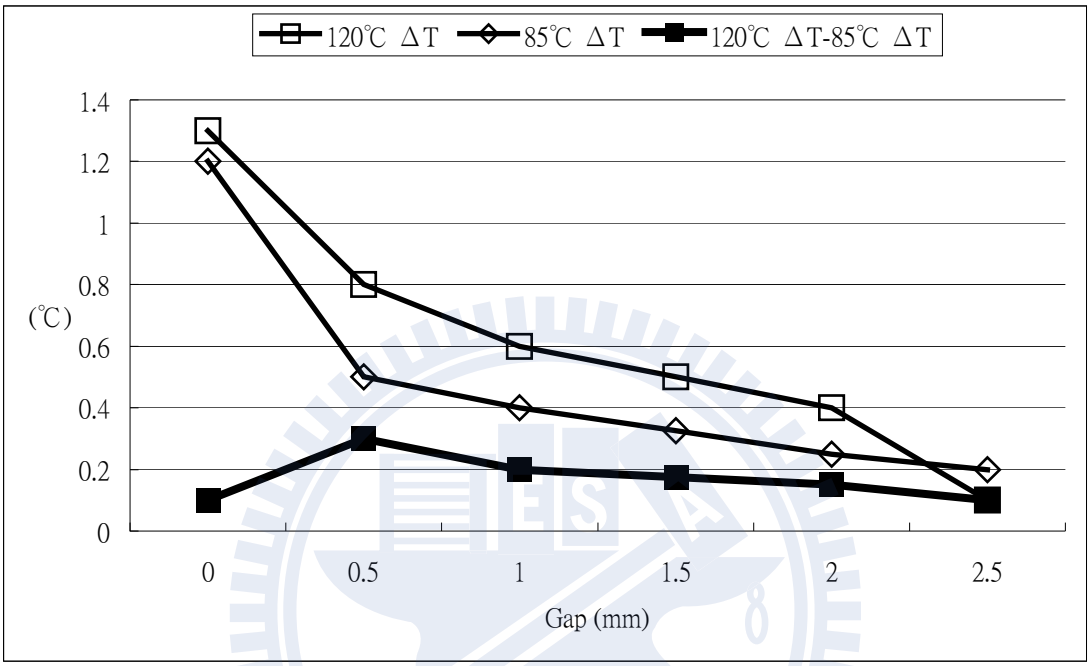

Figure 4.4 Comparative ΔT of 85℃ and 120℃

4.1.1.2 ANSYS simulation of plate temperature

The temperature is simulated using ANSYS software, with a very small wafer tilt of 0.05 mm while most of the wafer touches the plate. For a large plate temperature difference ΔT, e.g., between approximately 115.48℃ and 120.0℃, the range of the plate temperature profile is about 4.5℃ due to the temperature-detecting device of the plate. Notably, the temperature of the plate center must be used since the position is at the center of the plate. Consequently, ΔT is equal to 120℃-118.8℃=1.2℃, as shown in Figure 4.5.

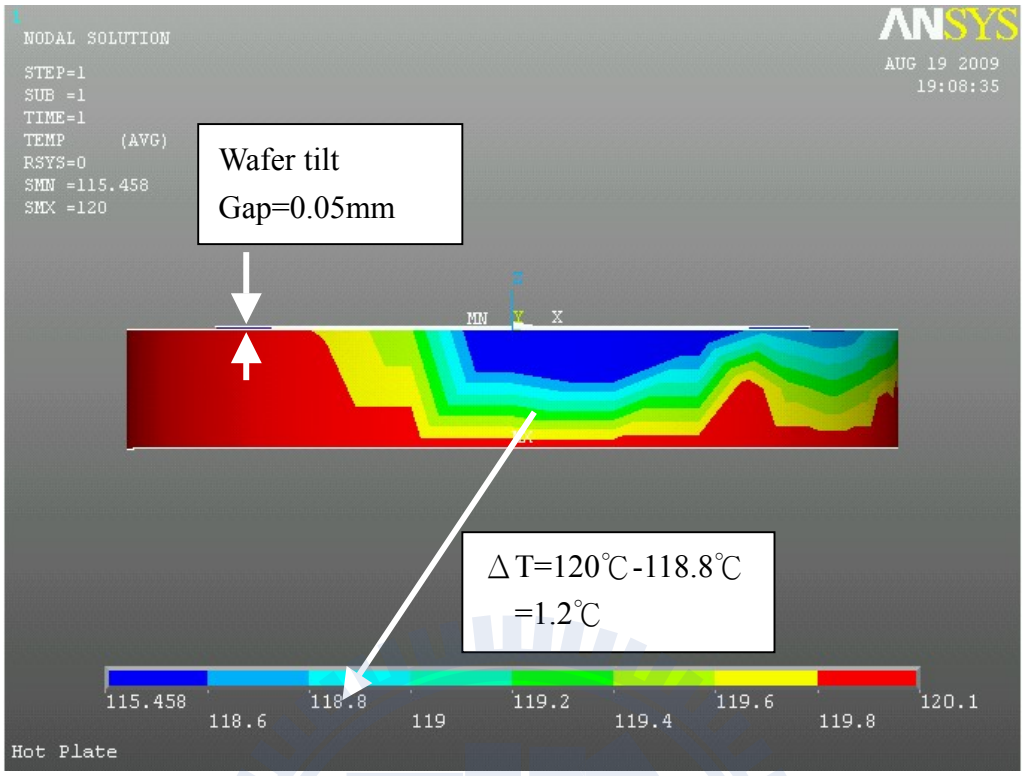

(a) ANSYS simulation result of plate temperature drop, ΔT =1.2℃ when wafer tilt gap=0.05 mm for plate temperature of 120℃

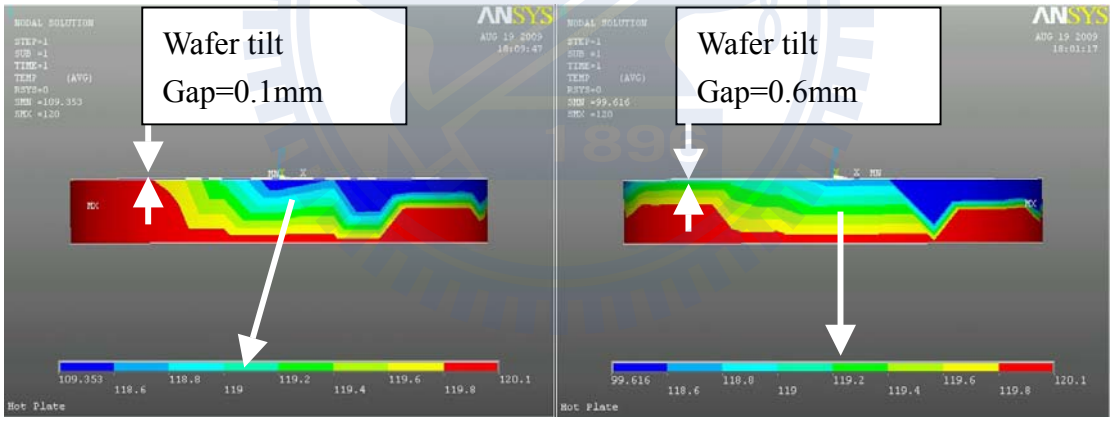

(b) tilt gap=0.1 mm, plate ΔT =0.9℃ **(c) tilt gap=0.6 mm, plate ΔT=0.8℃**

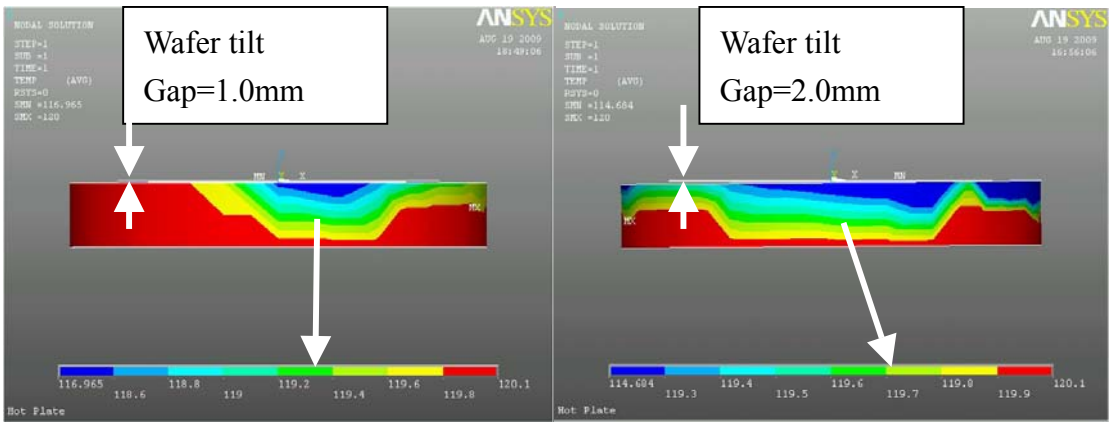

(d) tilt=1.0 mm, plate ΔT =0.6℃ **(e) tilt=2.0 mm, plate ΔT =0.5℃**

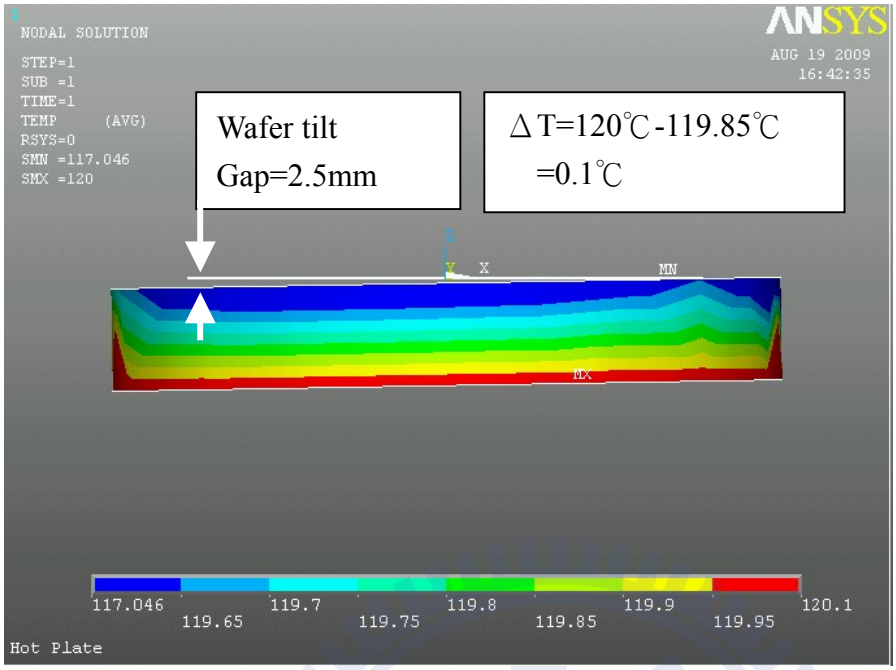

(f) tilt=2.5 mm, plate ΔT =0.1℃

Figures 4.5 ANSYS simulation results of plate temperature drop, ΔT for various gaps at plate temperature of 120℃

With a greater slope, the wafer tilt reach about 2.5 mm. Also, with the wafer barely touching the plate, the temperature drop is extremely small within the plate, between, *i.e.* 117.04℃ to 120.0℃. In addition, the plate temperature profile ranges by about 3℃. The temperature of the plate center is about 119.9℃, *i.e.* ΔT is about 120℃-119.85℃=0.1℃, as shown in Figure 4.5 (f).

4.1.1.3 Simulation error

Software simulation is set at 120℃ to test all contact situations. Figure 4.5 shows ΔT of the simulation plate position of the central point; Figure 4.5 shows the combined ΔT of data; Figure 4.2 shows the real plate temperature; and Figure 4.6 compares the results with a ±0.2℃ marginal error.

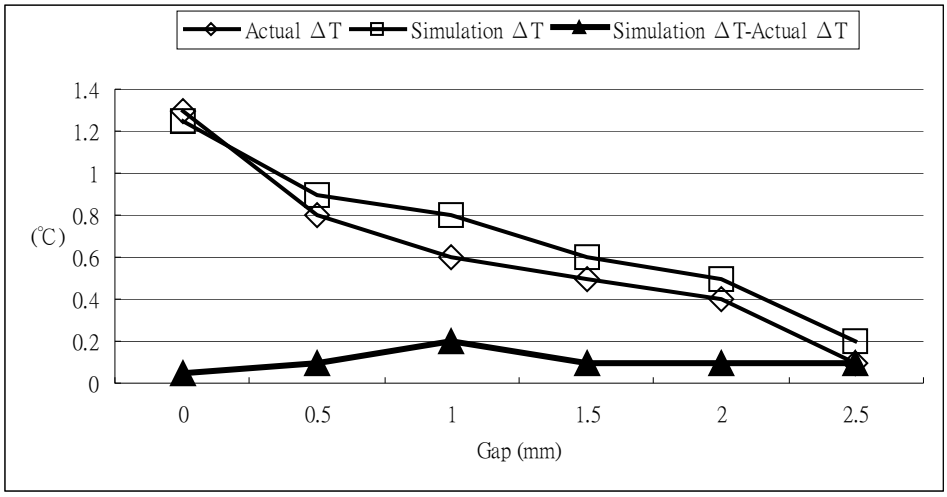

Figure 4.6 Compared simulation and actual ΔT of plate 120℃

4.1.2 Wafer surface temperature analysis

The wafer surface temperature for gaps ranges from 0 mm to 2.5 mm, as measured finest experimentally. These data will be used subsequently to compare with simulation data and to determine whether a simulation error occurs. The shift CD per ℃ is calculated as well.

4.1.2.1 Actual temperature of wafer surface

The wafer temperature is initially 23℃ because the wafer is above the plate. The wafer has not yet touched plate, and the wafer and the plate are about 2 cm apart from each other. The wafer is then heated to about 40℃. After about 10 seconds, the support wafer that falls into the plate is identified. At this moment, the wafer is in constant contact with the plate. Within 20 seconds, the wafer temperature rises to 115℃. This finding reveals not only a good uniformity, but also a good accumulation of all of the curves. The wafer remains in contact with the plate well, as shown in Figure 4.7.

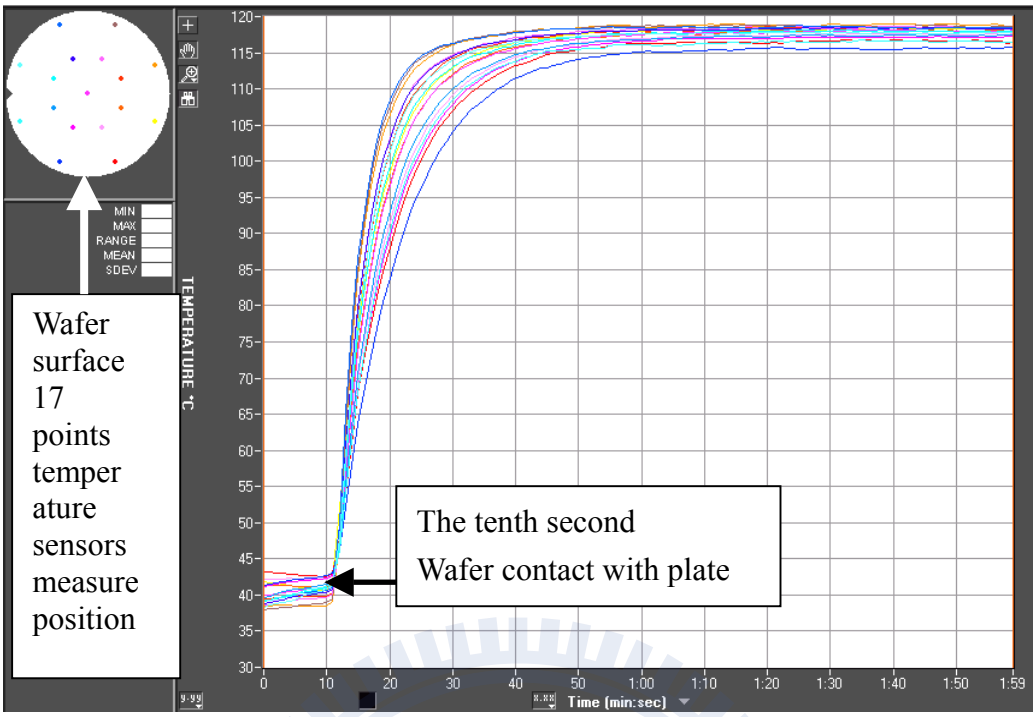

Figure 4.7 When wafer normal contact with the plate the wafer surface 17 points temperature good uniformity

From the surface temperature of the wafer, the minimum temperature is 113.2 ℃; the maximum temperature is 118.3℃, with a range of 5.11℃; and the average temperature of the wafer is 116.57℃, as shown in Figure 4.6. According to Figures 4.8~4.13, a larger tilt a shows broaden disperse distribution of the temperature curve. Moreover, a larger range implies less contact area between the wafer and the plate.

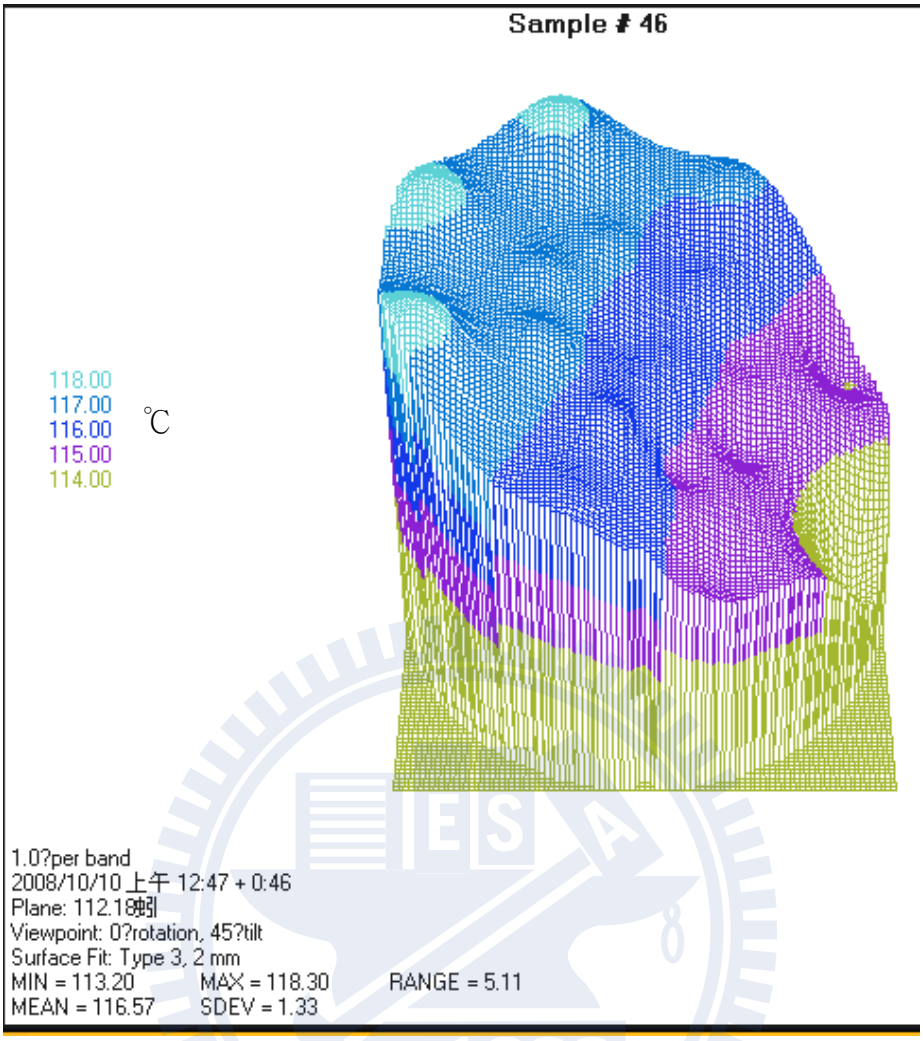

Figure 4.8 When wafer tilt gap=0 mm wafer surface temperature drop 5.11℃

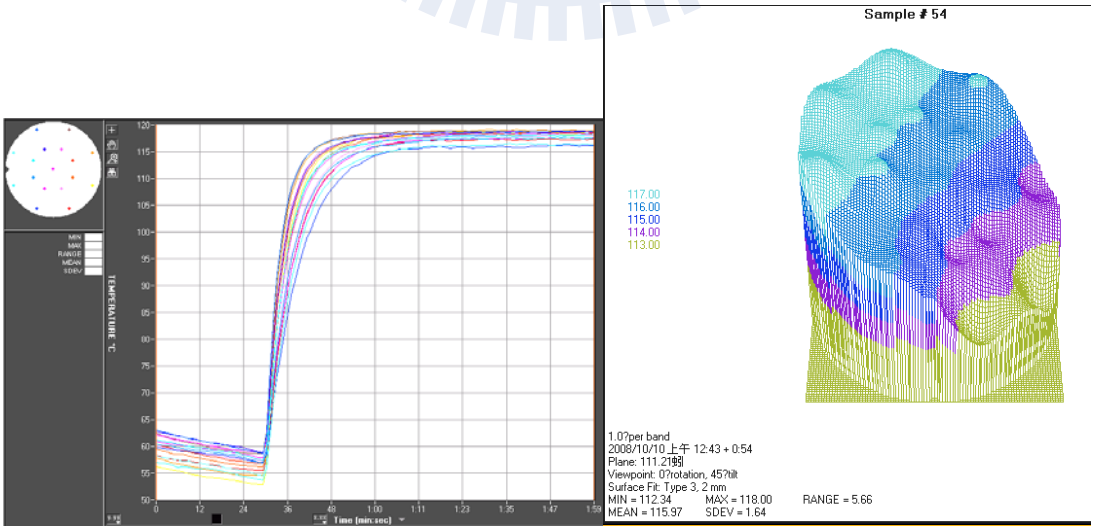

Figure 4.9 When wafer tilt gap=0.05 mm wafer surface temperature drop 5.66℃

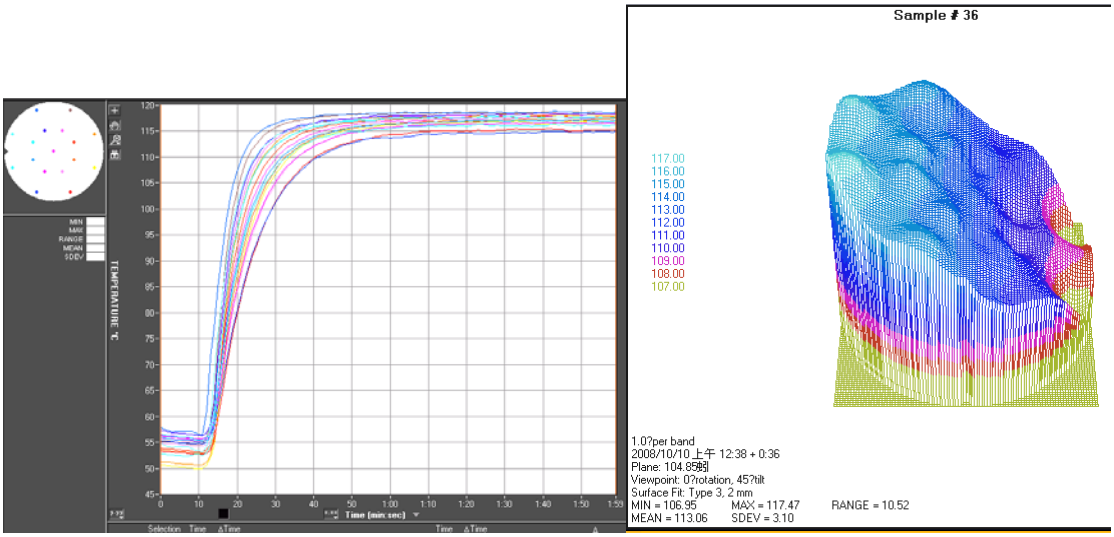

Figure 4.10 Wafer tilt gap=0.1 mm wafer surface temperature drop 10.52℃

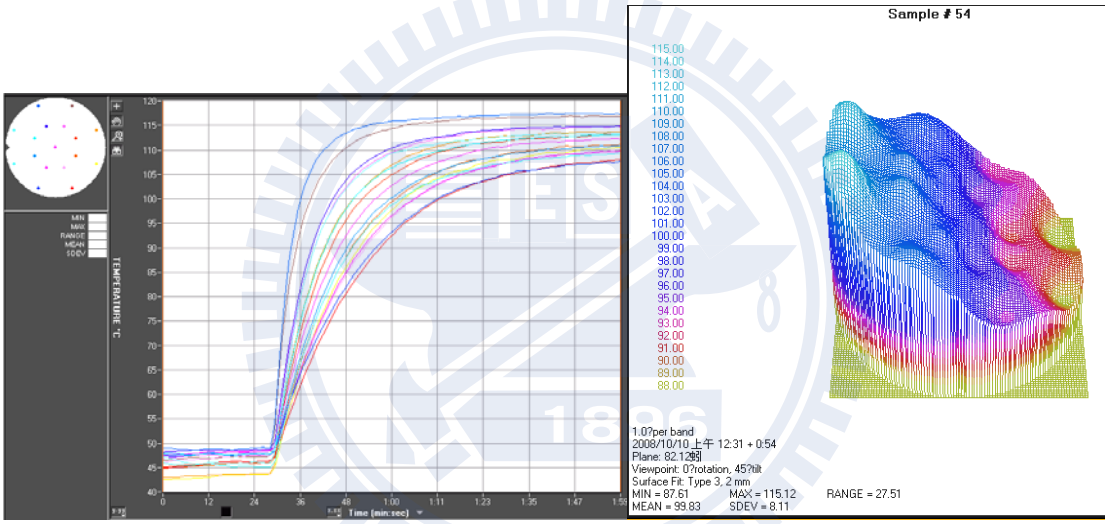

Figure 4.11 Wafer tilt gap=0.6 mm wafer surface temperature drop 27.51℃

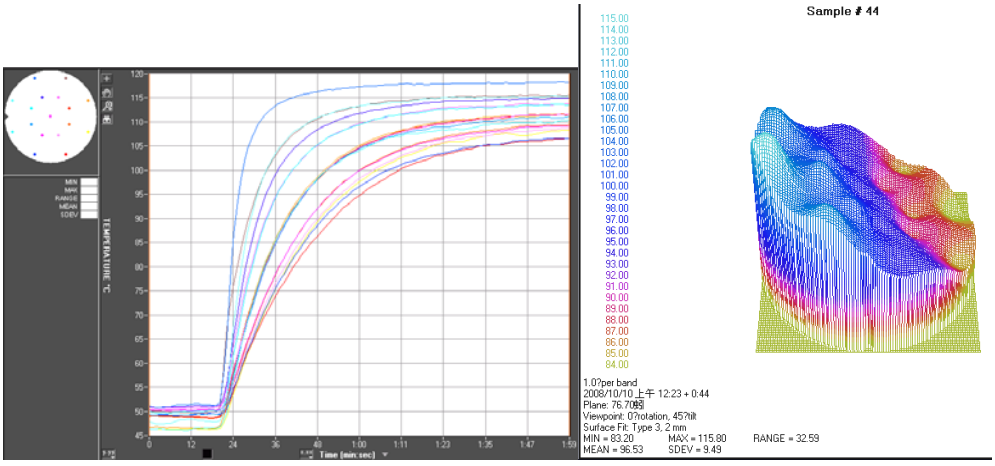

Figure 4.12 Wafer tilt gap=1.0 mm wafer surface temperature drop 32.59℃

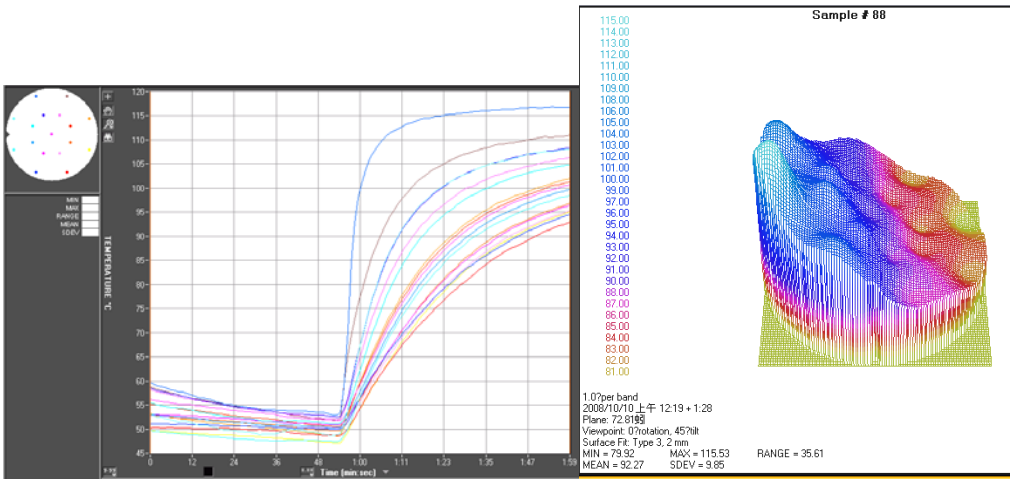

Figure 4.13 Wafer tilt gap=2.0 mm wafer surface temperature drop 35.61℃

When the wafer tilt is 2.5 mm, a time-lag must occur for the temperature to remain steady at 40℃. At the 36th second, wafer falls into the plate with the wafer still in contact with the plate. Although the wafer temperature has not reached 90℃, after one minute, the temperature curve is widely distributed. Figure 4.14, illustrates a small wafer and plate contact area, in which the energy can not be transferred from the plate to the wafer, resulting in a final temperature still under 100℃.

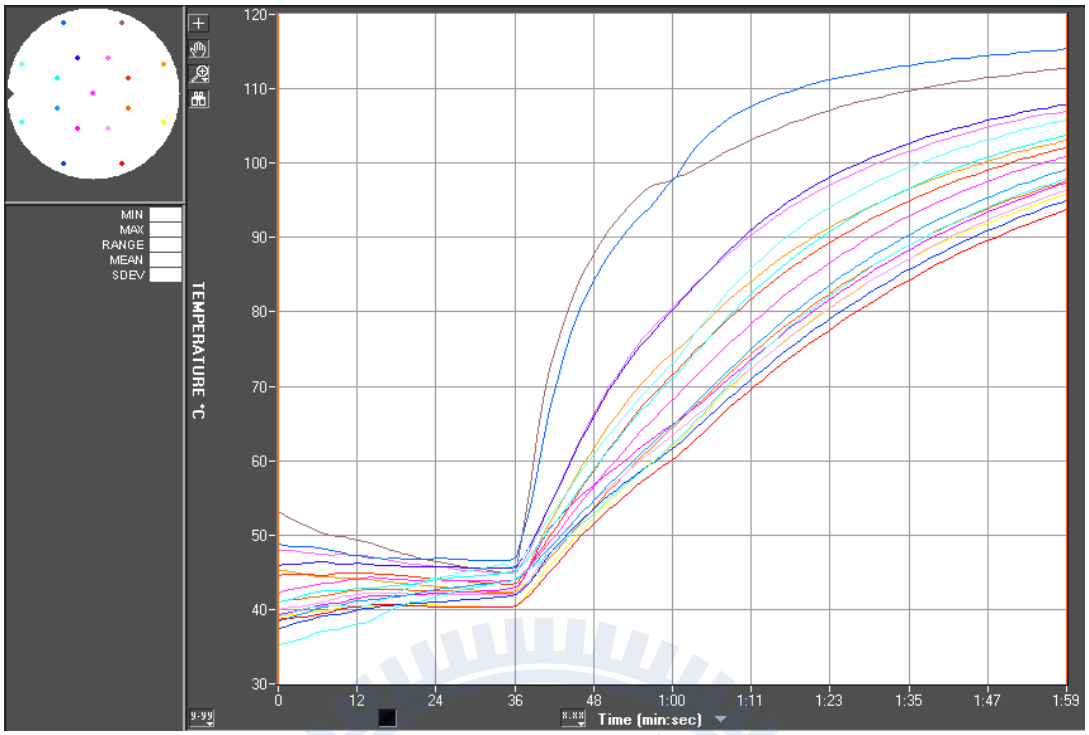

Figure 4.14 Wafer tilt gap=2.5 mm wafer surface 17 points temperature unbalanced

According to the surface temperature of the wafer, the minimum temperature is 60.43 ℃; the maximum temperature is 98.17℃, with a **r**ange of 37.74℃; and the average temperature of the wafer is 72.05℃. Moreover, the average surface temperature of the wafer is 44.52℃ *i.e.* lower than the normal wafer average temperature of 116.57 ℃, as shown in Figure 4.15

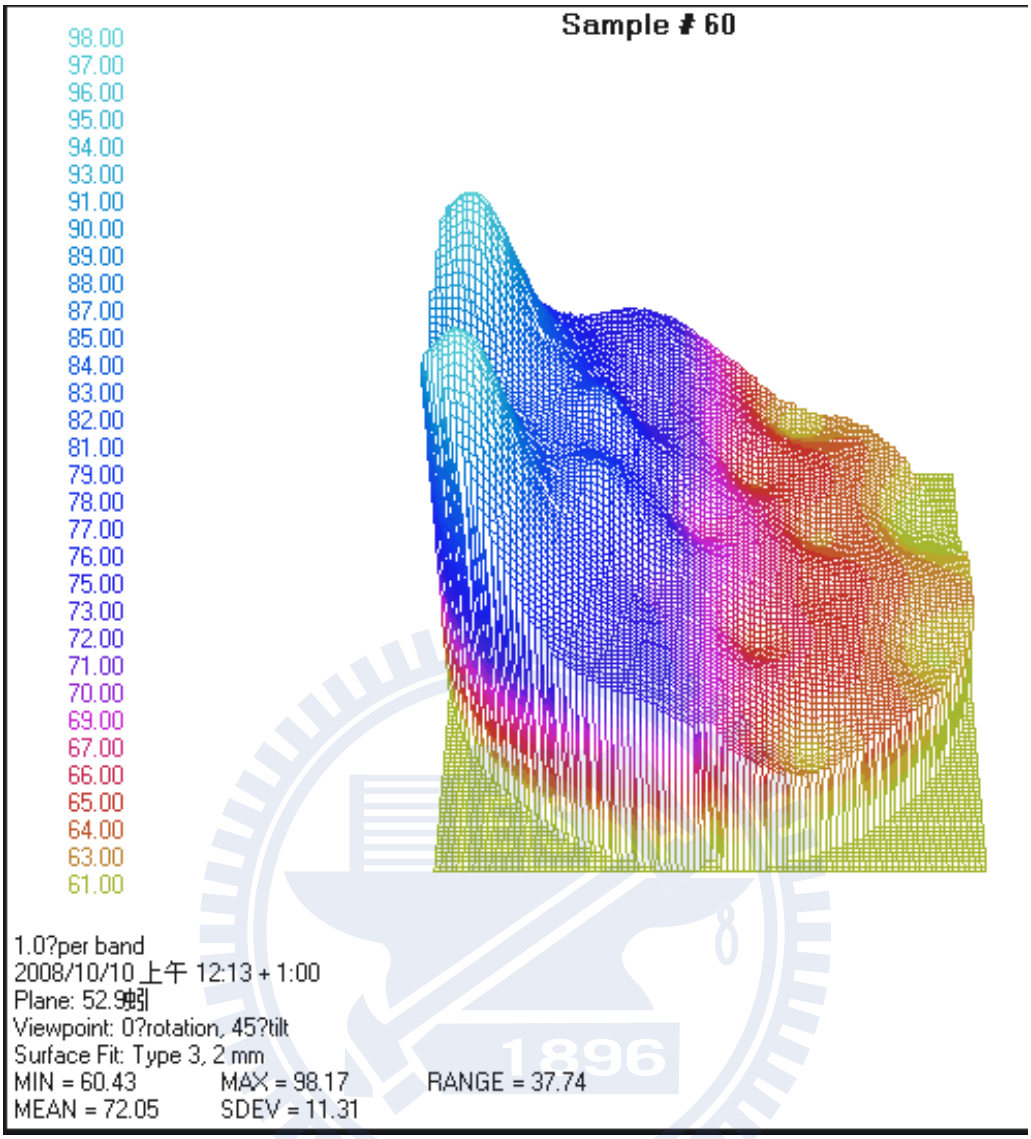

Figure 4.15 Wafer tilt gap=2.5 mm wafer surface temperature drop 37.74℃

4.1.2.2 ANSYS simulation temperature of wafer

The wafer temperature is simulated at an extremely small wafer tilt of 0.05 mm by using ANSYS software. As most of the wafer is in contact with the plate, the wafer surface temperature profile is not wide, ranging approximately between 116.03 ℃ and 120.03℃. The wafer temperature profile ranges by about 4℃, as shown in Figure 4.16.

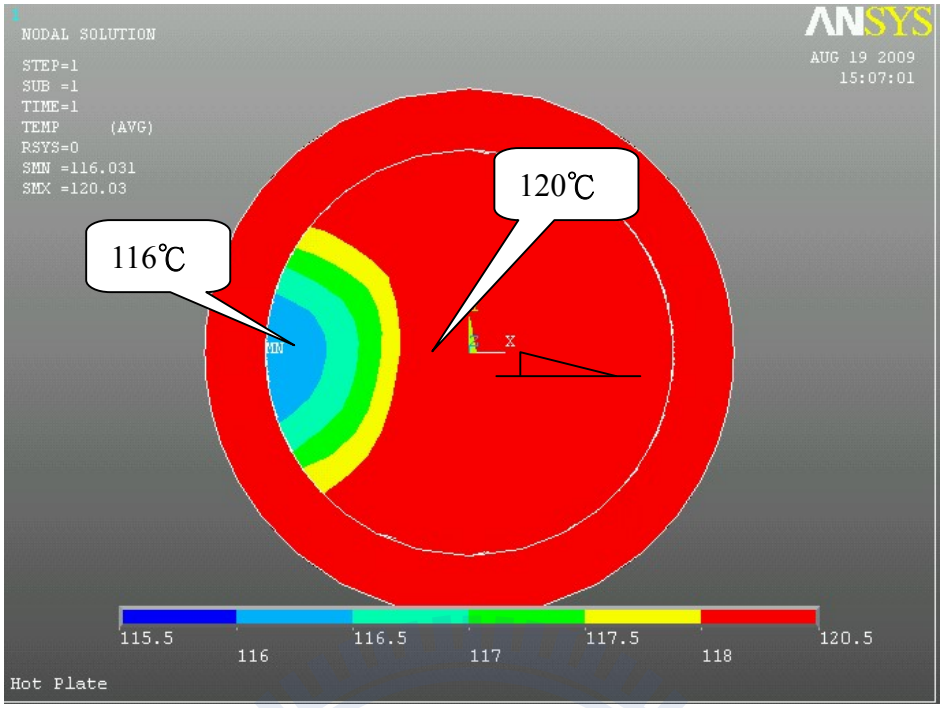

wafer tilt gap=0.05 mm, surface temperature dropped 4℃

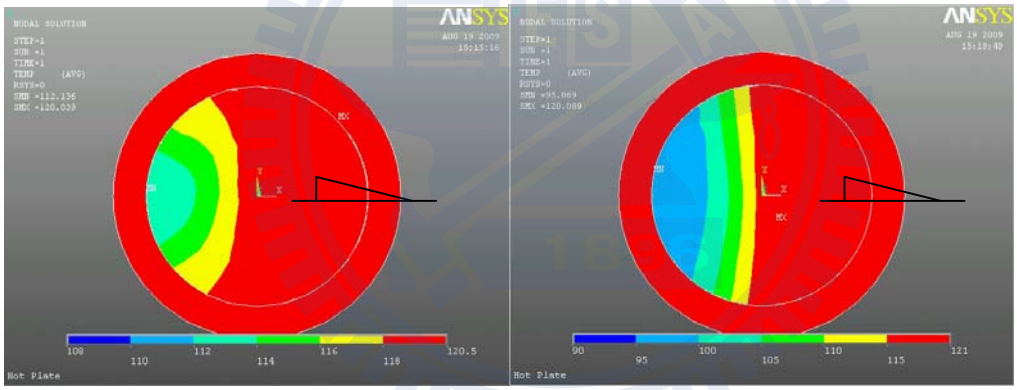

wafer tilt gap=0.1 mm, drop 7.9℃ **wafer tilt gap=0.5 mm, drop 25.5℃**

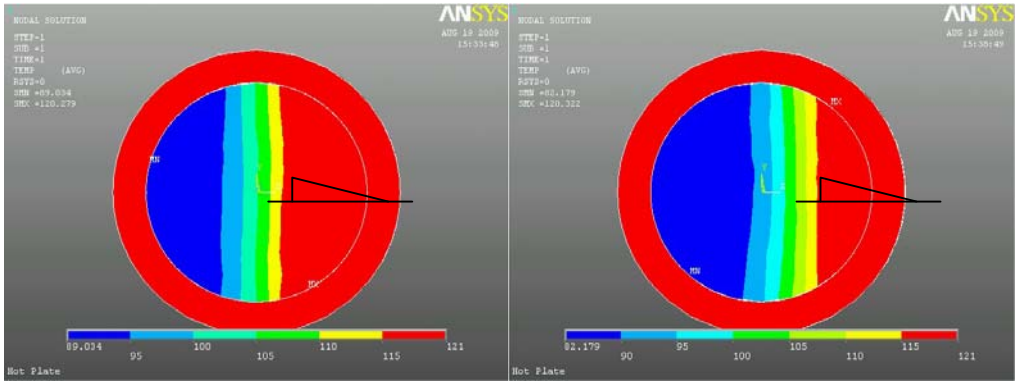

wafer tilt gap=1.0 mm, drop 31℃ **wafer tilt gap=2.0 mm, drop=36.9℃**

Figure 4.16 Simulation tilt gap from 0.05 to 2.0 mm wafer surface temperature

With a steeper slope, which reaches about 2.5 mm, the wafer is barely in contact with the plate, resulting in a wide wafer surface temperature profile between 82.02℃ to 120.0℃, as shown in Figure 4.17.

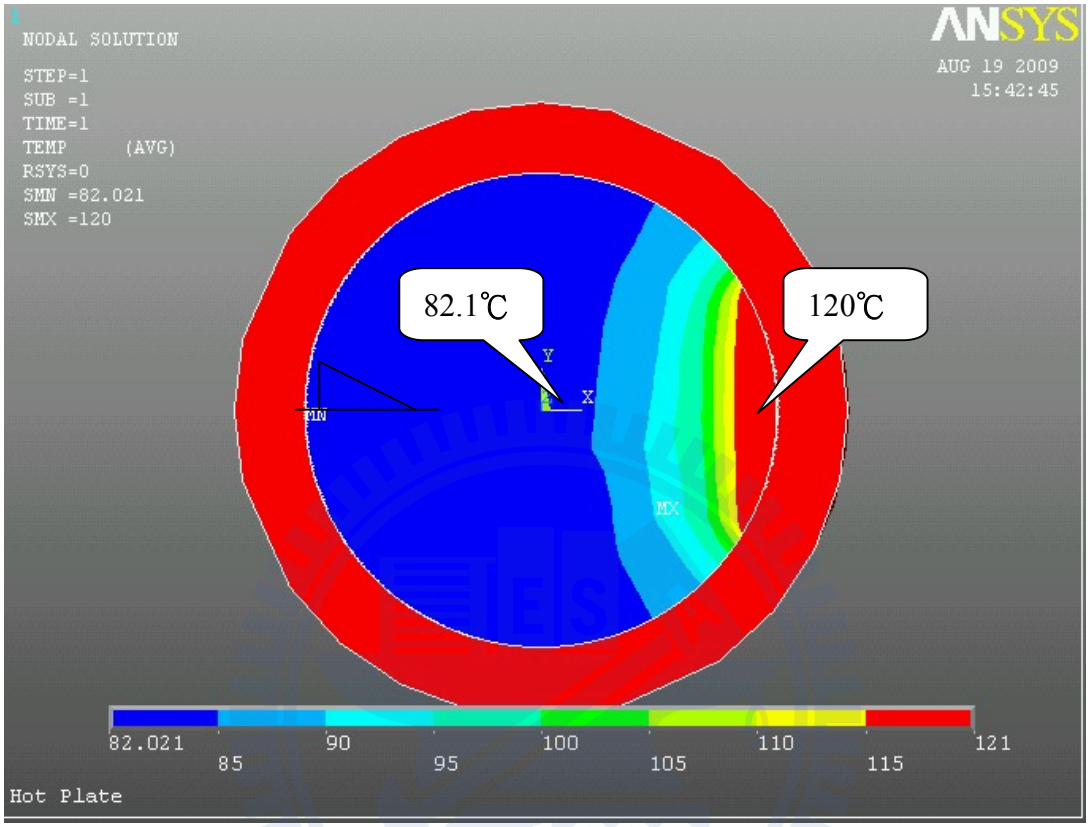

Figure 4.17 ANSYS simulation wafer tilt gap=2.5 mm, wafer surface temperature drop 38℃

4.1.2.3 Calculation of the simulation error

Figures 4.7-15 shows the surface temperature of an actual wafer. The simulated wafer surface temperature, as determined by the ANSYS software, is 120℃, *i.e.* similar to the one shown in Figures 4.16-17. The simulation condition is that for a plate at 120℃. Figure 4.18 compares the surface temperature of the real wafer with the simulated wafer surface, with a marginal error of ±2℃.

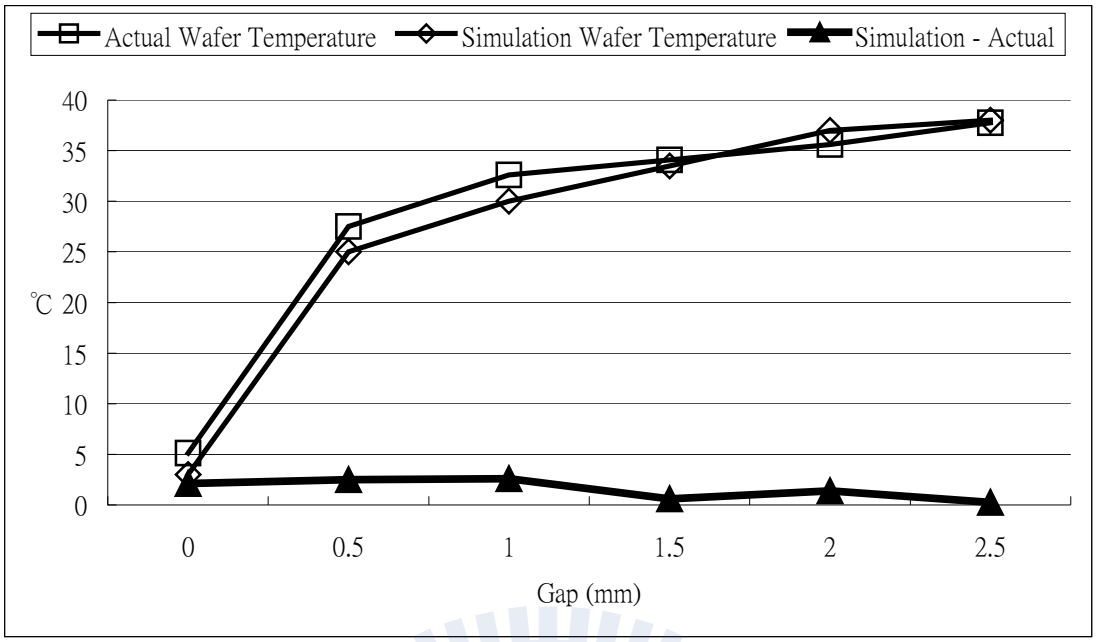

Figure 4.18 Simulation error of wafer temperature

This model can simulate an extremely narrow gap, especially when the spacer thickness is smaller than 400 μm. In an actual apparatus, placing the thin spacer on the plate and then taking it out of plate would be extremely difficult because it is likely to be crocked, subsequently making the experimental data unstable. Therefore, the ANSYS model is used to predict the wafer surface temperature and CD shift, when a particle makes the wafer tilt gap below 400 μm.

4.2 Analysis of wafer thickness

The thickness of three-type photoresists need to be determined. First, I-Line photoresist coating is normally thicker than DUV. I-Line uses Ar89 photoresist with a thickness at 12500Å. DUV248 uses SEPR203 with a thickness at 8000Å. DUV193 uses G48 with a thickness at 3000Å. The measuring points are recombined with the alignment of the wafer tilt direction, which is more convenient than the profit difference.

(1) For the XY position of the first wafer and the thickness value, the thickness value is inserted according to the actual position of the wafer;

(2) The maximum and minimum thicknesses are obtained and the relative position is confirmed as most remotely as possible, which is the wafer tilt direction;

(3) Measurement data is arranged from left to right deviation and from light to loud to arrange, as shown in Figure 4.19.

(4) Thickness data translation is performed at 12000 Å, by inserting from a minimum to maximum order of 1~25 materials, as shown in Figure 4.19.

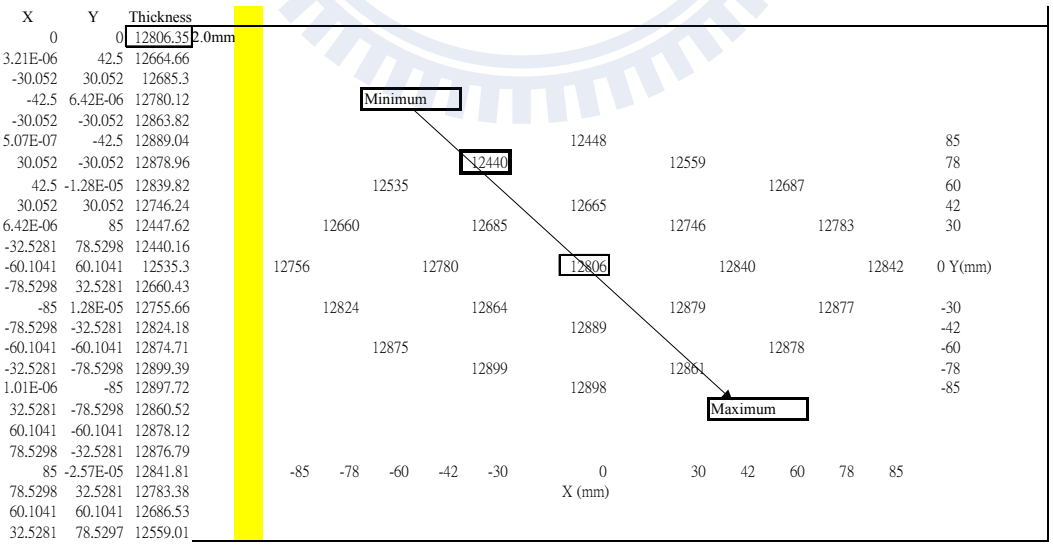

Figure 4.19 25 Positions of photoresist thickness measurement

(5) According to reference data for all wafers data up to 12000Å, thickness specifications of the I-line photoresist range from 12000Å to 12250Å, as shown in Figure 4.20;

(6) For wafers #1, #2, #3 and #4 with a wafer tilt gap of 0 mm, their thicknesses range from 12000 Å to 12050 Å, with good uniformity;

(7) For wafers #5, #6, #7 and #8 with a wafer tilt gap of 0.5 mm, their thicknesses range from 12000 Å to 12240 Å, in which the uniformity is worse but all within the range of designed specifications;

(8) For wafers #9 and #10 with a wafer tilt gap of 1.0 mm, their thicknesses range from 12000 Å to 12360 Å, which 50% of which is beyond the scope of designed specifications;

(9) For wafer #11 with a wafer tilt gap of 1.5 mm, the thickness ranges from 12000 Å to 12400 Å, which are all beyond the scope of designed specifications;

(10) For wafer #12 with a wafer tilt gap of 2.0 mm, the thickness ranges from 12000 Å to 12450 Å, which is totally out of specifications; and

(11) For wafers #13 and #14 with a wafer tilt gap of 2.5 mm, their thicknesses ranges from 12000 Å to 13097 Å, which are totally out of specifications.

4.2.1 I-Line photoresist thickness

Hi-thickness (12000Å) I-Line365 nm Ar89 photoresist is studied first. In the I-Line photoresist, when tilt range is within 0.5 mm, the thickness difference range is within specifications 250 Å. If the tilt increases to 1.0 mm, the thickness difference range increases above 250 Å, which is out of specifications, as shown in Figure 4.20.

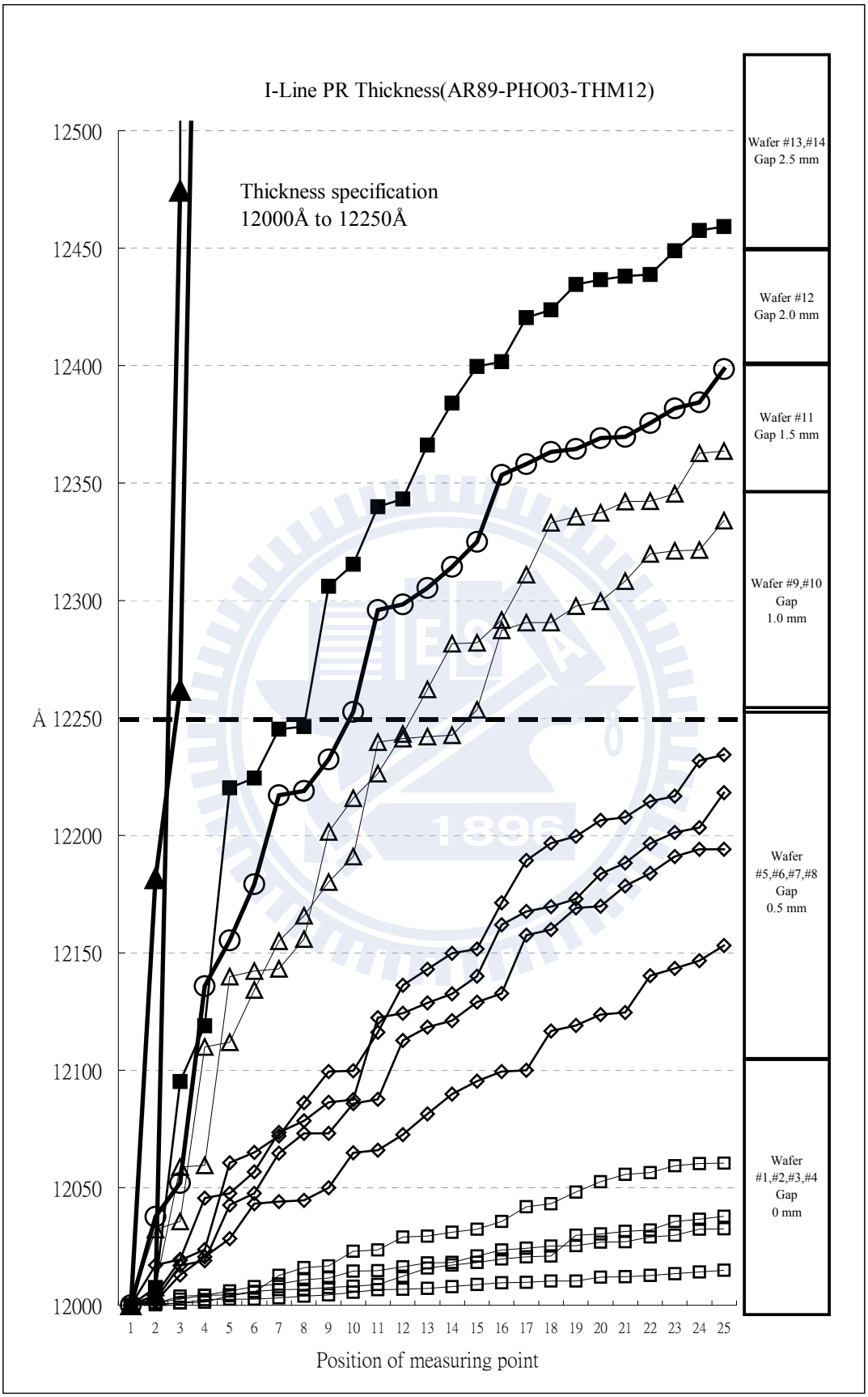

Figure 4.20 I-line photoresist thickness of wafer tilt gap from 0 to 2.5 mm

4.2.2 DUV 248 nm photoresist thickness

The second photoresist type is the intermediate thickness (8000Å) DUV248 nm SEPR203 photoresist. In the DUV photoresist, when the tilt range is within 0.1 mm, the thickness difference range is within specifications of 80 Å. If the tilt increases to 0.6 mm, the thickness difference range increases to 80~95Å; which is still within specifications (100Å). When the tilt increases to 0.6 mm, the thickness difference range increases above 100 Å, which is out of specifications, as shown in Figure 4.21.

(1) According to reference data for all wafers up to 8000Å, the photoresist thickness specifications range from 8000Å to 8100Å, as shown in Figure 4.21.

(2) For wafers #1~#10 with a wafer tilt gap of 0 mm, their thicknesses range from 8000 Å to 8050 Å with good uniformity;

(3) For wafers #11, #12 and #13 with a wafer tilt gap of 0.1 mm, their thicknesses range from 8000 Å to 8070 Å, which are all within specifications;

(4) For wafers #14 and #15 with a wafer tilt gap of 0.5 mm, their thicknesses range from 8000 Å to 8086 Å, which are all within specifications;

(5) For wafer #16 with a wafer tilt gap of 1.0 mm, their thicknesses range from 8000 Å to 8090 Å, which are all within specifications;

(6) For wafer #17 with a wafer tilt gap of 1.5 mm, their thicknesses range from 8000 Å to 8109 Å, which are partially out of specifications;

(7) For wafer #18 with a wafer tilt gap of 2.0 mm, their thicknesses range from 8000 Å to 8230 Å, which are partially out of specifications; and

(8) For wafer #19 with a wafer tilt gap of 2.5 mm, their thicknesses range from 8000 Å to 8235 Å, which are totally out of specifications.

According to our results, SEPR203 photoresist only slightly affects the thickness due to the wide specifications, which did not consider photoresist thickness.

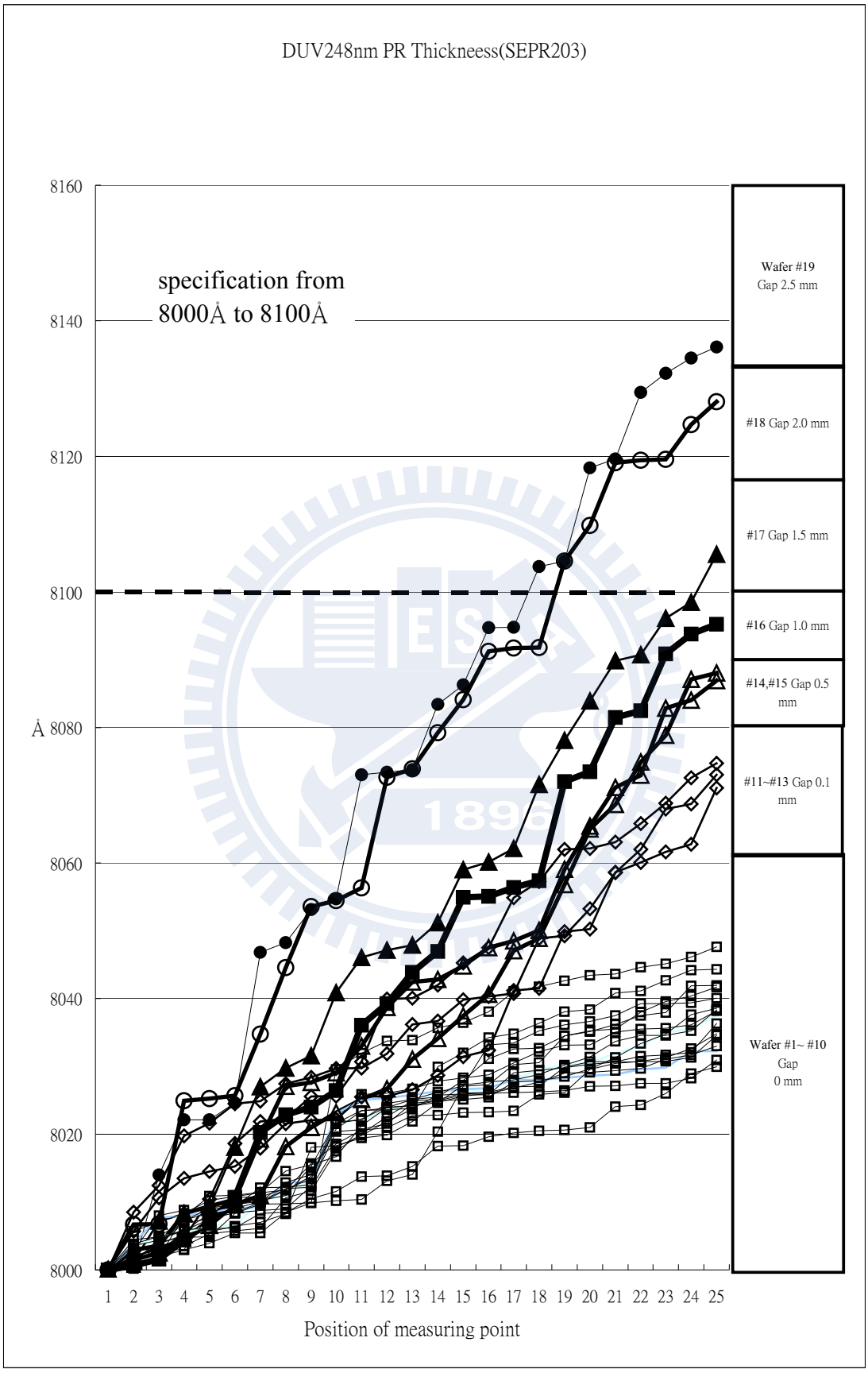

Figure 4.21 SEPR203 PR thickness of wafer tilt gap form 0 mm to 2.5 mm

4.2.3 DUV193 nm photoresist thickness

The third photoresist type is thin thickness (3000Å) DUV193 nm G48 photoresist. In the G48 photoresist, when the tilt range is within 0.5 mm, the thickness difference, which has a range of about 20 Å, is within specifications of 50 Å. If the tilt increases to 0.6 mm, the thickness difference range increases to 30 Å. The uniformity is slightly poor but still within a specification range designed at 50 Å. When the tilt increases to 2.0 mm, the thickness difference range increases above 80 Å, which is out of specifications, as shown in Figure 4.22.

(1) According to reference data for all wafers up to 3000Å, the thickness specifications of DUV 193 photoresist are from 3000Å to 3050Å;

(2) For wafers #1, #2 and #3 with a wafer tilt gap of 0 mm, their thicknesses range from 3000 Å to 3025 Å, with a good uniformity;

(3) For wafers #4 and #5 with a wafer tilt gap of 0.5 mm, their thicknesses range from 3000 Å to 3030 Å, with a good uniformity;

(4) For wafer #6 with a wafer tilt gap of 1.0 mm, their thicknesses range from 3000 Å to 3048 Å, which are within specifications;

(5) For wafer #7 with a wafer tilt gap of 2.0 mm, their thicknesses range from 3000 Å to 3075 Å, which are partially out of specifications; and

(6) For wafer #8 with a wafer tilt gap of 2.5 mm, their thicknesses range from 3000 Å to 3085 Å, which are partially out of specifications.

According to our results, G48 photoresist only slightly affects the thickness due to the wide specification, which does not consider the photoresist thickness.

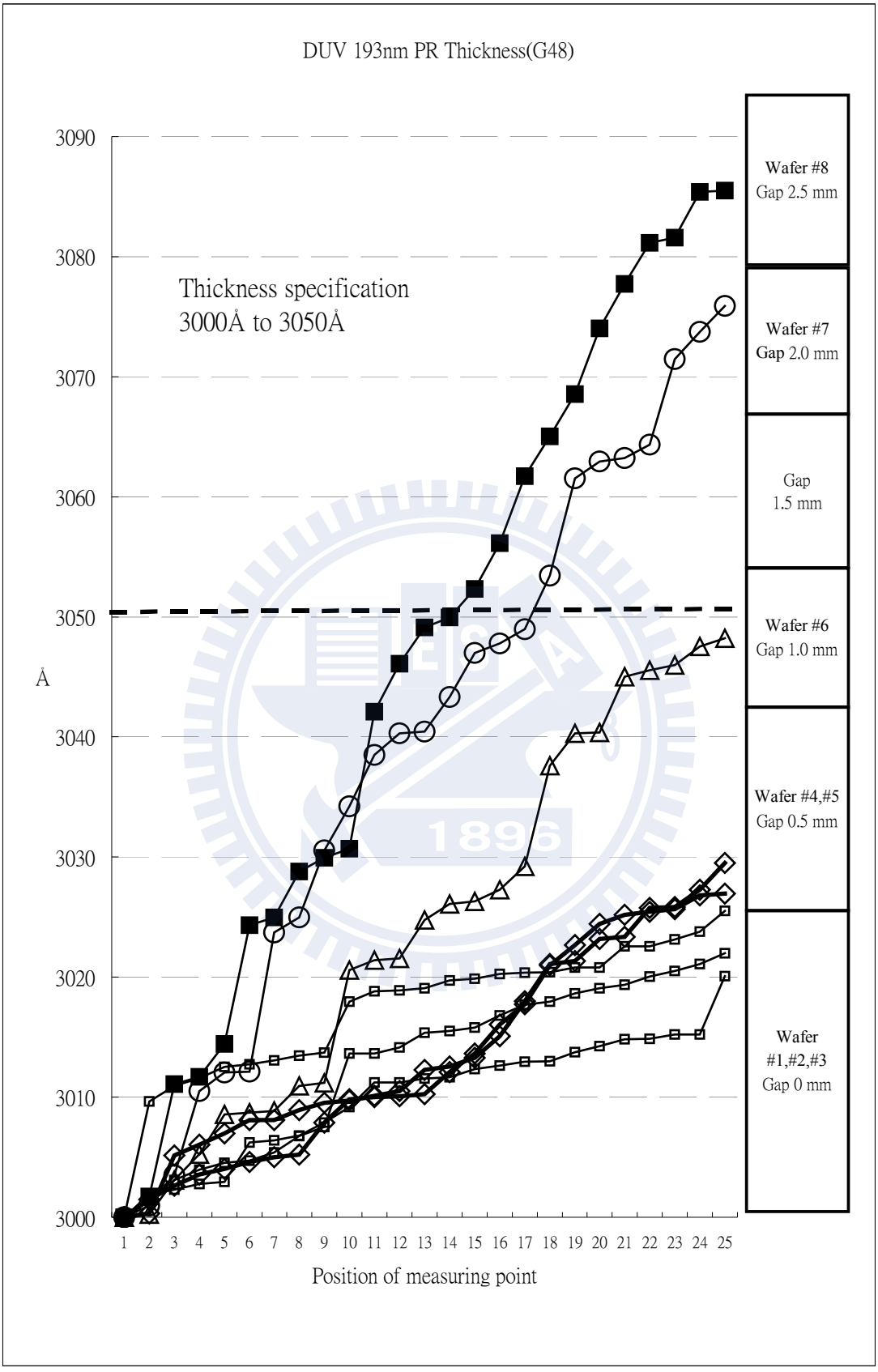

Figure 4.22 G48 photoresist thickness of wafer tilt gap form 0 mm to 2.5 mm

Closely examining different materials for the three photoresist types reveals that a greater wafer tilt implies a larger difference in the thickness range. As is roughly estimated, thickness influences a wafer tilt, with a greater thickness influencing the wafer tilts even more. However, this behavior still has not been verified.

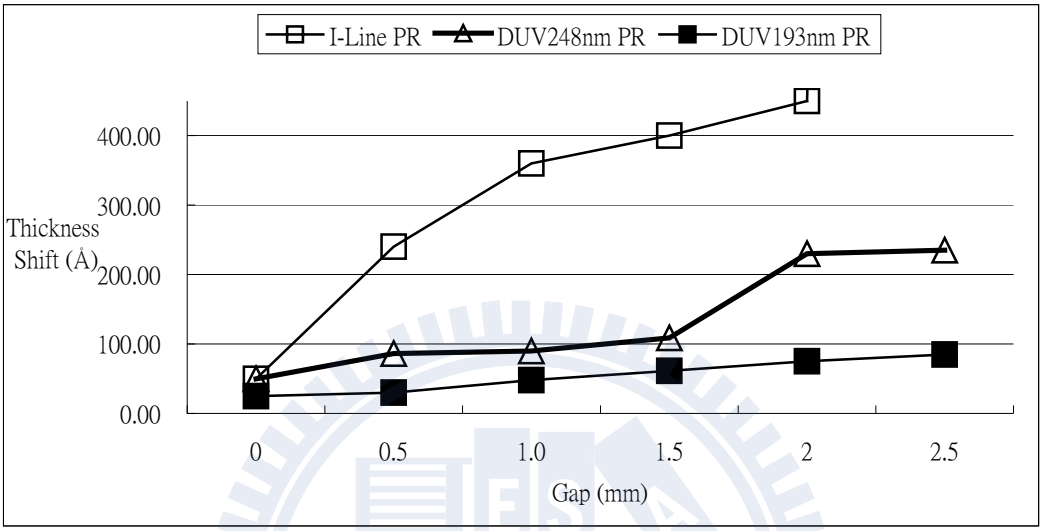

Figure 4.23 Compare three PRs thickness

The thickness factor in Figure 4.23 is obtained once again, and the range and thickness rate are used for analysis. The obvious I-Line is found to be greater than DUV193 and DUV248, as shown in Figure 4.24.

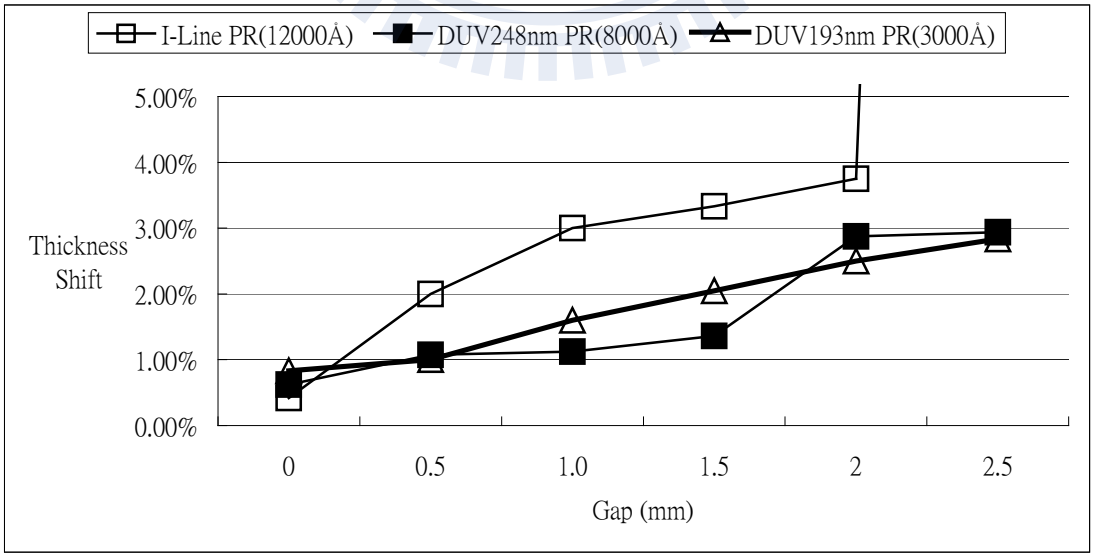

Figure 4.24 Compare three PRs thickness shift rate

4.3 Critical dimension analysis

4.3.1 CD analysis of I-line PR

The I-Line 0.35um photoresist specification is 250 Å, as the wafer tilt is smaller than the situation of 0.1 mm. It does not significantly affect CD, nor causes it to be out of specification, as shown in Figure 4.25. Since the CD specifications of the I-Line photoresist are relatively wide, tolerance for the wafer tilt is relatively high such that its influence on an extremely small CD should not be of concern.

(1) For wafers #1~#5 with a wafer tilt gap of 0 mm, the line CDs range from 2850 Å to 3123 Å, which are in specification with a good uniformity;

(2) For wafers #6~#8 with a wafer tilt gap of 0.5 mm, the line CDs range from 2850 Å to 3251Å, in which the uniformity is slightly poor but can still be up to specifications requirements;

(3) For wafers #9 and #10 with a wafer tilt gap of 1.0 mm, the line CDs range from 2850 Å to 3320 Å, in which the uniformity is worse and goes beyond the specifications requirements;

(4) For wafer #11 with a wafer tilt gap of 2.0 mm, the line CDs range from 2850 Å to 3426 Å, in which one point is out of specifications; and

(5) For wafer #12 with a wafer tilt gap of 2.5 mm, the line CDs range from 2850 Å to 3601 Å, in which 6 points are out of specifications.

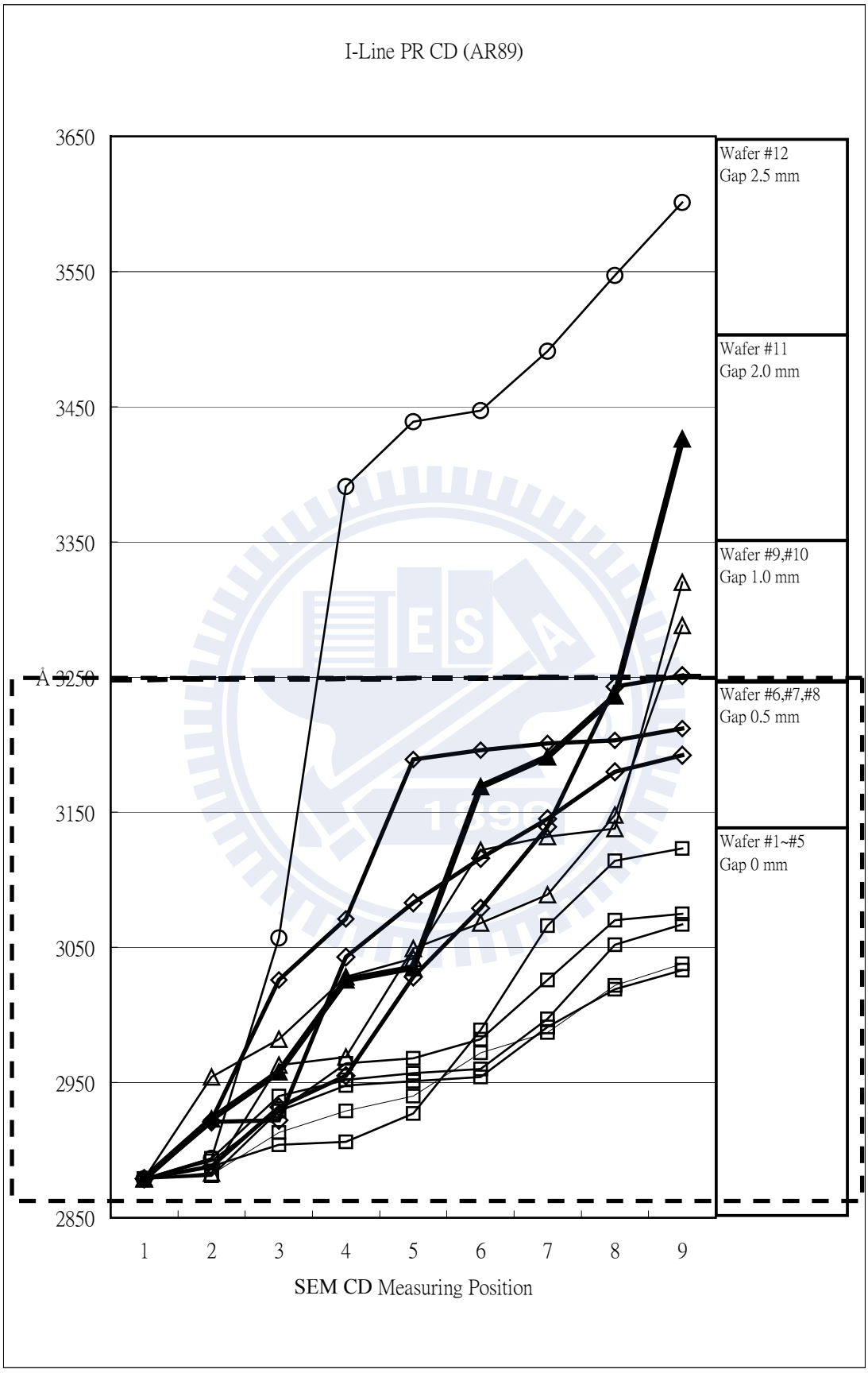

Figure 4.25 I-line photoresist CD impact of wafer tilt gap form 0 to 2.5 mm

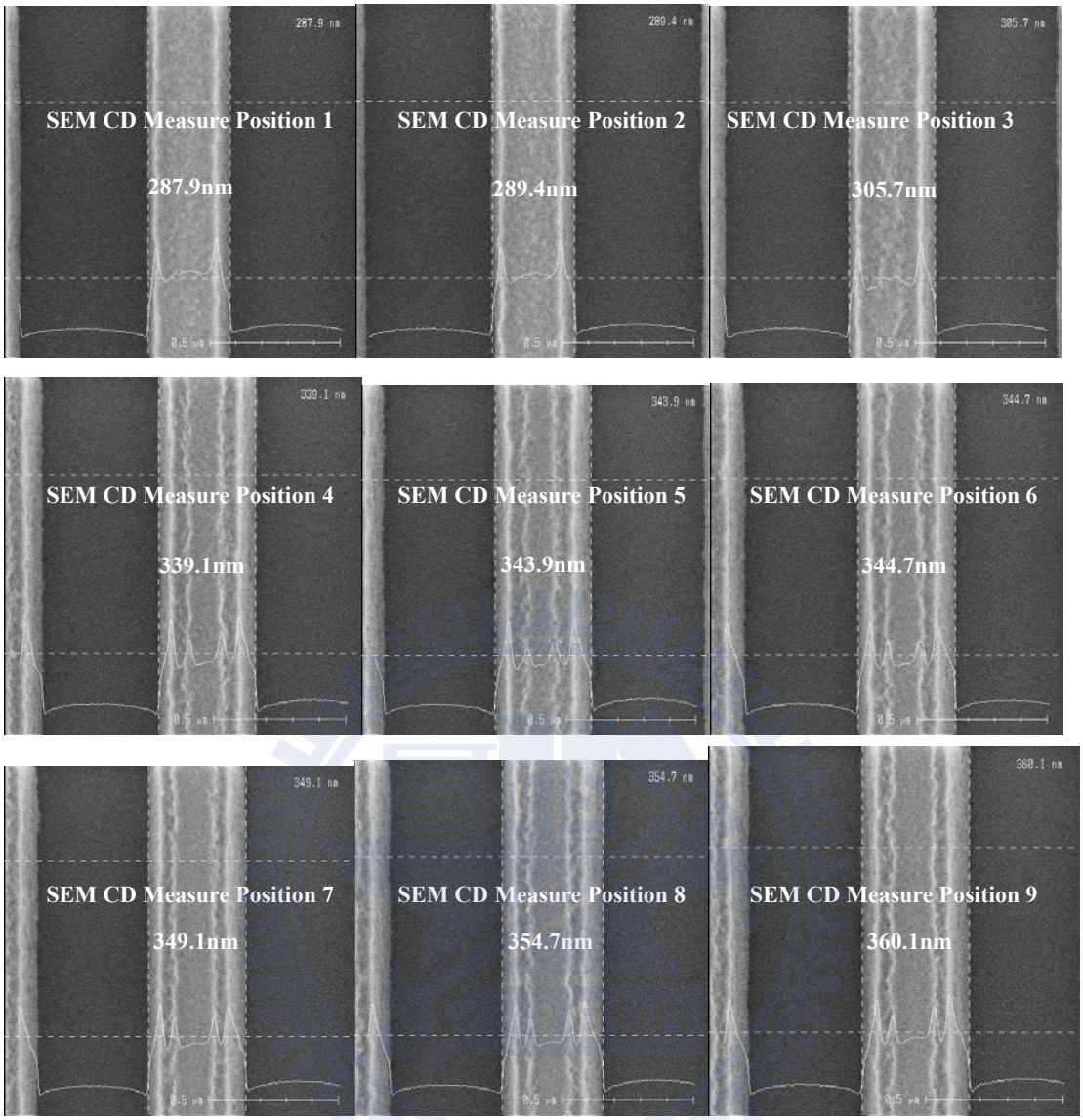

Figure 4.26 I-line photoresist CD impact of wafer tilt gap 2.5 mm

4.3.2 CD analysis of DUV248 nm SEPR203 photoresist

DUV 248 nm SEPR203 photoresist specification is 2925 Å ~3075 Å, as wafer tilt is smaller than the condition of 0.3 mm. Such a condition neither affects CD significantly, nor causes it to be out of specification as shown in Figure 4.27.

(1) For wafers #1~#4 with a wafer tilt gap of 0 mm, the line CDs range from 2950 Å to 3025 Å, which are in specification with a good uniformity;

(2) For wafers #5~#12 with a wafer tilt gap of 0.5 mm, the line CDs range from 2950 Å to 3090Å, which are some points out of specifications;

(3) For wafers #13 and #14 with a wafer tilt gap of 1.0 mm, the line CDs range from 2950 Å to 3150 Å, in which one point is out of specifications;

(4) For wafer #15 with a wafer tilt gap of 2.0 mm, the line CDs range from 2950 Å to 3175Å, in which all points are out of specifications; and

(5) For wafer #16 with a wafer tilt gap of 2.5 mm, the line CDs range from 2950 Å to 3180Å, in which all points are out of specifications.

When the wafer tilt is greater than 0.1 mm, CD goes beyond specifications ±50 Å. A situation in which all CD values are above the target, may be owing to that the PB photoresist does not harden sufficiently. When the making has a slight drift phenomenon in the film of photoresist, this drift phenomenon becomes more violent and the PEB hot energy causes the H^+ to move more violently, as shown in Figure 4.27.

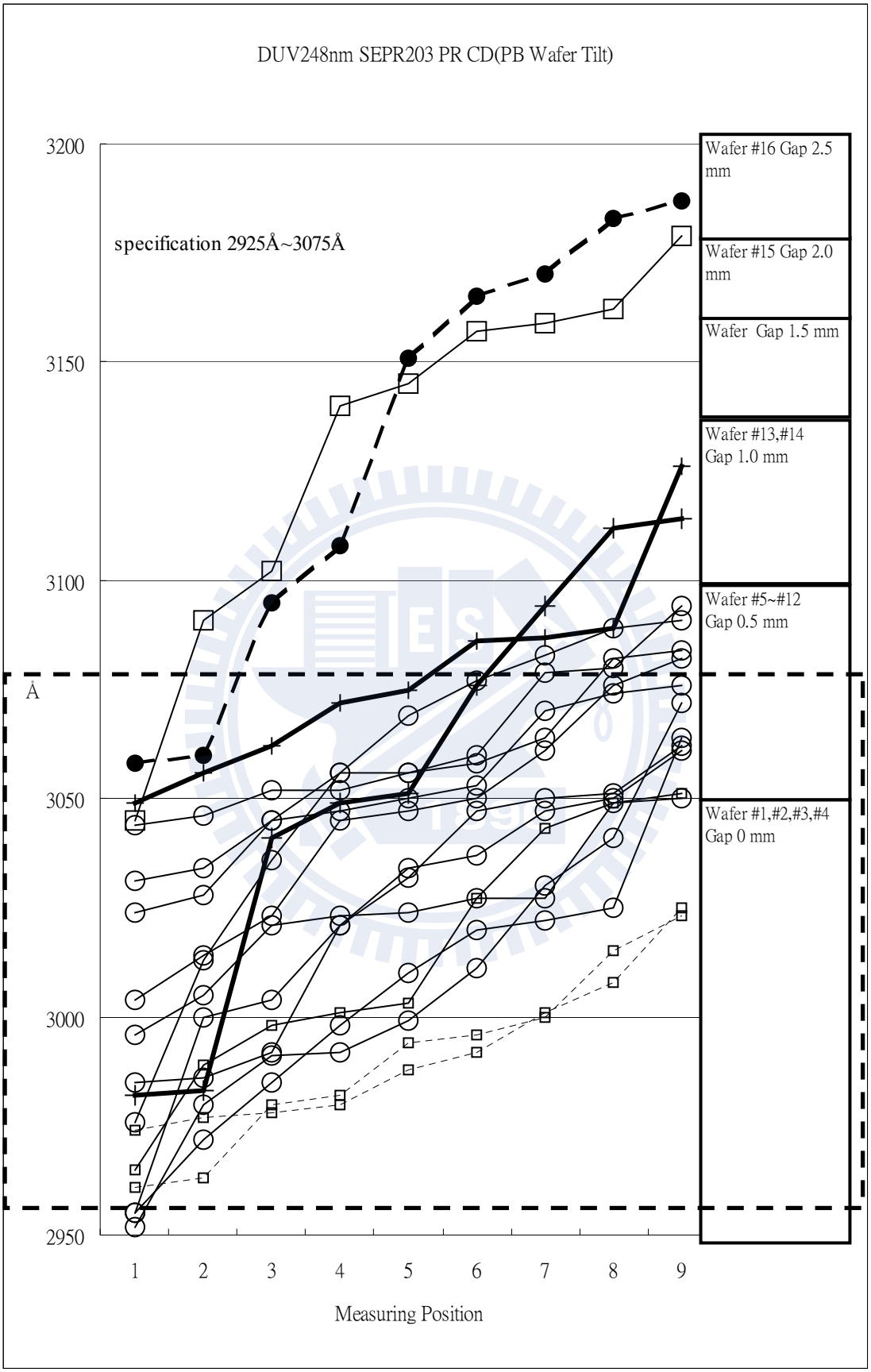

Figure 4.27 SEPR203 photoresist PB CD impact of wafer tilt gap 0 to 2.5 mm

The micro flow phenomenon in a photoresist film is attributed to a situation in which photoresist PB hardens insufficiently; after exposure, the micro flow still exists. It causes the exposed area and unexposed area interface to mix together, Due to the proton sour H^+ micro flow, a slight drift in position occurs and heat energy is generated for the next PEB process. As for the rapid micro flow phenomenon, in which the micro flow does not run in a certain direction, although H^+ inside the micro flow does not influence CD, but H^+ of the outward micro flow causes CD to expand at about 13 nm, as shown in Figure 4.28.

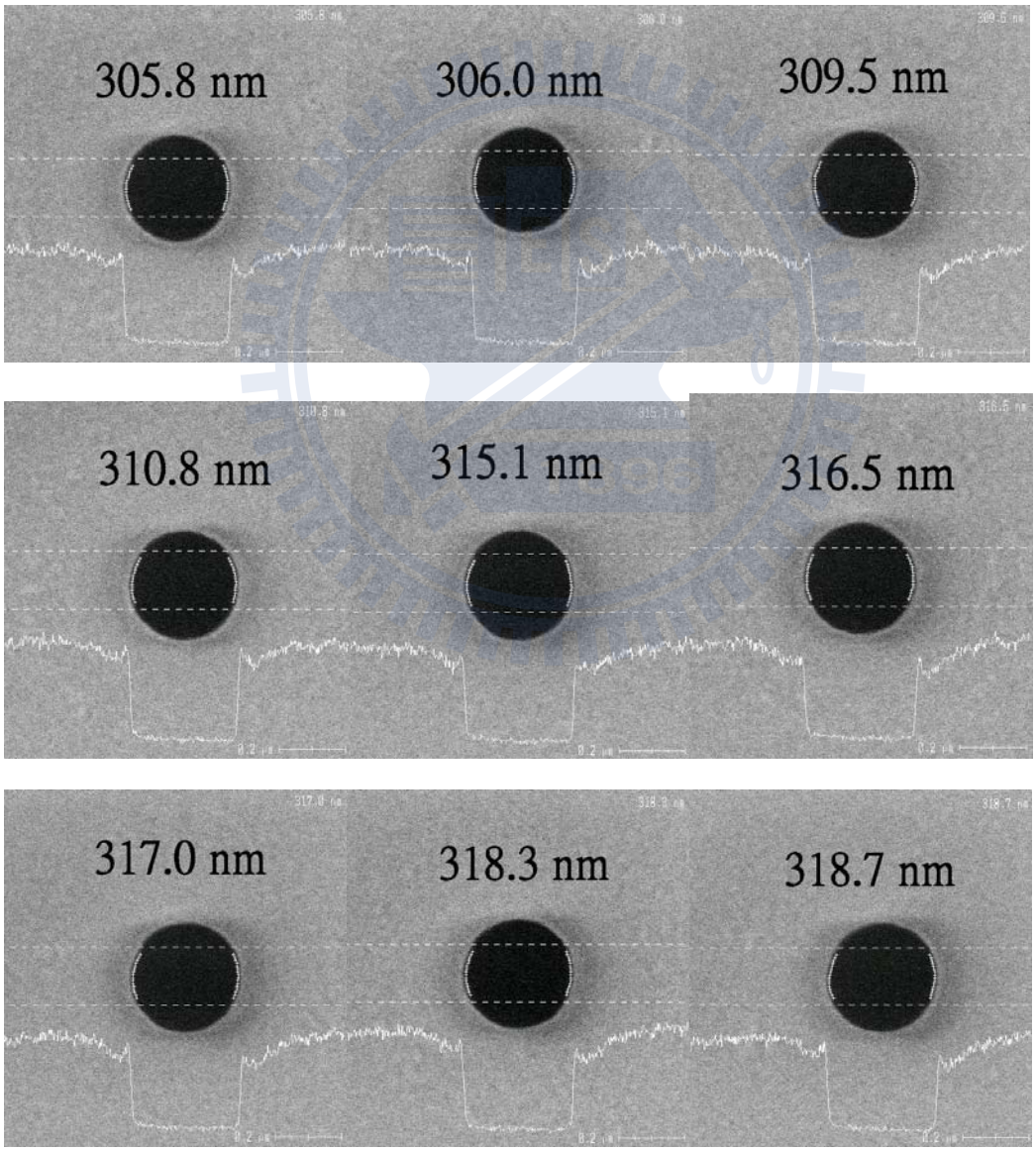

Figure 4.28 SEPR203 PB Wafer tilt, hole image

The DUV 248 nm SEPR203 photoresist SEM CD measurement, there are 9 points uniformity measure as shown in Figure 4.29.

(1) For wafer #1 with a wafer tilt gap of 0 mm, the line CDs range from 2955 Å 3035 Å, which are in specifications with a good uniformity;

(2) For wafers #2 and #3 with a wafer tilt gap of 0.5 mm, the line CDs range from 2939 Å to 3048Å, which are in specifications;

(3) For wafer #4 with a wafer tilt gap of 1.0 mm, the line CDs range from 2906 Å to 2911 Å, which are partially out of specifications;

(4) For wafer #5 with a wafer tilt gap of 1.5 mm, the line CDs range from 2892 Å to 3037Å, which are partially out of specifications;

(5) For wafer #6 with a wafer tilt gap of 2.0 mm, the line CDs range from 2879 Å to 3174Å, which are partially out of specifications; and

(6) For wafer #7 with a wafer tilt gap of 2.5 mm, the line CDs range from 2838 Å to 3122Å, which are partially out of specifications.

When the wafer tilt is greater than 0.1 mm and the CD goes beyond specifications ±50Å, all CDs can be distributed in a wide range. Targeted distribution from the start leads to a situation under the target, *i.e.* an insufficient phenomenon caused by heat energy. Excessive heat energy causes over targeting, as plate ΔT does not drop as expected, as shown in Figure 4.29.

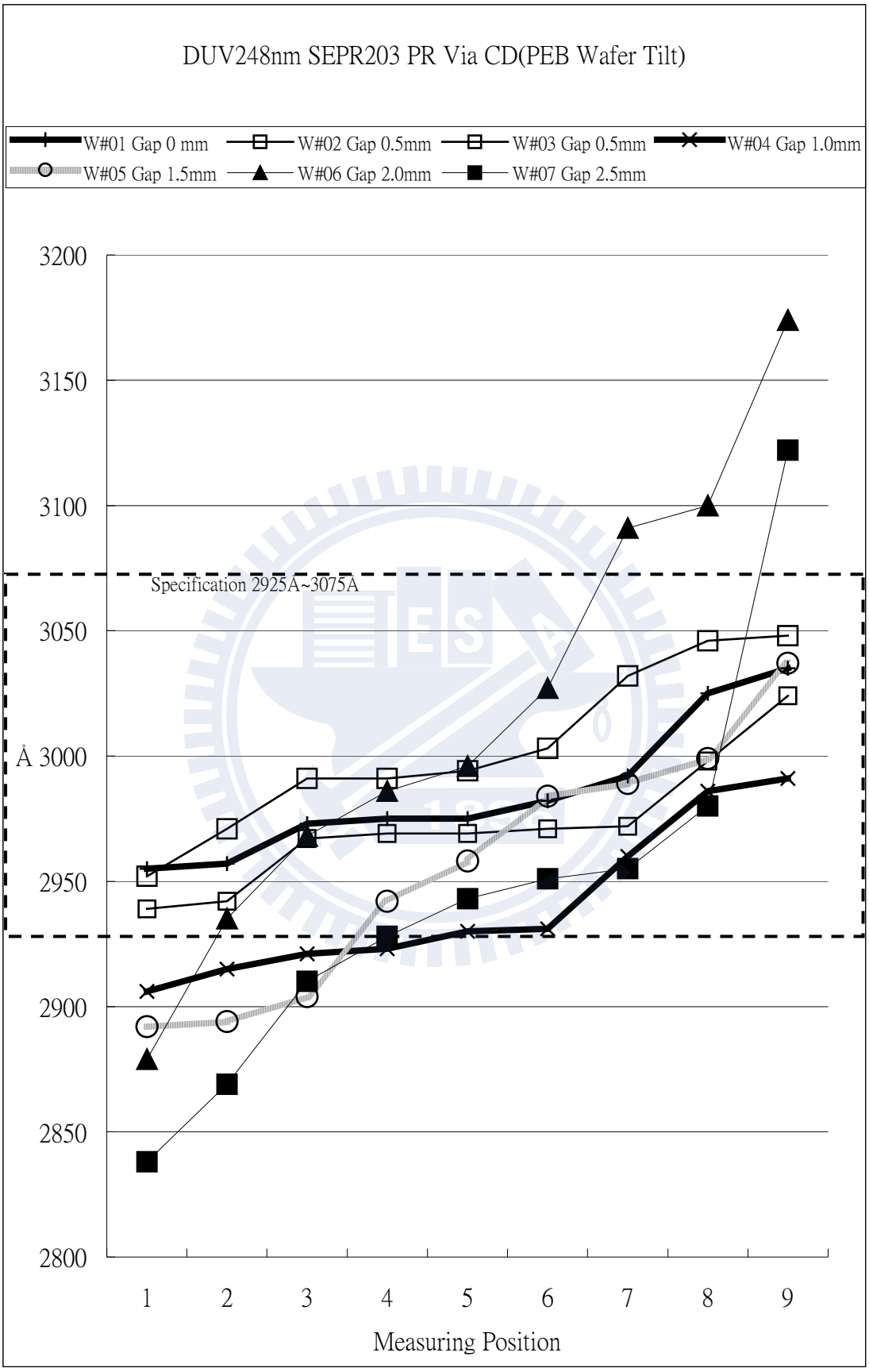

Figure 4.29 SEPR203 photoresist PEB CD impact of wafer tilt gap 0 to 2.5 mm

When PEB is insufficient, CD of 2879 Å is lower than target 3000 Å, with a difference of 121 Å because proton H^+ must have sufficient heat energy to proceed with the chain reaction. The contact area between a wafer and plate is relatively small. A situation in which the area is not large to consume heat causes a high temperature and excessive baking. Such conditions lead to proton acid H^+ with an excessive amount of heat energy to proceed with the chain reaction, causing CD to lean towards it. In addition, it is higher than target 100 Å, as shown in Figure 4.30.

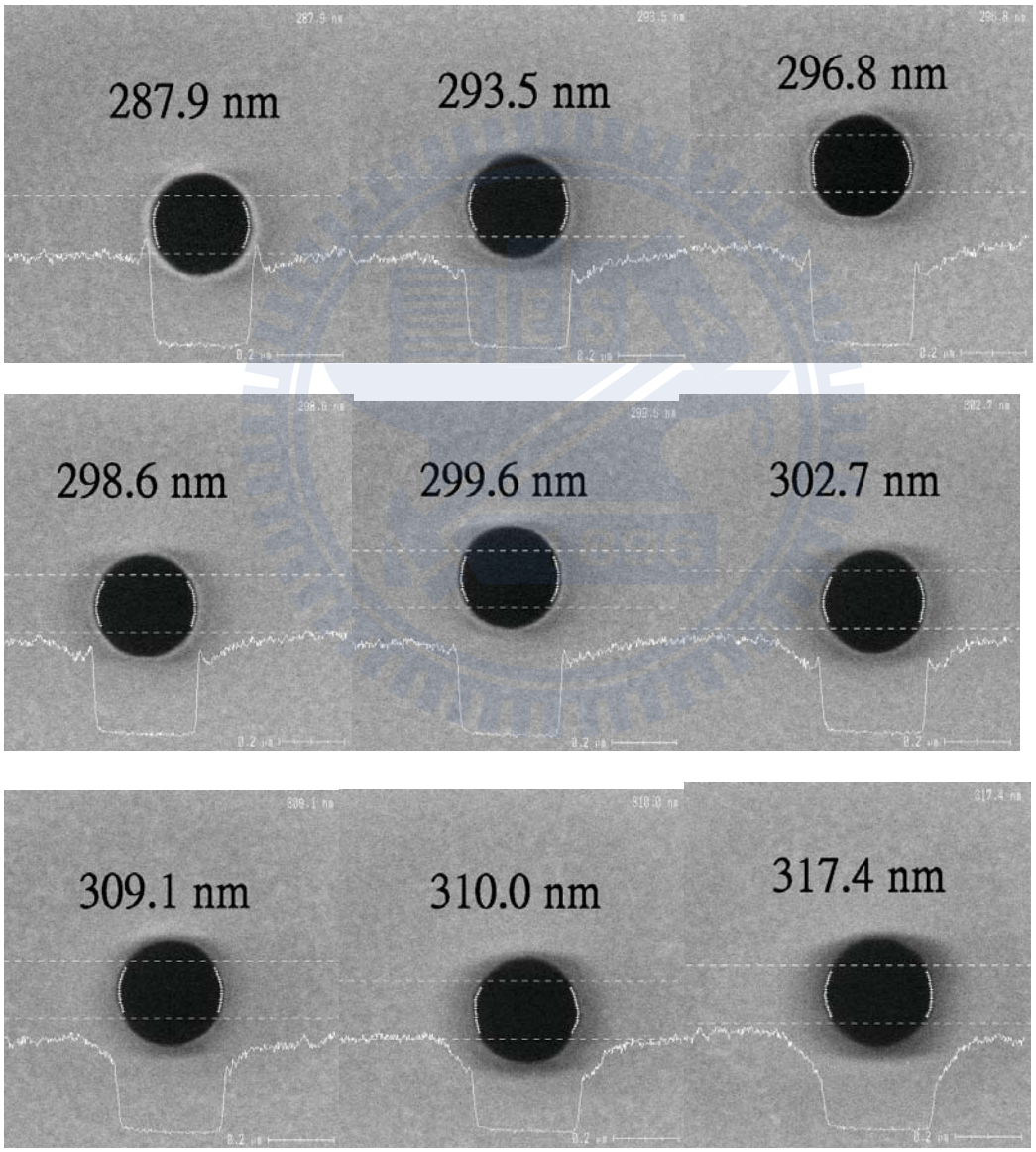

Figure 4.30 SEPR203 photoresist PEB wafer tilt hole image

4.3.3 DUV193 nm G48 photoresist CD

According to Table 4.3, this photoresist is more sensitive to CD, because many samples do not show a pattern. Because the feature size is reduced to 1000 Å, the line distance increases and reaches 1200 Å when it's at 0.1 mm tilt. Restated, the line is wide and leaves only 800Å. The estimated wafer tilt line might be reach 400Å at a distance of 0.6 mm in advance. Absorbing the insufficient area between the wafer and photoresist can lead to bursting and complete dissolution of the developer when no pattern is available.

Table 4.3 G48 photoresist PB Spacer CD impact of wafer tilt gap 0 to 0.1 mm

PB wafer tilt	SEM Spacer CD measuring (Å)									DUV193nm G48 PR Spacer CD impact (Å)					
	Pos 1	Pos 2	Pos 3	Pos 4	Pos 5	Pos 6	Pos 7	Pos 8	Pos 9	AVERAGE	Max	Min	Max-Min	Decrease	Average
2.0 mm	*	*	*	*	*	*	*	*	*	"*" Have no pattern					
1.0 mm	*	*	*	*	*	*	*	*	*	"*" Have no pattern					
0.5 mm	*	*	*	*	*	*	*	*	*	"*" Have no pattern					
0.5 mm	*	*	*	*	*	*	*	*	*	"*" Have no pattern					
0.1 mm	1086	1082	988	1068	1112	1090	1038	1065	1195	1080.4	1195	988	207	80.4	
0.1 mm	1003	1022	1153	1066	1052	959	1033	1134	1082	1056.0	1153	959	194	56.0	68.22222
0 mm	1011	1046	998	1058	1048	1042	1074	978	1042	1033.0	1074	978	96	33.0	
0 mm	975	966	944	921	929	970	971	943	975	954.9	975	921	54	-45.1	-6.05556

Spacer width increases by 68Å when the wafer tilt is 0.1 mm, as shown in Table 4.4. The situation contrast with pre bake, which does not have a pattern due to its relatively lower amount of measurement data. Since 900Å leaves a 0.6 mm tilt from the line distance, the line must be sufficiently wide to contain 1100 Å to ensure a remaining pattern. Notably, the 1.0 mm tilt of the proton acid H^+ on the wafer tilt 1.0 mm has too low of a heat energy to carry out the chain reaction. Additionally, with the insufficient solubility, the entire process can not be dissolved by the developer, resulting in a pattern-less situation.

Table 4.4 G48 photoresist PEB Spacer CD impact of wafer tilt gap 0 to 0.5 mm

PEB wafer tilt gap(mm)	SEM Spacer CD measuring (Å)									DUV193nm G48 PR Spacer CD impact (Å)					
	Pos 1	Pos 2	Pos 3	Pos 4	Pos 5	Pos 6	Pos 7	Pos 8	Pos 9	AVERAGE	Max	Min	Max-Min	Increase	Average
2.0 mm	*	*	*	*	*	*	*	*	*	"*" Have no pattern					
1.0 mm	*	*	*	*	*	*	*	*	*	"*" Have no pattern					
0.5 mm	934	944	897	924	1049	936	846	753	944	914.1	1049	753	296	-85.9	
0.5 mm	830	866	719	862	922	1031	871	829	871	866.8	1031	719	312	-133.2	-109.6
0.1 mm	959	983	955	907	955	1000	970	947	951	958.6	1000	907	93	-41.4	
0.1 mm	939	897	931	924	875	937	857	966	1022	927.6	1022	857	165	-72.4	-56.9
0 mm	1003	1039	969	981	974	1029	1016	988	989	998.7	1039	969	70	-1.3	
0 mm	1015	986	971	956	957	961	974	990	989	977.7	1015	956	59	-22.3	-11.8

The three photoresists are compared. The bake impact on CD, although slightly influenced by the I-Line, is not considered due to the loose specifications with wide window. Irrespective of the DUV photoresist type, *i.e.* 248 or 193, its influence by PB is greater than that by PEB. DUV193 G48 photoresist greater than 248 nm SEPR203 photoresist is taken to bake for the sensitivity of the bake progress again. Actually, the DUV photoresist contains no fixed direction in the proton acid H^+ movement. However, in PB, proton sour H^+ moves outwards due to the immature PB solidification, subsequently leading to swelling of the CD. The insufficient PEB energy results in a proton sour H^+ during the interface place, insufficient chain reaction and diminished CDs, thus causing PB and PEB to impact CD of DUV photoresist moving in the opposite direction, as shown in Figure 4.31.

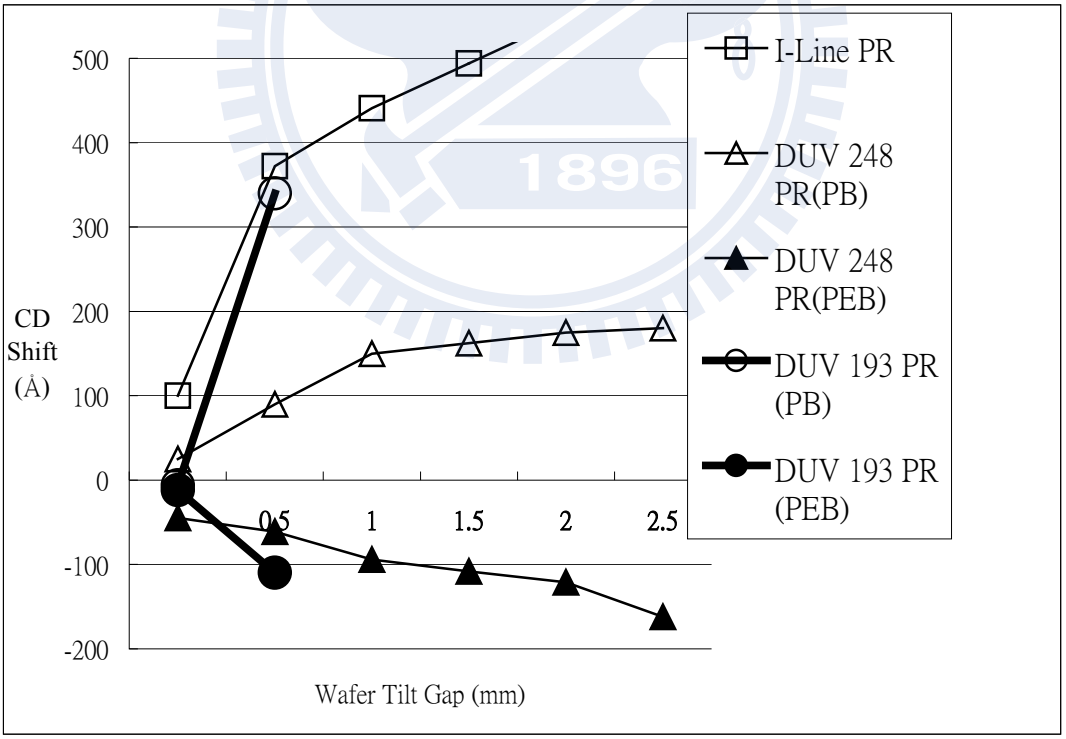

Figure 4.31 Compare three kinds of PR, bake impact on CD

4.4 Extremely narrow gap simulation

4.4.1 Particle on wafer backside simulation

A situation for a real apparatus in which the spacer thickness is less than 400 μm, makes it extremely difficult to put on and take out the plate, because a thin spacer is likely to be crocked, making the experiment data unstable. This model assumes that the particle is in the center of the wafer backside. For 0.1 mm, 0.2 mm, 0.3 mm, 0.4 mm, and 0.5 mm particles at the backside center of wafer, the surface temperature declines from 120 ℃ to 110.65~91.9 ℃, as shown in Figure 4.32.

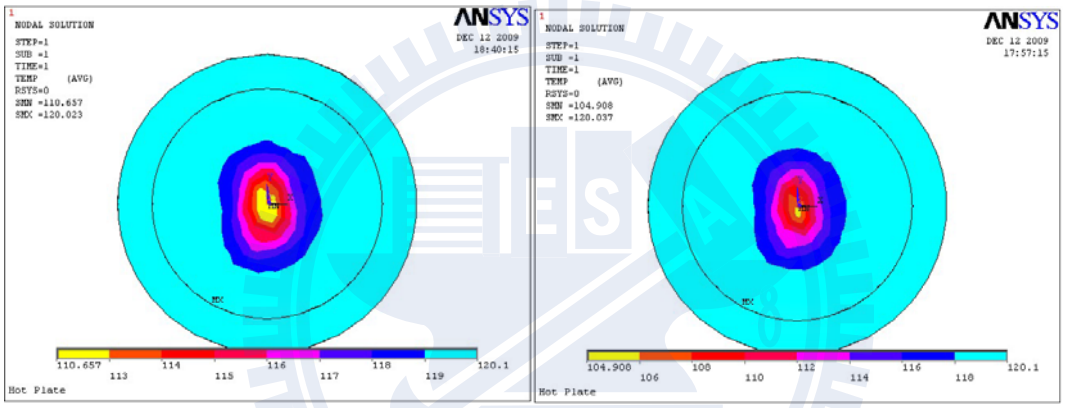

Particle size 0.1 mm **Particle size 0.2 mm**

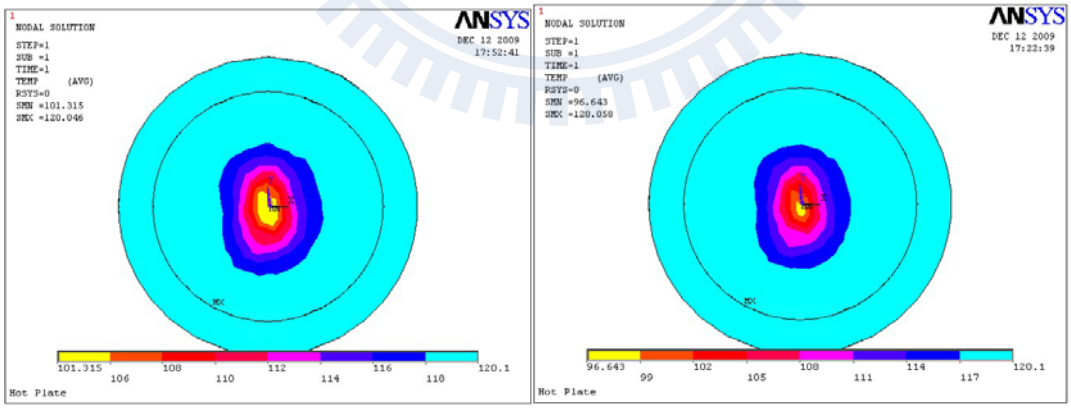

Particle size 0.3 mm **Particle size 0.4 mm**

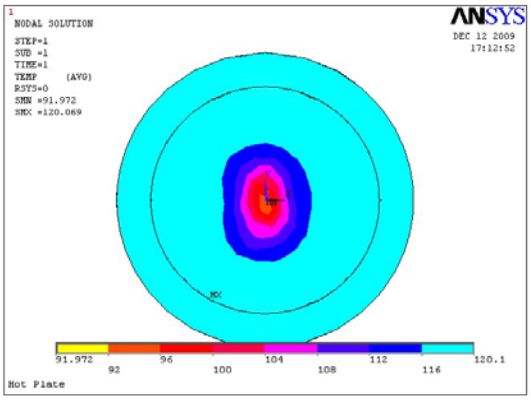

Particle size 0.5 mm

Figure 4.32 Simulation particle in wafer backside centre, particle size from 0.1 mm to 0.5 mm

Figure 4.33 summarizes the effect of PB wafer backside particle on the CD, in which the DUV193 nm photoresist is greater than the DUV248 nm photoresist. Meanwhile, the PEB wafer backside particle impacts then CD, of which the DUV193 nm photoresist is the same as DUV248 nm photoresist.

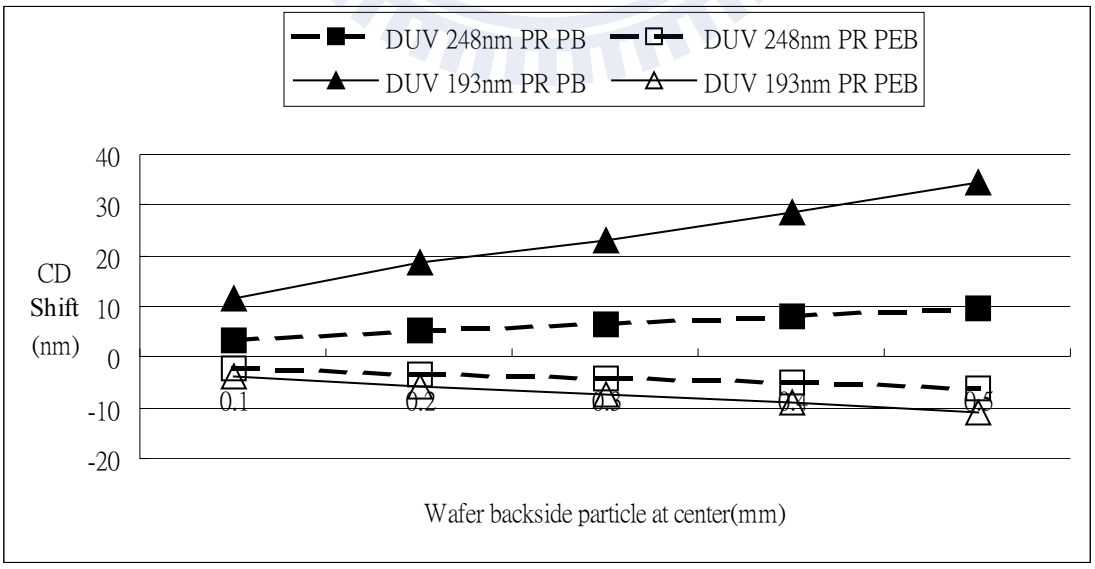

Figure 4.33 Compare DUV 193 and 248 photoresist CD shift of particle in wafer backside center

The above model assumes that the 0.1 mm particle is in the upper position of the wafer backside, in which the wafer surface temperature decrease from 120℃ to 110.72℃. When the 0.2 mm particle is in the right handed position of the wafer backside, the wafer surface temperature declines from 120℃ to 104.73℃. When the 0.3 mm particle is in the left handed position of the wafer backside, the wafer surface temperature decreases from 120℃ to 100.47℃. However, the 0.4 mm particle is in the upper position of the wafer backside, in which the wafer surface temperature declines from 120℃ to 95.49℃, Meanwhile, the 0.5 mm particle is in the lower position of the wafer backside, in which the wafer surface temperature decreases from 120℃ to 91.3℃, as shown in Figure 4.34.

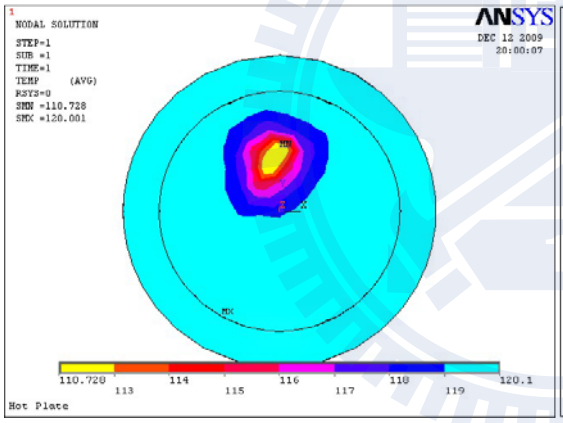

Particle size 0.1 mm

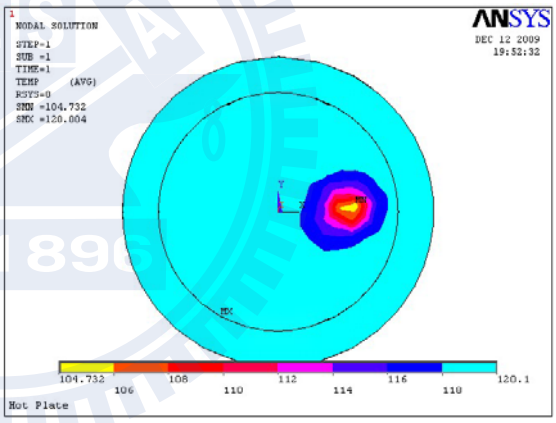

Particle size 0.2 mm

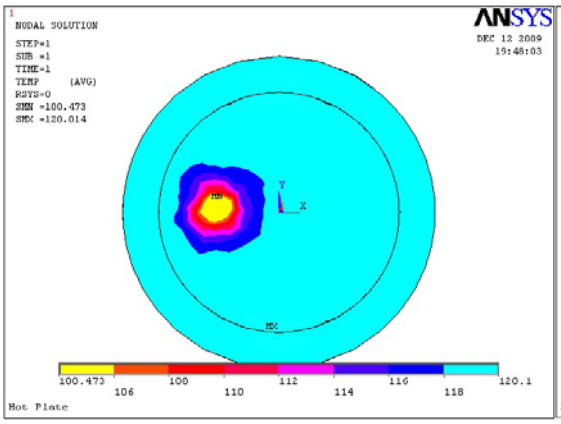

Particle size 0.3 mm

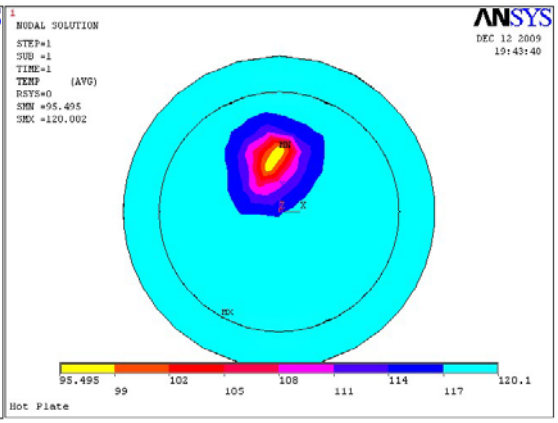

Particle size 0.4 mm

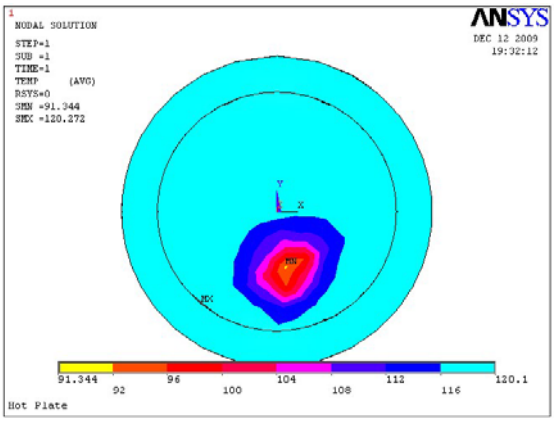

Particle size 0.5 mm

Figure 4.34 Simulation particle in wafer backside edge, particle size from 0.1 mm to 0.5 mm

According to Figure 4.35 for the PB wafer backside particle that influences the CD, DUV193 nm photoresist is greater than DUV248 nm photoresist. Additionally, for the PEB wafer backside particle that impacts the CD, DUV193 nm photoresist is the same as DUV248 nm photoresist.

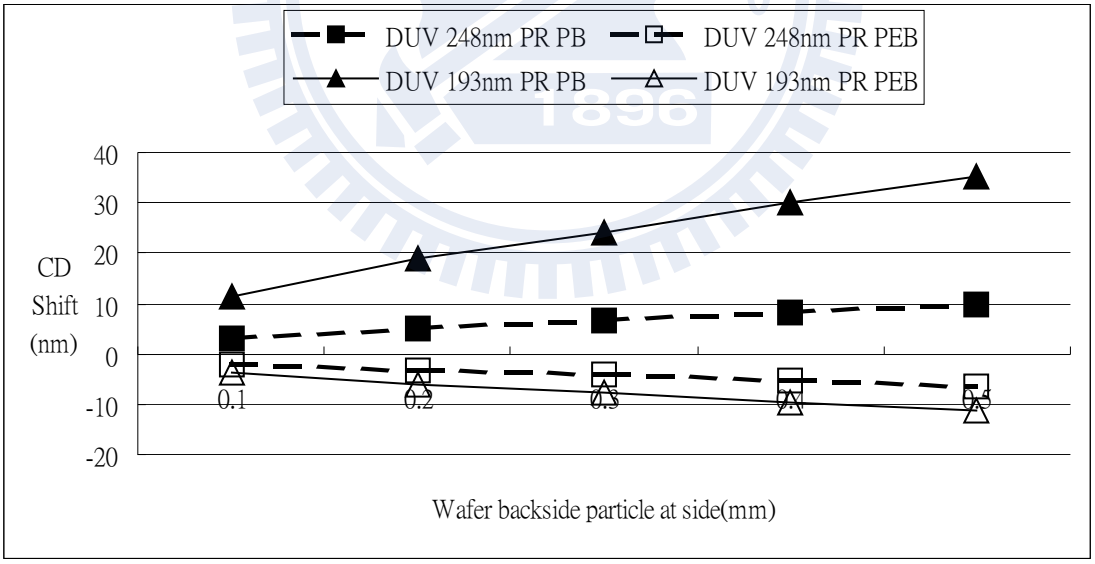

Figure 4.35 Compare DUV 193 and 248 photoresist CD shift of particle in wafer backside edge

Table 4.5 shows the wafer temperature on the simulation surface to calculate the photoresist CD shift. In DUV248 nm photoresist, PB influences CD shift 0.34 nm per ℃, in PEB influences CD shift –0.22 nm per ℃, In DUV193 nm photoresist PB

influences the CD shift 1.23 nm per ℃, in which PEB influences the CD shift –0.39 nm per ℃.

Table 4.5 Compare DUV center and edge 193 and 248 photoresist CD shift

Wafer backside particle Position	Particle Size Gap (mm)	Wafer suffice Minimum Temperature℃	Plate120℃ wafer Temp insufficient (℃)	DUV 248nm PR CD shift (nm)		DUV 193nm PR CD shift (nm)	
				PB	PEB	PB	PEB
				0.34	-0.22	1.23	-0.39
Center	0.1	110.65	9.35	3.179	-2.057	11.5005	-3.6465
	0.2	104.9	15.1	5.134	-3.322	18.573	-5.889
	0.3	101.31	18.69	6.3546	-4.1118	22.9887	-7.2891
	0.4	96.64	23.36	7.9424	-5.1392	28.7328	-9.1104
	0.5	91.9	28.1	9.554	-6.182	34.563	-10.959
Up	0.1	110.72	9.28	3.1552	-2.0416	11.4144	-3.6192
Right	0.2	104.73	15.27	5.1918	-3.3594	18.7821	-5.9553
Left	0.3	100.47	19.53	6.6402	-4.2966	24.0219	-7.6167
Up	0.4	95.49	24.51	8.3334	-5.3922	30.1473	-9.5589
Down	0.5	91.3	28.7	9.758	-6.314	35.301	-11.193

4.4.2 Pollution during the wafer backside simulation

Pollution that occurs on the wafer backside is simulated to examine the ring-pattern pollution on the wafer backside. Owing to the lack of an effective means of coating a ring pattern on the wafer backside experimentally, simulation is performed to predict the 60 μm pollution on the wafer backside at the backside center when the wafer surface temperature declines from 120 ℃ to 118.5 ℃, Estimates are also made of 70 μm pollution on the wafer backside at backside center when the wafer surface temperature decreases from 120 ℃ to 116.4 ℃. Additionally, estimates are made to predict 80 μm pollution on the wafer backside at backside center when the wafer surface temperature declines from 120 ℃ to 114.6 ℃. Moreover, estimates are made to predict 90 μm pollution on the wafer backside at the backside center when the wafer surface temperature decreases from 120 ℃ to 109.2 ℃. Furthermore, estimates are made to predict the 100 μm pollution on the wafer backside at the backside center when the wafer surface temperature declines from 120 ℃ to 106.4 ℃, as shown in Figure 4.36-37.

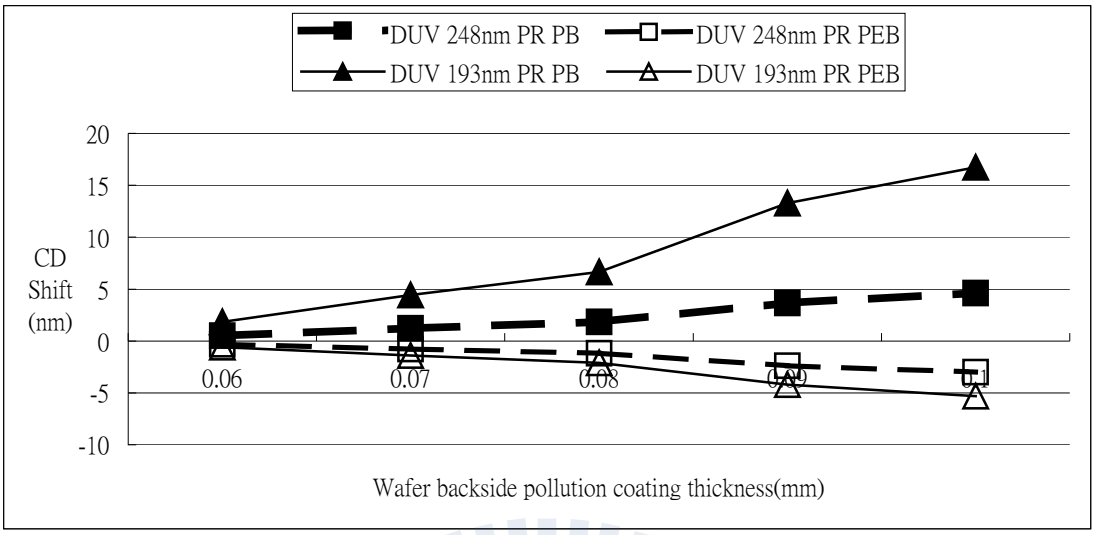

Figure 4.36 CD shift simulation pollutions at wafer backside center, film thickness from 60 µm to 100 µm

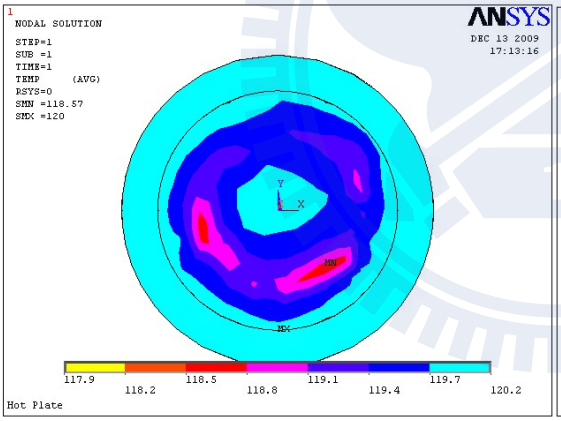

60 µm

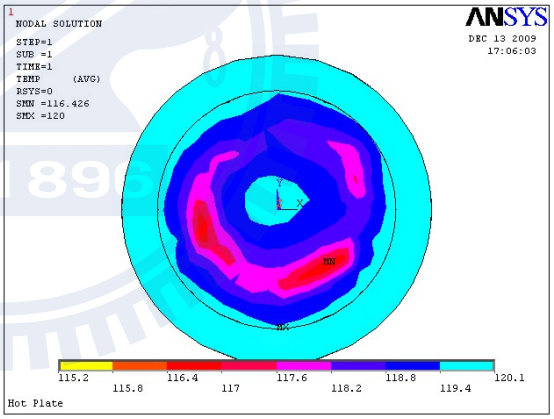

70 µm

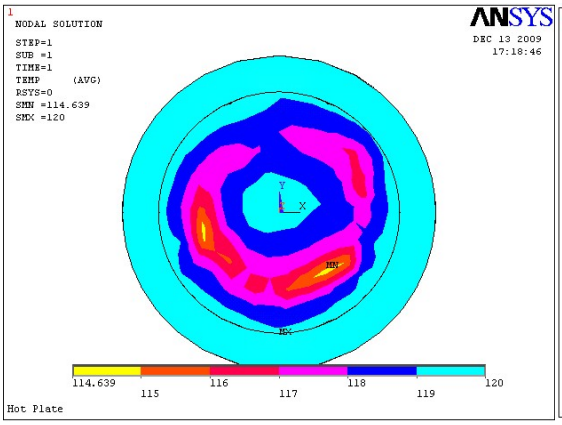

80 µm

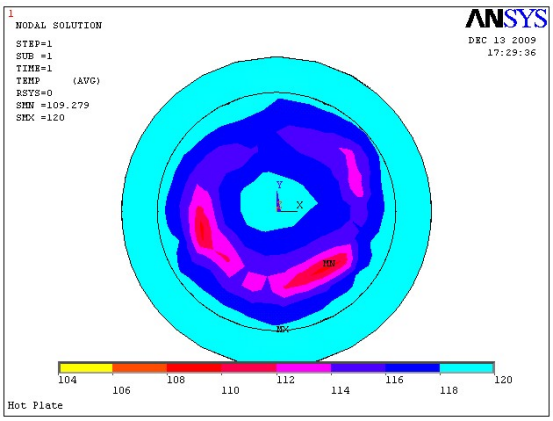

90 µm

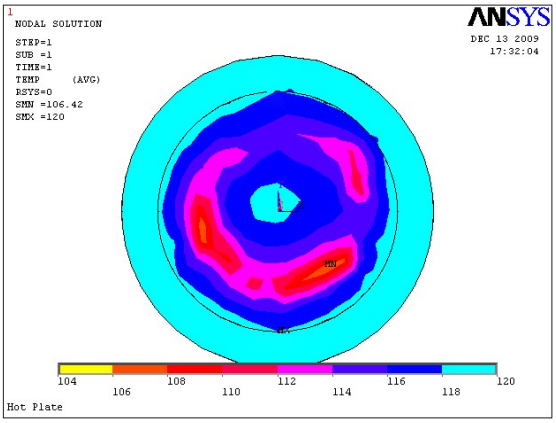

100 μm

Figure 4.37 Simulation wafer temperature, pollutions at wafer backside center, film thickness from 60 μm to 100 μm

Table 4.6 summarizes the model predictions, in which DUV 248 nm photoresist simulation is performed for 60 μm pollution on the PB wafer backside CD shift of 0.51 nm, on the PEB wafer backside CD shift –0.33 nm. DUV 193 nm photoresist simulation is performed for 100 μm pollution on the PB wafer backside CD shift 16.72 nm, on the PEB wafer backside CD shift –5.30 nm.

Table 4.6 Simulation predict 60 μm~100 μm pollutioin film at the wafer backside center photoresist CDs shift

pollution on wafer back side	pollution thickness Gap (mm)	Wafer sufface Minimum Temperature℃	Plate120℃ wafer Temp insufficient (℃)	DUV 248nm PR CD shift (nm)		DUV 193nm PR CD shift (nm)	
				PB	PEB	PB	PEB
				0.34	-0.22	1.23	-0.39
Ring-1	0.06	118.5	1.5	0.51	-0.33	1.845	-0.585
Ring-2	0.07	116.4	3.6	1.224	-0.792	4.428	-1.404
Ring-3	0.08	114.6	5.4	1.836	-1.188	6.642	-2.106
Ring-4	0.09	109.2	10.8	3.672	-2.376	13.284	-4.212
Ring-5	0.1	106.4	13.6	4.624	-2.992	16.728	-5.304

Table 4.7 This experimental data materials summary

Hot Plate 120℃	Gap of wafer and plate (mm)	0	0.5	1	1.5	2	2.5
	ΔT plate drops temperature (℃)	1.3	0.8	0.6	0.5	0.4	0.1
	Simulation plate drop ΔT (℃)	1.25	0.85	0.6	0.55	0.5	0.1
	Wafer surface temperature drop (℃)	5.11	27.51	32.59	34.09	35.61	37.74
	Simulation Wafer surface temperature drop (℃)	4	25.5	31	33.9	36.9	38
I-Line PR	Thickness 12000~12250, Shift (Å)	25	175	350	400	450	6796
	CD spec 3500~3900, Shift (Å)	200	350	420	480	540	820
248 nm DUV PR CD Spec 2925~3075 (Å)	Thickness 8000~8100, Shift (Å)	30	70	105	115	125	135
	PB Wafer Tilt CD Shift (Å)	25	94	126	152	179	187
	PEB Wafer Tilt CD Shift (Å)	-40	-61	-96	-108	-121	-162
193 nm DUV PR CD Spec 950~1050 (Å)	PR Thickness spec 3000~3050, shift (Å)	20	28	48	61.5	75	85
	PB Wafer Tilt CD Shift (Å)	33	340	no pattern	no pattern	no pattern	no pattern
	PEB Wafer Tilt CD Shift (Å)	-25	-109	no pattern	no pattern	no pattern	no pattern

Table 4.7 shows the DUV 248 nm photoresist prebake plate and a wafer tilt gap of 0.5 mm, in which the wafer surface temperature declines to 27.51℃; the CD shifts 9.4 nm; the DUV 248 nm photoresist post exposed bake plate and a wafer tilt gap of 0.5 mm, in which the wafer surface temperature decrease to 27.51℃ the CD shift –6.1 nm. Calculations are made of how the pre bake wafer surface temperature impacts the DUV 248 nm photoresist CD shift 9.4 nm in 27.5℃. Therefore, for each ℃ shift 0.34 nm (0.34 nm per ℃), the PEB wafer surface temperature impacts the DUV 248 nm photoresist CD shift –6.1 nm/27.5℃, –0.22 nm per ℃. Calculations are made of how pre bake wafer surface temperature impacts the DUV193 nm photoresist CD shift 34 nm/27.5℃, 1.23 nm per ℃. Moreover, the PEB wafer surface temperature impacts the DUV193 nm photoresist CD shift 10.9 nm/27.5℃, –0.39 nm per ℃.

Chapter 5 Conclusion

The plate ΔT provides bake condition impact on CD, and workable simplify judge abnormal bakes of wafer. Thickness influence I-Line greater than DUV193 and DUV248. The I-line CD will not be considered due to the wide specification. DUV PR, 248 or 193 PB influences will be greater than PEB. PB and PEB impact on CD DUV193 G48 photoresist greater than 248 nm SEPR203 PR. PB and PEB impact on CD in the opposite direction.

The wafer surface temperature impact on DUV248 nm PR, at PB CD shift 0.34 nm per ℃, at PEB CD shift –0.22 nm per ℃. The wafer surface temperature impact on DUV193 nm PR, at PB CD shift 1.23 nm per ℃, at PEB CD shift –0.39 nm per ℃.

In addition, a three-dimensional finite-element model using commercial software, ANSYS^{TM} was employed to examine the wafer surface temperature of various hardware and contact gap conditions. Compare surface temperature of the real wafer with simulated wafer surface with a marginal error of ±2℃. Wafer and instantaneous plate-plate contact temperature drop ΔT, actual plate temperature drop ΔT and ΔT data difference are predicted to reach below ±0.2℃.

This ANSYS model simulated very narrow gap especially when the spacer thickness smaller than 400 μm. In the real apparatus is too difficult to put on the plate and take out of plate, in such thin spacer is likely to be crocked and make the experiment data unstable. So use this model predict wafer surface temperature and CD shift, when a particle make wafer tilt gap under 400 μm. Use this model predict 100 μm particle on PB plate the wafer surface temperature drop from 120 ℃ to 110.65 ℃ and the CD shift about 3.179~11.5 nm, particle on PEB plate the CD shift about –2.05~-3.64 nm.

Also, ANSYS can be used to simulate a ring pattern pollution on wafer backside,

because there is no good method to do a ring pattern coating at wafer backside for experiment. Used this model to predict that 100 μm pollution on wafer backside at backside center of PB wafer surface temperature drop from 120 ℃ to 106.4 ℃ and the via CD shift from 4.624 to 16.72 nm, at PEB the via CD shift from –2.992 to –5.304 nm.

References

[1] Scotten W. Jones, IC Knowledge LLC Photo Lithography, (2008).

[2] Adam R. Pawloski, Alden Acheta, Bruno La Fontain, Scott Bell, Harry J. Levinson, Lithographically Generated Line Edge Roughness in Photoresist, January 13 (2005).

[3] Paul D. Friedberg, Cherry Tang, Bhanwar Singh, Thomas Brueckner, Wolfram Gr dke, Bern Schulz, Costas J. Spanos, Time-based PEB adjustment for optimizing CD distributions, (2005).

[4] 邱俊達, 張雍政 ,「淺談LER成因與改善對策」, 半導體科技技術專文 , P48-52 , July (2005).

[5] Bryan Rice, Heidi Cao, Jeanette Roberts, Manish Chandhok Intel Corporation, Effects of Processing Parameters on Line Edge Roughness (LER), 2 (2002).

[6] Donald A. Neamen, Semiconductor Physics & Devices, (2003).

[7] Bart Van Zeghbroeck, Principles of Semiconductor Devices, (2002).

[8] Wen-Li Wu, Jim Leu, "Small angle x-ray scattering measurements of lithographic patterns with sidewall roughness from vertical standing waves", American Institute of Physics, 1 (2007).

[9] International Technology Working Group (ITWG), "Lithography", International Technology Roadmap for Semiconductors 2007 edition, 20 (2007).

[10] Ko Fu-Hsiang, Wang Chung-Cheng, "Research on Lithographic In-line Process Control from Scatterometry Measurements", 國立交通大學, 碩士論文, (2009).

[11] Cymer Southeast Asia, Service manual, (2000).

[12] Komatsu, KLES-G10K 1k Hz KrF 10W Laser, (2001).

[13] Lambda Physic Company, Service manual, (2000).

[14] Harry J. Levinson, Principles of Lithography Second Edition, (2004).

[15] Will Conley, "International Sematech Universities 157nm Photoresist Research Project", 半導體科技, **22**, 1, (2001/8).

[16] 李世鴻, 積體電路製程技術, 206 (2001).

[17] Michael Quirk, Julian Serda, Semiconductor Manufacturing Technology, 401 (2003).

[18] 朱文聰, 有機化學精要, 18 (2002).

[19] 曾國輝, 化學HYDROGEN BONDS, 258 (2005).

[20] Nixon Shen, 正型光阻內容物介紹, (2002).

[21] TOKYO OHKA KOGYO CO., LTD., Chemistry of Novolak-DNQ Based Resists, (1994).

[22] 宋心琦, 周福添, 劉劍波, 光化學, 五南圖書出版公司, 295 (2004).

[23] 莊達人, VLSI 製造技術, 239 (2000).

[24] Robin Nagel, "Optical lithography", Technische Universitat Munchen, 12 Januar (2009).

[25] Sean David Burns, B.S. Ch.E., "Understanding FundamentalMechanisms of Photoresist Dissolution", The University of Texas at Austin, Doctor of Philosophy, May (2003).

[26] Pavlos C. Tsiartas, Lewis W. Flanagin, Clifford L. Henderson, "The Mechanism of Phenolic Polymer Dissolution", Macromolecules, **30,** 4657, (1997).

[27] 龍文安, 半導體微影技術, (2004).

[28] Saburo Nonogaki, Takumi Ueno, Toshio lto, "Chemistry of Photoresist Materials", SPIE, **1262,** 493 (1990).

[29] Hiroshi iTO, Greg BREYTA, Don HOFER, R. SOORiYAKUMARAN, "ENVIRONMENTALLY STABLE CHEMICAL AMPLIFICATION POSITIVE RESIST", Journal of Photopolymer Science and Technology, **7,** 448

(1994).

[30] Donald C. Hofer, Robert Allen, Greg Wallraff, Hiroshi Ito, Phil Brock and Rick DiPietro, "193 nm Photoresist R&D The Risk & Challeng", Journal of Photopolymer Science and Technology, **9,** 387, (1996).

[31] Andrew Jamiesion, Mark Somervell, Hoang Vi Tran, Raymond Hung, Scott A, "Top Surface Imaging at 157 nm", The University of Texas at Austin, 3 (2005).

[32] Saeed Moaveni, Finite Element Analysis Theory and Application with ANSYS, (2007).

[33] 賴育良, ANSYS電腦輔助工程分析, (1997).

[34] 劉博文, ULSI 製程技術, 283 (2003).

[35] 吳昌崙, 張景學, 半導體製程技術, 298 (2003).

[36] 張勁燕, 半導體製程設備, 59 (2004).

[37] ASML Corporation, PAS5500 Service Manual, Aug (1995).

[38] HONG XIAO, Introduction to Semiconduction Manufacturing Technology, 113 (2002).

[39] Tokyo Electron Limited, Clean Track ACT8, Mark8 Manual, (1999).

[40] Therma-wave Inc, Opti-Probe Getting Started Manual, TFMS3.00, June(1997).

[41] Hitachi High-Technologies Corporation, CD Measurement SEM, (2001).

[42] SensArray, Thermal MAP3 User Manual, (1998).

[43] Atmel Corporation, 8-bit Microcontroller with 4k Bytes In-System Programmable Flash AT89S51, (2001).